Dissertation

Zur Erlangung eines Doktorgrades der Naturwissenschaften

The Effect of Oncogenic HRas on the RTK-PTP Reaction Network

vorgelegt von

Rabea Stockert

bei der Fakultät für Chemie und Chemische Biologie

Technische Universität Dortmund

August 2017

Diese Arbeit wurde angefertigt am
Max-Planck-Institut für molekulare Physiologie in Dortmund

1. Gutachter: Prof. Dr. Philippe I.H. Bastiaens

2. Gutachter: Prof. Dr. Roger S. Goody

Eidesstattliche Versicherung (Affidavit)

Name, Vorname
(Surname, first name)

Matrikel-Nr.
(Enrolment number)

Belehrung:

Wer vorsätzlich gegen eine die Täuschung über Prüfungsleistungen betreffende Regelung einer Hochschulprüfungsordnung verstößt, handelt ordnungswidrig. Die Ordnungswidrigkeit kann mit einer Geldbuße von bis zu 50.000,00 € geahndet werden. Zuständige Verwaltungsbehörde für die Verfolgung und Ahndung von Ordnungswidrigkeiten ist der Kanzler/die Kanzlerin der Technischen Universität Dortmund. Im Falle eines mehrfachen oder sonstigen schwerwiegenden Täuschungsversuches kann der Prüfling zudem exmatrikuliert werden, § 63 Abs. 5 Hochschulgesetz NRW.

Die Abgabe einer falschen Versicherung an Eides statt ist strafbar.

Wer vorsätzlich eine falsche Versicherung an Eides statt abgibt, kann mit einer Freiheitsstrafe bis zu drei Jahren oder mit Geldstrafe bestraft werden, § 156 StGB. Die fahrlässige Abgabe einer falschen Versicherung an Eides statt kann mit einer Freiheitsstrafe bis zu einem Jahr oder Geldstrafe bestraft werden, § 161 StGB.

Die oben stehende Belehrung habe ich zur Kenntnis genommen:

Official notification:

Any person who intentionally breaches any regulation of university examination regulations relating to deception in examination performance is acting improperly. This offence can be punished with a fine of up to EUR 50,000.00. The competent administrative authority for the pursuit and prosecution of offences of this type is the chancellor of the TU Dortmund University. In the case of multiple or other serious attempts at deception, the candidate can also be unenrolled, Section 63, paragraph 5 of the Universities Act of North Rhine-Westphalia.

The submission of a false affidavit is punishable.

Any person who intentionally submits a false affidavit can be punished with a prison sentence of up to three years or a fine, Section 156 of the Criminal Code. The negligent submission of a false affidavit can be punished with a prison sentence of up to one year or a fine, Section 161 of the Criminal Code.

I have taken note of the above official notification.

Ort, Datum
(Place, date)

Unterschrift
(Signature)

Titel der Dissertation:
(Title of the thesis):

Ich versichere hiermit an Eides statt, dass ich die vorliegende Dissertation mit dem Titel selbstständig und ohne unzulässige fremde Hilfe angefertigt habe. Ich habe keine anderen als die angegebenen Quellen und Hilfsmittel benutzt sowie wörtliche und sinngemäße Zitate kenntlich gemacht.
Die Arbeit hat in gegenwärtiger oder in einer anderen Fassung weder der TU Dortmund noch einer anderen Hochschule im Zusammenhang mit einer staatlichen oder akademischen Prüfung vorgelegen.

I hereby swear that I have completed the present dissertation independently and without inadmissible external support. I have not used any sources or tools other than those indicated and have identified literal and analogous quotations.

The thesis in its current version or another version has not been presented to the TU Dortmund University or another university in connection with a state or academic examination.*

*Please be aware that solely the German version of the affidavit ("Eidesstattliche Versicherung") for the PhD thesis is the official and legally binding version.

Ort, Datum
(Place, date)

Unterschrift
(Signature)

The scariest moment is always just before you start.

Stephen King

CONTENTS

LIST OF FIGURES

LIST OF TABLES

ABBREVIATIONS

-SH	thiol
-SOH	sulfenic acid
°C	degree Celsius
a.u.	arbitrary units
aa	amino acid
Ab	antibody
Akt/PKB	protein kinase B
ATP	adenosine triphosphate
Bis-Tris	bis-(2-hydroxyethyl) aminotris (hydroxymethyl) methane
bp	base pair
BSA	bovine serum albumin
C-terminus	carboxyl terminus
CIP	calf intestinal phosphatase
ddH_2O	double distilled water
Dimedone	5,5-dimethyl-1,3-cyclohexanedione
DMEM	Dulbecco's minimal essential medium
DMSO	dimethyl sulfoxide
DNA	deoxyribonucleic acid
dsDNA	double stranded DNA
DTT	dithiothreitol
DUSP	dual-specificity phosphatase
e.g.	*exempli gratis*
EB	elution buffer
EDTA	ethylenediaminetetraacetic acid
EGF	epidermal growth factor
EGFP	enhanced green fluorescence protein
EGFR	epidermal growth factor receptor
ER	endoplasmic reticulum
Erk	extracellular signal-regulated kinase
FCS	fetal calf serum
FLIM	fluorescence lifetime imaging microscopy
FRET	Förster resonance energy transfer
GDP	guanosine diphosphate
GF	growth factor
GFP	green fluorescent protein
GTP	guanosine triphosphate
H_2O_2	Hydrogen Peroxide
hr(s)	hour(s)
IP	immunoprecipitation
IRF	instrument response function
kb	kilo base pair
kD	kilo dalton
l	liter
L-Glu	L-glutamine
LB	lysogeny broth
MAPK	mitogen-activated protein kinase
MeOH	methanol

min	minute
N-terminus	amino-terminus
n.s.	not significant
NAPDH	nicotinamide adenine dinucleotide phosphate
NEAA	non-essential amino acids
nm	nanometer
NOX	NAPDH oxidase
ns	nanosecond(s)
o.n.	over night
PAGE	polyacrylamide gel electrophoresis
PBS	phosphate buffered saline
pH	*potentium hydrogenii*
PH domain	pleckstrin homology domain
PI3K	phosphoinositide-3-kinase
PIP3	phosphatidylinositol (3,4,5)-triphosphate
PM	plasma membrane
PMT	photomultiplier tube
PRX	peroxiredoxin
PTB	phosphotyrosine binding
PTEN	phosphatase and tensin homolog
PTP	protein tyrosine phosphatase
pTyr	phosphotyrosine
PVDF	polyvinylidene fluori
RE	recycling endosome
ROS	reactive oxygen species
rpm	rounds per minute
RT	room temperature
RTK	receptor tyrosine kinase
s	second
SDS	sodium dodecyl sulphate
SEM	standard error of mean
SFM	serum free media
SH2	src homology 2
SHP1	SH2-containing tyrosine phosphatase 1
SHP2	SH2-containing tyrosine phosphatase 2
SOD	superoxide dismutase
TAE	Tris-acetate-EDTA
TBS	Tris buffered saline
TCSPC	time correlated single photon counting
Tris	Tris[hydroxymethyl]aminomethane
UV	ultraviolet
V	volt
wt	wild type
µ	micro
τ	lifetime
τ_{av}	average lifetime
τ_{D}	donor-only lifetime
τ_{DA}	donor-acceptor lifetime

ABSTRACT

The production of reactive oxygen species (ROS) was long thought to be a necessary consequence of aerobic metabolism causing non-specific damage to proteins, lipids and DNA. In the last years, however, several studies showed that at low levels ROS can act as cellular signaling molecules. In particular, hydrogen peroxide (H_2O_2) gained interest as second messenger due to its long half-life, its compartmentalized production and its ability to reversibly oxidize specific thiol groups of proteins. Reversible oxidation leads to the formation of sulfenic acid (-SOH), altering protein structure and thereby protein function. One of the most established targets of H_2O_2-mediated oxidation are protein tyrosine phosphatases (PTPs). Their active site is characterized by the same signature motif including one cysteine with a low pKa, which is essential for catalyzing the dephosphorylation of tyrosines but also renders PTPs highly susceptible for oxidation resulting in their inactivation. Interestingly, it was shown that receptor tyrosine kinase (RTK) activation initiates the production of H_2O_2 by activating NAPDH oxidases (NOXs). This local burst of H_2O_2 leads to the coupling of RTK activation with PTP inhibition.

So far, it was difficult to detect the spatial-temporal dynamics of H_2O_2 production and the resulting oxidation of proteins, remaining the precise role of PTP oxidation in RTK signal propagation unspecified. Here, we investigated the causal connectivity between PTP inhibition and activation of the epidermal growth factor receptor (EGFR) and how this network might be affected by oncogene-induced H_2O_2 production. We could show that ligand-dependent and -independent EGFR activation result in the production of H_2O_2. Cellular transformation through the constitutively active form of HRas (G12V mutant) even increases H_2O_2 levels in unstimulated cells and upon EGF stimulation. As a consequence, HRas G12V transformed cells are more susceptible for autonomous EGFR activation. In addition, we could show that proliferation and survival of oncogenic cells are dependent on elevated H_2O_2 levels. For a better understanding of the link between RTK activation and PTP inactivation, we developed a FRET-FLIM approach to monitor the spatial-temporal oxidation of proteins, tested here with the Src-homology protein tyrosine phosphatase 2 (SHP2). By using this method, we could show that SHP2 is more oxidized in HRas G12V transformed cells, most likely involved in the higher autonomous EGFR activation. A further investigation of how H_2O_2-mediated oxidation of other PTPs is affecting the RTK-PTP reaction network could give new insights into how the final RTK response is shaped under physiological and pathophysiological conditions.

ZUSAMMENFASSUNG

Lange Zeit wurde die Bildung von reaktiven Sauerstoffspezies (*Reactive oxygen species*, ROS) als notwendiges Übel eines aeroben Stoffwechsels angesehen, das zur Schädigung von Proteinen, Lipiden und DNA führt. Allerdings zeigten mehrere Studien, dass bei niedrigen Konzentrationen ROS als zelluläre Signalmoleküle fungieren können. Vor allem Wasserstoffperoxid (H_2O_2) rückte in den Fokus als sekundärer Botenstoff, charakterisiert durch seine lange Halbwertszeit, die kompartimentalisierte Bildung und die Eigenschaft spezifische Thiolgruppen von Proteinen reversibel zu oxidieren. Die reversible Oxidierung führt zur Bildung von Sulfensäure (-SOH) und einer daraus resultierenden Modifikation der Proteinstruktur, was zu einer Änderung der Proteinfunktion führt. Zu der bekanntesten Zielgruppe von H_2O_2 vermittelter Oxidierung gehören Protein-Tyrosin-Phosphatasen (PTPs). Das aktive Zentrum von PTPs ist durch das gleiche Motiv gekennzeichnet, was ein Cystein mit niedrigem pKa beinhaltet. Dieser Cystein-Rest ist wichtig für die Phosphotyrosin-Hydrolyse, macht PTPs aber gleichzeitig anfällig für eine oxidative Modifikation und einer damit verbundenen Inaktivierung. Interessanterweise konnte auch gezeigt werden, dass die Aktivierung von Rezeptortyrosin-Kinasen (RTKs) die Bildung von H_2O_2 verursacht. Der lokale Anstieg von H_2O_2 führt somit zur einer Kopplung zwischen der Aktivierung von RTKs und der Inhibierung von PTPs.

Bis jetzt war es schwierig, die räumlichen und zeitlichen Dynamiken der H_2O_2 Bildung und der daraus resultierenden Proteinoxidierung zu detektieren, weswegen der Einfluss der PTP Oxidierung auf die RTK Signalweiterleitung weitestgehend ungeklärt ist. Der Fokus dieser Arbeit liegt auf der Untersuchung des kausalen Zusammenhangs zwischen PTP Inhibierung und der Aktivierung des epidermalen Wachstumsfaktor Rezeptors (*epidermal growth factor receptor*, EGFR) und ob dieses Netzwerk durch Onkogen-induzierte H_2O_2 Produktion beeinflusst wird. Wir konnten zeigen, dass die Liganden-abhängige und -unabhängige Aktivierung von EGFR zu der Produktion von H_2O_2 führt. Maligne Zelltransformation durch die konstitutiv-aktive Form von HRas (G12V Mutante) erhöht die intrazellulären H_2O_2 Level zusätzlich, sowohl in unstimulierten als auch in EGF-stimulierten Zellen. Daraus resultiert, dass HRas G12V transformierte Zellen eine besonders hohe Anfälligkeit für eine autonome EGFR Aktivierung aufweisen. Zusätzlich konnte gezeigt werden, dass die Zellproliferation und das Überleben transformierter Zellen von der erhöhten H_2O_2 Produktion abhängig ist. Für einen tiefer Einblick in die Kopplung zwischen RTK Aktivierung und PTP Inhibierung wurde ein FRET-FLIM Ansatz entwickelt, um die

räumliche und zeitliche Oxidierung von Proteinen aufzulösen. Getestet wurde diese Methode an Hand der Oxidierung von der Src-homology Proteintyrosin Phosphatase 2 (SHP2). Es konnte gezeigt werden, dass HRas G12V transformierte Zellen eine erhöhte SHP2 Oxidierung aufweisen, was sehr wahrscheinlich zu der verstärkten autonomen EGFR Aktivierung beiträgt. Weiterführende Untersuchungen könnten Aufschluss darüber geben, inwieweit die Oxidierung von weiteren PTPs das RTK-PTP Reaktionsnetzwerk beeinflusst und wie dadurch die finale RTK Reaktion unter physiologischen und pathophysiologischen Bedingungen bestimmt wird.

1 INTRODUCTION

1.1 ROS signaling

Reactive oxygen species (ROS) is a collective term that describes O_2-derived species including superoxide anion (O_2^-), hydrogen peroxide (H_2O_2) and hydroxyl radical (HO•)[1]. The intracellular production of ROS was long believed to be a necessary evil of aerobic life that cannot be avoided[2]. Nearly every metabolic process is coupled to the generation of small amounts of ROS due to incomplete reduction of oxygen, with the mitochondrion as one of the major intracellular sources[3]. High concentrations, referred to as oxidative stress, are implicated in various disease states such as atherosclerosis, diabetes, cancer, neurodegeneration and aging[4]. However, ROS involvement in the pathogenesis of diseases is not confined to macromolecular damage but rather their specific role in affecting cellular signaling. Furthermore, many studies now provided evidence for the role of ROS not only in pathologies but also in physiological signaling processes.

The implication of ROS as possible second messenger is still controversial but raising more and more interest in the scientific community. The paradox that a rather toxic byproduct should mediate important signaling processes and regulate cellular functions such as survival and proliferation is still not fully explained yet. How can a molecule, which recognition occurs at the atomic and not the macromolecular level, that has short half-lives and targets ranging from proteins to lipids to DNA and RNA, guarantee specificity in cellular signaling cascades? With this work we want to render the understanding of ROS signaling activities more precisely with the focus on hydrogen peroxide (H_2O_2).

Going back in the history of ROS biology, the first proteins found important for redox (reduction/oxidation) signaling were ROS scavengers such as catalase, peroxiredoxins (PRXs) and superoxide dismutases (SODs). They are part of the antioxidant machinery of cells removing excess radicals. Their discovery supported the view of ROS as an unavoidable component of aerobic metabolism that need to be reduced quickly upon formation. On the other hand, high H_2O_2 levels near the endoplasmic reticulum, necessary for proper protein folding, was an accepted exception for biological relevant ROS production. It was shown that the protein ER oxidoreductin 1 (Ero1) initiates the formation of disulphide bonds by triggering a two-electron oxidation of the thioredoxin protein disulfide isomerase (PDI) leading to the production of H_2O_2[5]. Another biological function of controlled ROS production

is long known for leucocytes, cells of the innate immune response. During phagocytosis ROS gets produced in high levels to kill harmful microbial intruders resulting in the so called 'respiratory burst'[6]. Otherwise, elevated ROS levels were only associated with cellular damage and genomic instability prompting cell death, aging and carcinogenesis[7].

Rethinking started with a few reports in the 1980s showing that low concentrations of exogenous H_2O_2 could stimulate cell proliferation[8]. Further investigations focused on the phagocytic enzyme gp91phox (now known as NOX2) responsible for the respiratory burst in leucocytes. Through gene profiling, seven isoforms (NOX1-5 and DUOX 1 and 2) of NOX2 were found with a ubiquitous expression also in non-phagocytic cells[3,9]. It became apparent that production of ROS has a more global role than just for microbe killing. In particular O_2^- and H_2O_2, the main products of NOX enzymes, can act as second messengers and fall in the same class such as other ubiquitous small-molecule messengers such as calcium ions (Ca^{2+})[10] and nitric oxide (•NO)[11]. In particular, H_2O_2 is relatively stable with a cellular half-life of 1 ms and steady state levels of 10^{-7} M making it a suitable signaling molecule.

1.1.1 NOX proteins as source of intracellular H_2O_2

The first evidence that cells produce ROS in a controlled fashion was shown for the innate immune system, where a so-called respiratory burst produced by leucocytes results in pathogen killing. Identification of the NAPDH oxidase in phagosomes (phox; NOX2) of these cells gave evidence of a signaling-mediated activation of this enzyme and subsequent generation of O_2^-. Later homologues of the catalytic subunit gp91phox were found in other cell types and with different intracellular localizations, primarily in the plasma membrane (PM) and later also in other membranes including the nucleus, mitochondria, and the endoplasmic reticulum (ER)[9,12]. Due to their ubiquitous expression profile it became obvious that production of ROS is not just a side effect of aerobic life but rather a general process in cellular signaling controlling protein activities on any kind of level.

So far, the NADPH oxidase (NOX) family consists of seven members; NOX1, NOX2, NOX3, NOX4, NOX5 and the dual oxidases DUOX1 and DUOX2, which are localized to various cellular membranes forming either O_2^- or H_2O_2. All members share a common structure, the catalytic subunit gp91phox consisting of six transmembrane domains, which form a channel to allow the successive transfer of electrons[13]. Those electrons are then transferred from NADPH (converting it to $NADP^+$) to flavin adenine dinucleotide (FAD) to

haeme and finally to oxygen to form superoxide anions ($O_2^{\cdot-}$)[3]. Superoxide dismutases (SODs) located at different intra- and extracellular compartments catalyze the dismutation from the superoxide radical to H_2O_2. The isoform SOD1 is expressed in the cytosol and the mitochondrial intermembrane space, SOD2 in the mitochondrial matrix and SOD3 in the extracellular space[14,15].

Activation of NOX enzymes is stimulus-regulated and the different NOX isoforms differ in their regulatory subunits. NOX1, NOX3 and NOX4 are nearly identical in size and structure to gp91phox/NOX2[3]. Upon activation, the membrane-associated p22phox forms a mutually stabilizing complex with the catalytic subunit gp91phox, whose carboxyl terminus contains a proline-rich sequence that serves as targeting site for the two SH3 domains of the cytoplasmic subunit p47phox[16,17]. Other cytoplasmic regulatory subunits, which are getting recruited to the transmembrane complex, include homologue NoxO1, p40phox, p67phox and homologue NoxA1, and Rac1/2 depending on the NOX isoform (

Figure 1.1)[3]. The other isoforms including NOX5, DUOX1 and DUOX2 share that they are calcium regulated owing to EF-hand Ca^{2+} binding domains[7]. NOX1, 2, 3 and 5 produce $O_2^{\cdot-}$ whereas DUOX1 and 2, and more recently discovered NOX4, are known to produce H_2O_2 directly due to a peroxidase-like domain at their N-terminus[7].

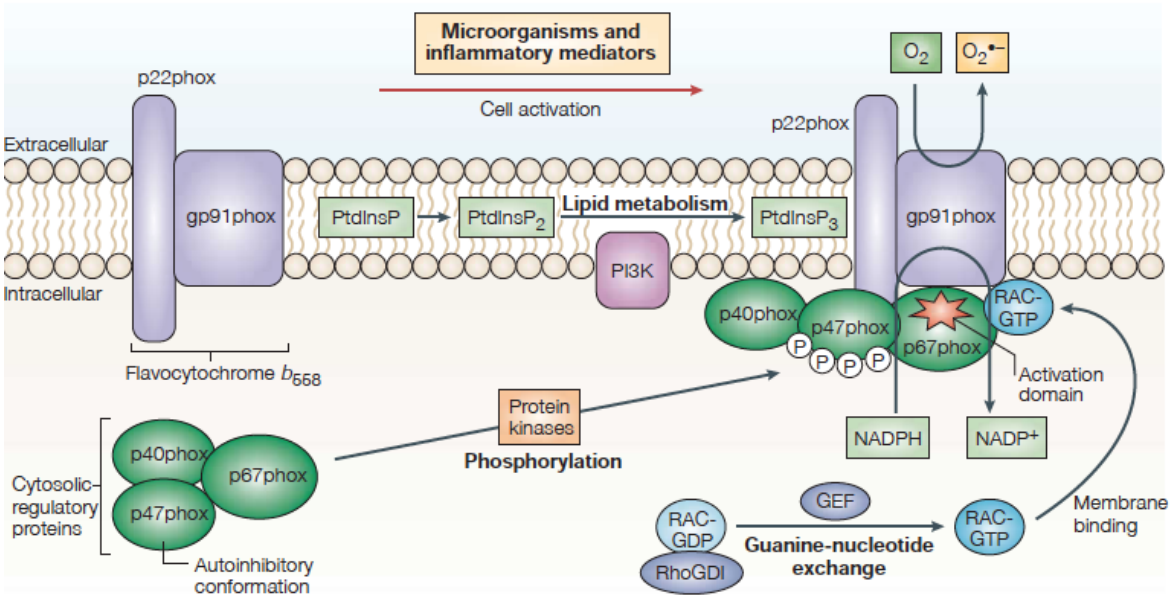

Figure 1.1: Schematic representation of the activation of NOX2 in phagocytes
Activation of NOX2 in phagocytes occurs upon assembly of the cytosolic regulatory proteins (p40phox, p47phox, p67phox) with the transmembrane domain flavocytochrome b_{558} (gp91phox and p22phox). In addition, Rac-GTP, which is masked by RhoGDI in its GDP-bound state, associates with the membrane and p67phox, stabilizing the active NOX complex. (adapted from[3])

Various subcellular localizations of NOX1 have been reported including the nuclear membrane[18], PM distribution[19] and expression in early endosomes[20]. NOX2 is the most intensively studied isoform and is expressed in various cell types including neutrophils, where it was discovered first. Its subcellular localization is mostly restricted to the PM with a high accumulation in protrusions and membrane ruffles[21,22]. NOX4 has a unique role among the NOX family members. In contrast to the other NOX isoforms, it only requires the membrane subunit phox22 for its superoxide-producing activity and appears to be constitutively active[17,23]. This suggests that its activity is proportional its to protein expression alone. In addition, most studies report that NOX4 is solely expressed in the endoplasmic reticulum (ER) independent of the investigated cell type[24].

1.1.2 Compartmentalization of H_2O_2

Among the different ROS, H_2O_2 seems to be the most promising species in mediating physiological relevant signaling activities. It was shown that it gets produced upon several growth-related stimuli including platelet-derived growth factor (PDGF)[25] and EGF stimulation[26], which activate NOX proteins via Ras and PI3K. However, it is still not fully understood how H_2O_2 concentrations can exceed normal intracellular levels needed for oxidative protein modifications, while the cell is packed with antioxidant enzymes.

Two mechanisms have been discovered, which are initiated by GF stimulation. In contrast to other ROS, H_2O_2 detoxification occurs mainly through the highly abundant PRXs, whereat the human PRX2 shows a reaction rate of ~10^7 $M^{-1}s^{-1}$ with H_2O_2[27,28] compared to a rate constant of ~20 $M^{-1}s^{-1}$ for other thiols[29]. Thus, spatially confined inactivation of PRXs would serve as effective strategy for compartmentalized H_2O_2 accumulation. Indeed, it was shown that the membrane-associated PRX1 gets phosphorylated in a Src-dependent manner upon PDGF and EGF stimulation resulting in its local inactivation[30]. This enables H_2O_2 concentrations above the threshold required to selectively oxidize target molecules near the PM. Another strategy, which allows spatially restricted accumulation of H_2O_2, was found in context with PRX2. In contrast to other proteins, PRX2 is easily hyperoxidized leading to the inhibition of this enzyme and providing a 'floodgate' permitting H_2O_2 mediated signaling activities (Figure 1.2)[2,31]. So one of the first targets of H_2O_2 are its own inhibitors, allowing a fast and confined accumulation of H_2O_2 at the PM.

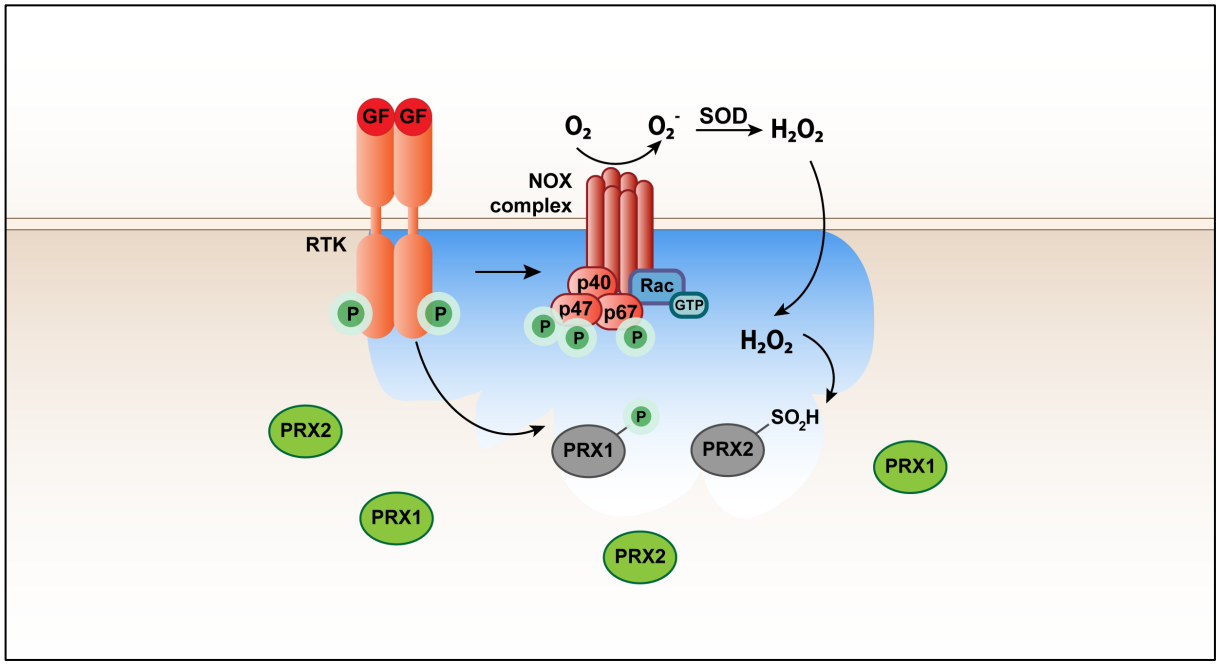

Figure 1.2: Accumulation of H_2O_2 at the PM upon GF stimulation
RTK activation by GF leads to superoxide (O_2^-) production with subsequent dismutation to H_2O_2 by SOD. H_2O_2 can pass the cellular membrane by diffusion or via aquaporins. RTK activation leads in turn to PRDX1 phosphorylation and inactivation, decreasing the redox-buffering capacity near the PM. An increase in H_2O_2 concentrations can inactivate PRDX2 by overoxidation. These regulatory mechanisms promote the confined accumulation of H_2O_2 near the PM. (adapted from[2])

Another paradigm for local H_2O_2 signaling is given by the fact that NOX enzymes, when expressed at the PM, produce O_2^- and subsequently H_2O_2 in the extracellular space and not directly in the cytoplasm. This seems ineffective when intracellular target molecules should be reached. H_2O_2 is thought to freely cross membranes by diffusion thereby having the ability to reach back to the producing cell in an autocrine loop. In addition, it was found that specialized aquaporins facilitate the uptake of H_2O_2 into cells providing another layer of controlled accumulation close to the PM[32,33].

Compartmentalized production of H_2O_2 is also thought to occur through the formation of redox-active endosomes, so-called 'redoxosomes'[34]. Similarly to ROS signaling, endosome signaling is a fairly new concept since endocytosis of proteins was long thought to be solely a mechanism facilitating the shut down of signaling activities. However, the mobility of endosomes can offer new spatial platforms for signaling events, recruitment of specific proteins can transduce an incoming signal to new targets and their unique geometry can influence protein activities[35,36]. When NOX proteins are expressed in endosomes, H_2O_2 gets no longer produced outside of the cell but rather inside of those specialized vesicles creating high local concentrations needed for oxidative protein modifications. In summary, compartmentalization of ROS is a prerequisite for its signaling activity and in addition one of

the main determinants ensuring signaling specificity. Restraining the action radius of an oxidant to the localization of its target molecule can thereby generate local activity patterns of proteins.

1.1.3 Protein oxidative modifications

1.1.3.1 Oxidation of protein thiols

As already discussed above, one of the first H_2O_2 targets are the highly reactive antioxidants PRX1 and PRX2 ensuring localized accumulation of high H_2O_2 concentrations needed to oxidize less reactive target molecules[27]. In general, H_2O_2 shows high reactivity with cysteine (Cys) residues, oxidizing the thiol (-SH) side chain of this amino acid to sulfenic acid (-SOH). However, not every cysteine shows the same susceptibility towards oxidation. The pKa value of the target cysteine needs to be lower than the physiological pH value (pH 7.4), which changes the thiol group to a redox reactive thiolate anion ($-S^-$)[37]. The pKa value of a given cysteine residue can be lowered by many factors including hydrogen bonding, an adjacent basic amino acid residue, the microenvironment of the target cysteine residue or substrate binding[37].

The oxidation of cysteine residues starts with the formation of sulfenic acid. Depending on the target molecule, formation of further oxidation products is possible including disulfide formation (S-S), S-glutathionylation (R-SSG) or S-nitrosylation (-SNO)[38]. These secondary redox modifications are necessary to prevent further oxidation to irreversible states such as sulfinic ($-SO_2H$) or sulfonic acid ($-SO_3H$), which would cause protein degradation and are linked rather to oxidative stress than oxidative signaling (Figure 1.3).

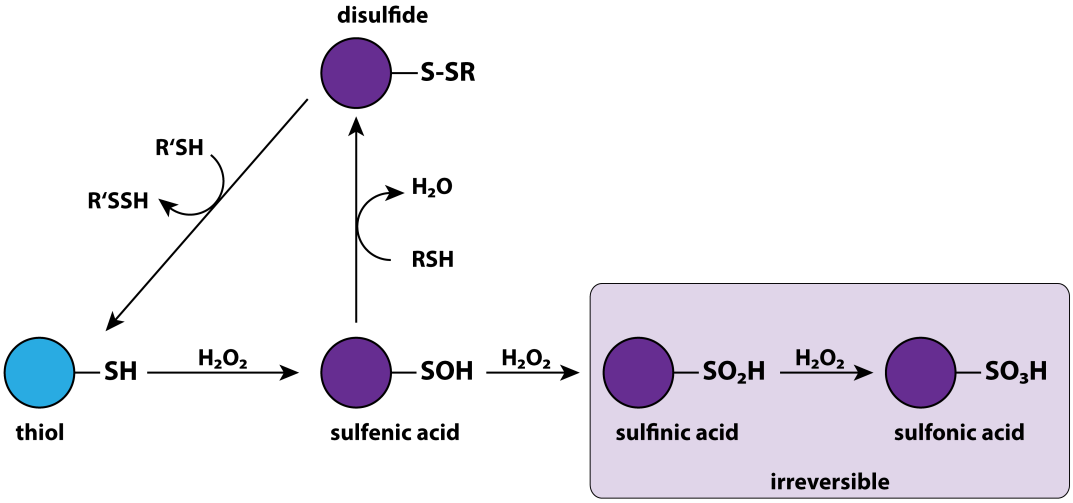

Figure 1.3: Oxidative modifications of protein cysteines
Cysteines with a low pKa thiol are susceptible to H_2O_2-mediated oxidation resulting in the formation of –SOH (sulfenic acid), also known as sulfenylation. This modification is either stabilized by the protein microenvironment or it reacts with a second thiol to form an intra- or intermolecular disulfide. When H_2O_2 concentrations reach a critical level, sulfenic acid can undergo further oxidation to irreversible states like sulfinic or sulfonic acid.

The formation of sulfenic acid seems to be a simple chemical modification but it can have dramatic effects on protein functionality. The inhibition of several phosphatases upon oxidation is widely accepted and will be discussed in more detail in the next chapter (1.1.3.2). In addition to the catalytic inactivation, oxidation of proteins can also lead to an enhancement of their catalytic activity as shown for the monophosphate-activated protein kinase (AMPK). S-glutathionylation of the AMPKα subunit caused by an increase of intracellular H_2O_2 levels leads to the activation of AMPK in an ATP-independent manner[39]. Recently, it was also shown that direct sulfenylation of a critical cysteine (Cys797) in the catalytic domain of EGFR increases its kinase activity[40], illustrating the diverse functions of redox protein modifications in cellular signaling.

1.1.3.2 Phosphatase oxidation

The protein tyrosine phosphatase (PTP) superfamily comprises 38 'classical PTPs', which are broadly classified in non-receptor and receptor PTPs, and is specialized in dephosphorylating tyrosine residues. In addition, 61 dual-specificity phosphatases (DUSPs) are known, which are characterized by the ability to dephosphorylate protein-phosphoserine/threonine residues and phosphotyrosine residues[41]. The lipid phosphatase PTEN (Phosphatase and Tensin homolog), which dephosphorylates phosphatidylinositol (3,4,5)-triphosphate (PIP3), is structurally related to PTPs[42]. Classical PTPs, DUSPs and PTEN share a cysteine-based mechanism characterized by a conserved $HC(X_5)R$ motif to catalyze dephosphorylation, defining them as cysteine-based phosphatases (CBPs)[43]. This PTP signature motif creates a unique environment for the catalytic cysteine residue. The presence of a conserved arginine residue confers an unusually low pKa (4.5 and 5.5) ensuring that the catalytic cysteine exists as a thiolate anion ($Cys\text{-}S^-$) at physiological pH, enabling the nucleophilic attack on phosphorylated substrates[44]. But this feature also renders the cysteine residue highly susceptible to oxidation, in contrast to protonated cysteine thiols (Cys-SH), which usually exhibit a pKa value of around 8.3[45]. Thus, H_2O_2 shows a reaction rate of 20 $M^{-1}s^{-1}$ for PTP1B, whereas it reacts very slowly with glutathione and free cysteine residues (2–20 $M^{-1}s^{-1}$)[46]. In addition, oxidant bursts are often associated with an in increase in protein

phosphorylation, consistent with the acceptance that PTPs are one of the main targets of ROS signaling[47]. However, the members of the PTP family differ in their intrinsic susceptibility to oxidation, and different types of oxidative modifications of the PTP catalytic cysteine can occur[42].

One of the first PTPs that has been shown to undergo reversible redox modifications was PTP1B. Cells that were treated with Insulin or EGF produced H_2O_2, which led to the reversible inhibition of PTP1B[48,49]. The structurally related PTPN2 (TCPTP) is also an important regulator of the insulin signaling pathway and, as PTP1B, undergoes reversible oxidation upon insulin stimulation[50,51]. Later, crystallographic analysis of PTP1B showed that after the formation of sulfenic acid, oxygen gets rapidly eliminated to produce an intramolecular cyclic sulfonamide, which protects the protein against overoxidation[52]. Reactivation of oxidized PTP1B was shown to occur mainly through the thioredoxin system, underlining the concept of the reversibility of PTP oxidation[53]. A similar mechanism exists for the phosphatases PTEN and CDC25c. Both enzymes contain a second cysteine in addition to the catalytic cysteine within their active site. Upon oxidation of the nucleophilic cysteine, a disulfide bond is formed with the vicinal cysteine residue, which serves as protection from a further irreversible oxidation[54,55]. The receptor PTP (RPTP) α is also susceptible to oxidation, forming intermolecular dimers with neighboring molecules resulting in the inhibition of the protein[56]. Interestingly, the second domain D2, which is not catalytically active, is much more prone to be oxidized and responsible for the dimer formation than the catalytically active domain D1. In addition it was shown that the recruitable SH2 domain containing PTP, SHP2, is oxidized in cells upon treatment with PDGF and EGF depending on a complex formation with the respective receptor[40,45].

In conclusion, it is now known that several PTPs are inhibited by H_2O_2-mediated oxidation and that different mechanisms have evolved to prevent further irreversible redox modifications. By promoting PTP inactivation, oxidation can be considered as an amplifier of protein phosphorylation. Novel tools for monitoring protein oxidation are giving a more detailed picture about physiological relevant redox modifications. However, the field is still vague and systemic approaches are needed to unravel the actual impact of PTP oxidation in cell signaling.

1.1.4 Detection of protein oxidation

The implication of protein oxidation in physiological and pathophysiological cell signaling made the development of strategies to detect oxidative modifications essential. But so far, available methods for monitoring protein oxidation are not as sophisticated as for other posttranslational modifications such as protein phosphorylation due to the labile nature of sulfenic acid. Nonetheless, various strategies were developed to unravel protein oxidation *in vitro* and *in vivo*.

The analysis of protein oxidation by spectroscopic methods gave great insights into sulfenic acid formation and the resulting structural changes of oxidized proteins but is limited to *in vitro* analysis of purified or recombinant proteins. A complicated strategy is the indirect detection of sulfenic acid by protection of free thiols using alkylating agents and subsequent conversion of sulfenic acid to a thiol or sulfonic acid[57]. The main drawbacks include that protein samples undergo extensive processing under denaturing conditions, false positive signals from incomplete thiol blocking and several steps of chemical manipulation of cell lysates[58]. The most promising approaches are based on the reaction of sulfenic acid with a chemical probe. This strategy is based on both the electrophilic and weak nucleophilic character of the sulphur atom making nucleophiles, electrophiles and reducing agents suitable for the detection[58]. One of the most used probes for sulfenic acid detection is the nucleophile 5,5-dimethyl-1,3-cyclohexanedione (dimedone), which reacts in a chemoselective reaction with the oxidized sulfur atom (Figure 1.4 A)[59]. However, the resulting dimedone-derivatized product is not distinguishable from unmodified proteins, e.g. by SDS-PAGE gel analysis. Therefore, radiolabeling or mass spectrometry analysis was needed to monitor adduct formation. Recently, dimedone-analogues with fluorescent- or biotin-tags were developed to facilitate an easy biochemical detection[60]. But analysis of fluorescein (DCP-FL) and rhodamine (DCP-Rho) linked dimedone derivatives indicated a partially quenched emission upon –SOH binding, which can falsify results. Furthermore, bulky detection tags limit cell permeability and can lead to a significant bias in protein target labeling. Hence, these probes are rather suitable for detection of sulfenic acid in recombinant proteins or cell lysates but not for detection in live cells. Due to the labile and transient nature of sulfenic acid modifications, in situ labeling is the preferable strategy to detect endogenous protein oxidative modifications[61]. By reducing the size of the chemical tag of dimedone to a minimum, Carroll and colleagues developed the probe DYn-2[40]. DYn-2 is a small alkyne-functionalized probe that can be coupled to any azide-functionalized reporter through a cupper-catalyzed reaction

known as 'click chemistry' (Figure 1.4 B). The same study showed that in situ incubation of DYn-2 is suitable for monitoring changes in protein sulfenylation upon EGF stimulation including oxidation of PTP1B, SHP2, PTEN and EGFR[40]. Another strategy for detecting dimedone-derivatized proteins without changing the chemical features of dimedone itself, is the use of an antibody raised against a synthetic hapten mimicking dimedone-modified cysteines[62]. However, immunochemical methods in general have the disadvantage of a varying affinity of the primary antibody to the epitope and high background staining due to the secondary antibody making a precise quantification difficult.

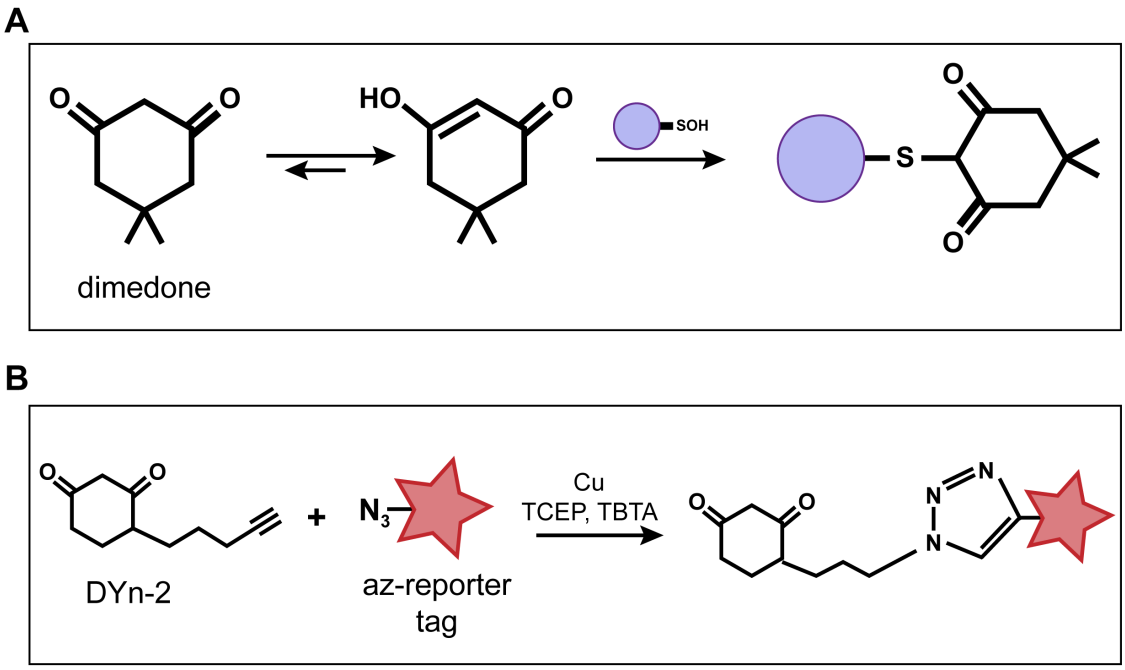

Figure 1.4: Probes for detection of protein cysteine oxidation
(A) Chemoselective reaction between an oxidized protein (-SOH) and dimedone results in the covalent binding of dimedone to the sulfur atom. (B) DYn-2, an alkyne-modified homologue of dimedone can be coupled to an azide-modified reporter tag (e.g. biotin or fluorescent tag) via the cupper-catalyzed click chemistry reaction. This approach enables downstream detection via fluorescence or enrichment for proteomic analysis.

1.2 RTK-PTP reaction network

Nearly 30 years ago, Tony Hunter and colleagues uncovered the existence of protein tyrosine kinases (PTKs), which led to the expansion of the new field of tyrosine phosphorylation and the associated signaling pathways[63]. PTKs play a central role in nearly every biological process including the regulation of development, cell motility, proliferation, differentiation, glucose metabolism, and apoptosis[64]. This work focuses on receptor tyrosine kinases (RTKs), a family of receptors with intrinsic kinase activity mediating the signal

transduction from extracellular ligands to specific cellular responses. The RTK family comprises more than 50 cell-surface receptors structurally characterized by three major domains: an extracellular domain for ligand binding, a membrane-spanning segment, and a cytoplasmic domain, which possesses tyrosine kinase activity and contains phosphorylation sites[64]. Phosphorylated tyrosine residues serve as docking sites for effector proteins, which recognize the active receptor via phosphotyrosine-binding (PTB) domains or Src-homolgy 2 (SH2) domains[65]. RTK activity gets counterbalanced by PTPs, which catalyze the dephosphorylation of tyrosine residues and therefore initiating the shut down of signal transduction.

1.2.1 EGFR activation and signaling

The first growth factor discovered was the epidermal growth factor (EGF) activating its cognate receptor, the epidermal growth factor receptor (EGFR)[66,67]. EGFR belongs to the EGFR/ErbB family of RTKs including 4 family members; EGFR (ErbB1), ErbB2, ErbB3 and ErbB4. Abnormal activation of ErbB family members is found in many cancers, in fact making EGFR the first receptor identified as an oncogene[67,68]. In general, ligand binding induces EGFR dimerization, stabilizes the active form of the receptor and promotes the autophosphorylation of tyrosine residues. In addition to ligand-binding, it was shown that enhanced expression of the receptor can trigger the formation of ligand-free dimers, resulting in autonomous receptor activation found in several cancer types[69].

EGFR consists of an extracellular module (separated in domains I, II, III and IV), connected by a single-helix transmembrane segment and a juxtamembrane segment to an intracellular kinase domain followed by a long regulatory C-terminal tail[70]. The extracellular domain exists either in a closed 'tethered' form shielding the sites important for dimer formation or an 'open' conformation, which is primed for dimerization (Figure 1.5)[71]. Both conformations exist in the absence of ligand with a preference for the closed, autoinhibited conformation. Upon ligand binding, the extracellular domains of two receptors dimerize 'back-to-back', which propagates to an enzymatically active kinase domain[72]. The extracellular dimer interface is solely receptor-mediated with the ligand bound on the outside (Figure 1.5)[70,73].

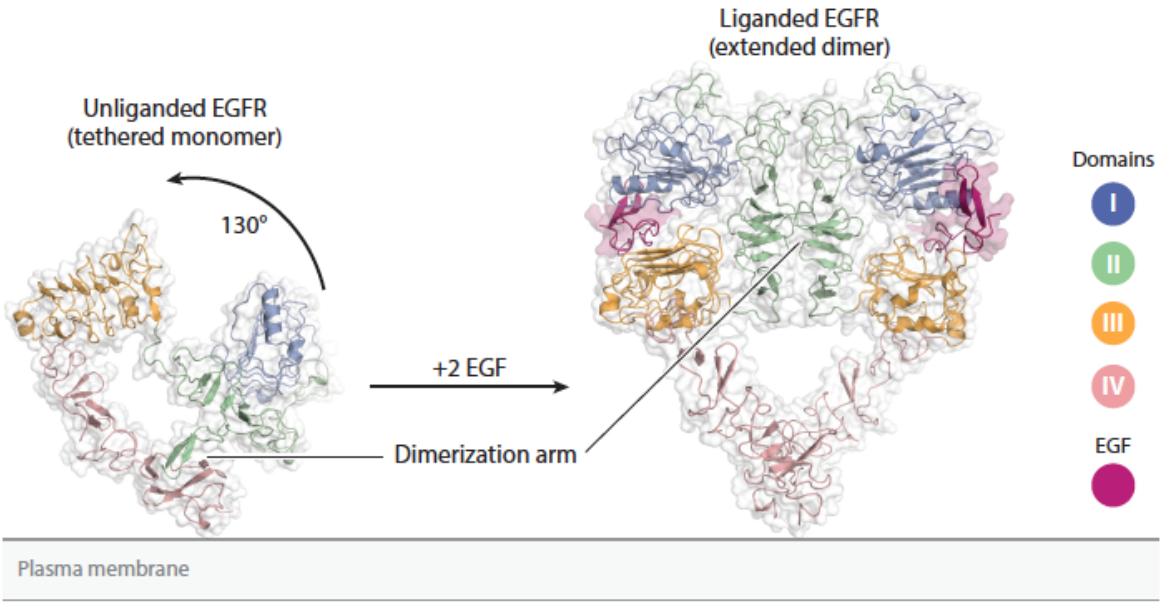

Figure 1.5: Structure of the extracellular module of EGFR
Structural model of the ligand-induced, conformational change of the extracellular domain of EGFR. Domain I and III are important for ligand binding whereas domain II and IV form the dimer interface. (adapted from[69])

In contrast to other kinases, it is still unclear, which impact the phosphorylation of the activation loop in EGFR has in adopting an active kinase conformation[74]. So far, it was shown that upon activation two EGFR kinase domains interact in an asymmetric fashion, where one (activator) switches on the other (receiver) in an allosteric mechanism (Figure 1.6)[72]. Phosphorylation of Y845, the critical tyrosine within the kinase domain, is not necessary to adopt this conformation but enhances the catalytic activity of the receptor and is proposed to suppress the intrinsic disorder of the kinase domain[75]. EGF-binding favors N-terminal dimerization of the transmembrane domains translating in a further dimerization of the juxtamembrane segments, and formation of the asymmetric kinase dimer. In contrast, C-terminal dimerization of the transmembrane helices was found in ligand-free dimers leading to a dissociation of the juxtamembrane segments resulting in the formation of a symmetric, inactive kinase dimer[70,73]. Upon EGF stimulation, EGFR can also form higher-order multimers initiated by domain IV of the extracellular module[76,77]. The same study also showed that multimerization is necessary for full autophosphorylation *in trans*. When EGFR only exists in dimers, tyrosine residues that are proximal to the kinase domain are phosphorylated just in one subunit[76].

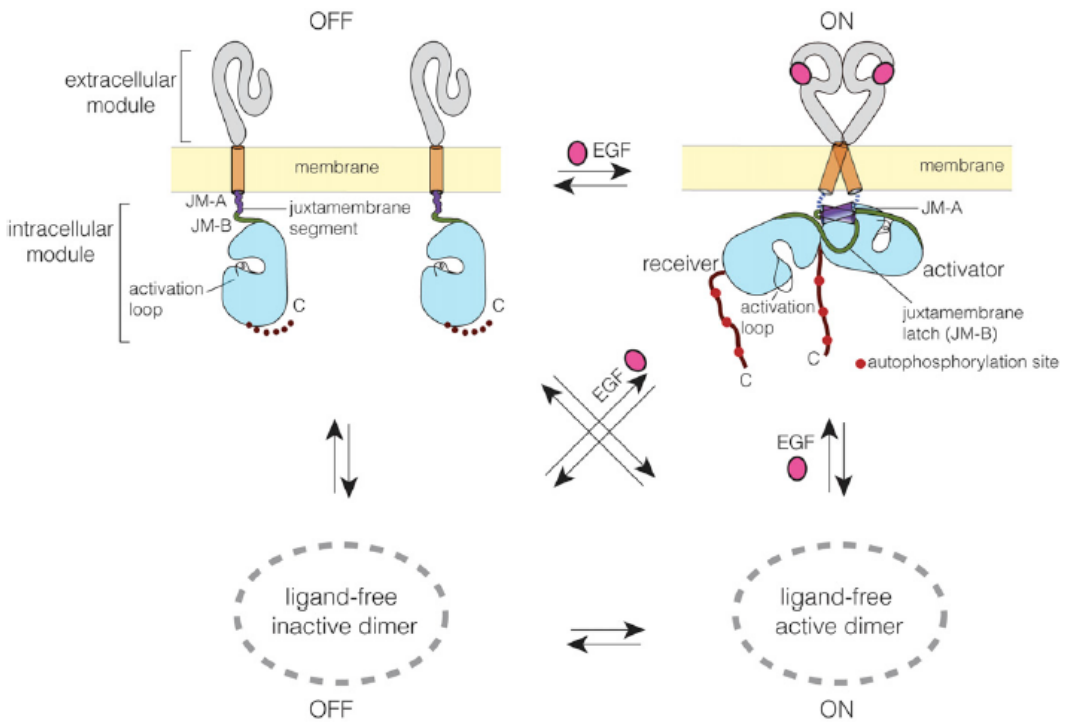

Figure 1.6: Model for monomer-dimer equilibrium of EGFR
Scheme shows the transition of inactive monomers to an active, asymmetric dimer. In addition, other states are possible like ligand-free active dimers at high expression level or ligand-free inactive dimers depending on the structural conformation. (adapted from[73])

Once activated, the first substrate for EGFR phosphorylation is the receptor itself. Several tyrosine residues are getting phosphorylated including the autophosphorylation sites Y992, 1045, 1068, 1086 and 1173. Y992, 1068, 1086 and 1173 are generally linked to an activation of the Ras/MAPK and PI3K/AKT signaling pathways, while Y1045 serves as docking site for the E3 ubiquitinase Cbl resulting in receptor ubiquitination and degradation[78]. The tyrosine residue 845 however has a special role when it comes to EGFR activation. Considered as transphosphorylation site activated by Src[79], structural studies suggest a role in stabilizing EGFR dimers, thereby promoting catalytic activation even in the absence of ligand[75]. Thus, Y845 gets described as 'autocatalytic' site of EGFR.

Autocatalytic activation of EGFR enables fast and robust activation upon stimulation but comes with the prize of spontaneous receptor activation and the chance for spurious signaling. The autoinhibition facilitated by structural features of EGFR discussed above represents one strategy to prevent receptor activation in the absence of ligand. In addition to this intrinsic safeguard mechanism, it was shown that continuous recycling of spontaneous activated RTK molecules to the perinuclear area, which is characterized by high PTP activity, keeps basal receptor activation low[80,81]. Therefore, it is important to consider EGFR signaling as the sum of autocatalytic receptor activation and the recursive interaction with PTPs.

1.2.2 Coupling between RTK and PTP activity by ROS

The traditional view of EGFR signaling comprises linear signaling pathways resulting in the transcription of a specific set of genes leading to a distinct cellular response such as proliferation or survival. However, several key studies have shown that the signaling pathways downstream of every RTK are highly interconnected representing a complicated signaling network with the receptor as conserved processing core[82,83]. Therefore, EGFR signaling should be understand as an integrated system, in which specificity is determined by the spatial-temporal dynamics of activation of signaling proteins[84]. For instance, feedforward and feedback loops embracing interacting EGFR pathways make the input–output response of one pathway dependent on the activity of the other pathway, thereby creating a context-dependent signaling output[84,85]. The interaction of EGFR with PTPs plays in this context an important role. By dephosphorylating the receptor itself or different downstream molecules, PTP activity is one of the major determinants in shaping the dynamic behaviour of RTK signaling, converting a transient or sustained growth factor activation into distinct responses, such as all or none, oscillatory, and pulsatory responses[84].

RTK and PTP activity show at any time a tight interplay. For instance, it was shown that inhibition of PTP activity leads to autonomous EGFR activation indicating that even at basal level, receptor phosphorylation is the result of a continuous cycle of phosphorylation and dephosphorylation[86-88]. When stimulated with EGF, receptor phosphorylation displays hysteresis, meaning that the stimulus needs to exceed a threshold value to flip the system from a low to high activity state, which may even remain when the stimulus returns to its initial value[84]. This is in general the property of a bistable system, which is created here by the coupling of RTK activity to PTP inhibition through the production of H_2O_2[26,86]. In general, a bistable system can switch between two distinct stable states, but cannot rest in intermediate states[89]. In the time course of ligand stimulation, EGFR gets dephosphorylated when internalized showing that intracellular PTP activity has to overcome RTK activity. This is ensured through a spatial partitioning of RTK and PTP activity with PTP activity peaking around the perinuclear area generating a robust EGFR activation at the PM and shut down of the signal upon internalization[90].

EGFR activation leads to H_2O_2 production by activating NOX complexes at the PM. The phosphorylated receptor recruits the adapter protein Grb2[91], which leads to activation of the Ras/MAPK pathway. Active Ras in turn activates the guanine nucleotide exchange factor (GEF) Tiam1 important for the conversion of GDP-bound Rac1 into the active GTP-bound

form, a subunit of NOX1, NOX2 and NOX3[92]. Rac activation can also be catalyzed by other GEFs including Son of sevenless (SOS), Vav or Pix depending on the activated RTK and NOX isoform. For EGFR it was shown that βPIX activation by PI3K is important for Rac activation and NOX1 mediated H_2O_2 production[93]. In addition, active PI3K catalyzes the phosphorylation of phosphatidylinositol (4,5)-biphosphate (PIP2) to phosphatidylinositol (3,4,5)-triphosphate (PIP3). The NOX subunit p47phox binds to PIP3 via its PH domain after the release of an autoinhibitory structural conformation. It was shown that serine/threonine phosphorylation catalyzed by AKT and PKC are crucial for p47phox recruitment to the membrane and full assembly of the NOX complex[16]. As a consequence, H_2O_2 can accumulate near the PM inactivating PTPs and thereby promoting full EGFR activation. Hence, autocatalytic activation of EGFR and inhibition of PTPs upon EGF binding leads to a shift in the kinase-phosphatase balance in favour of the kinase allowing signal transduction[94].

Depending on the network architecture either lateral propagation of a stimulus or distinct pattering can be generated, illustrating the extremely rich repertoire of different dynamic behaviours of EGFR signaling (Figure 1.7). The emergence of large-scale patterns from random local fluctuations was already proposed by Turing in 1952[95]. Recently, it was shown that a similar mechanism is used to keep the mean amount of phosphorylated EGFR per endosome constant, even forming distinct activity clusters[96]. The authors proposed that the phosphatase SHP2 gets recruited to active EGFR on endosomes where EGFR activates SHP2 by phosphorylation promoting its own dephosphorylation in a negative feedback loop. This strategy could be one aspect of the analogue-to-digital conversion of RTK signaling, necessary to elicit distinct cellular responses out of continuous variables like extracellular growth factor concentrations. In addition, it illustrates how the causality of the RTK-PTP network shapes RTK response properties enabling the formation of different activity patterns.

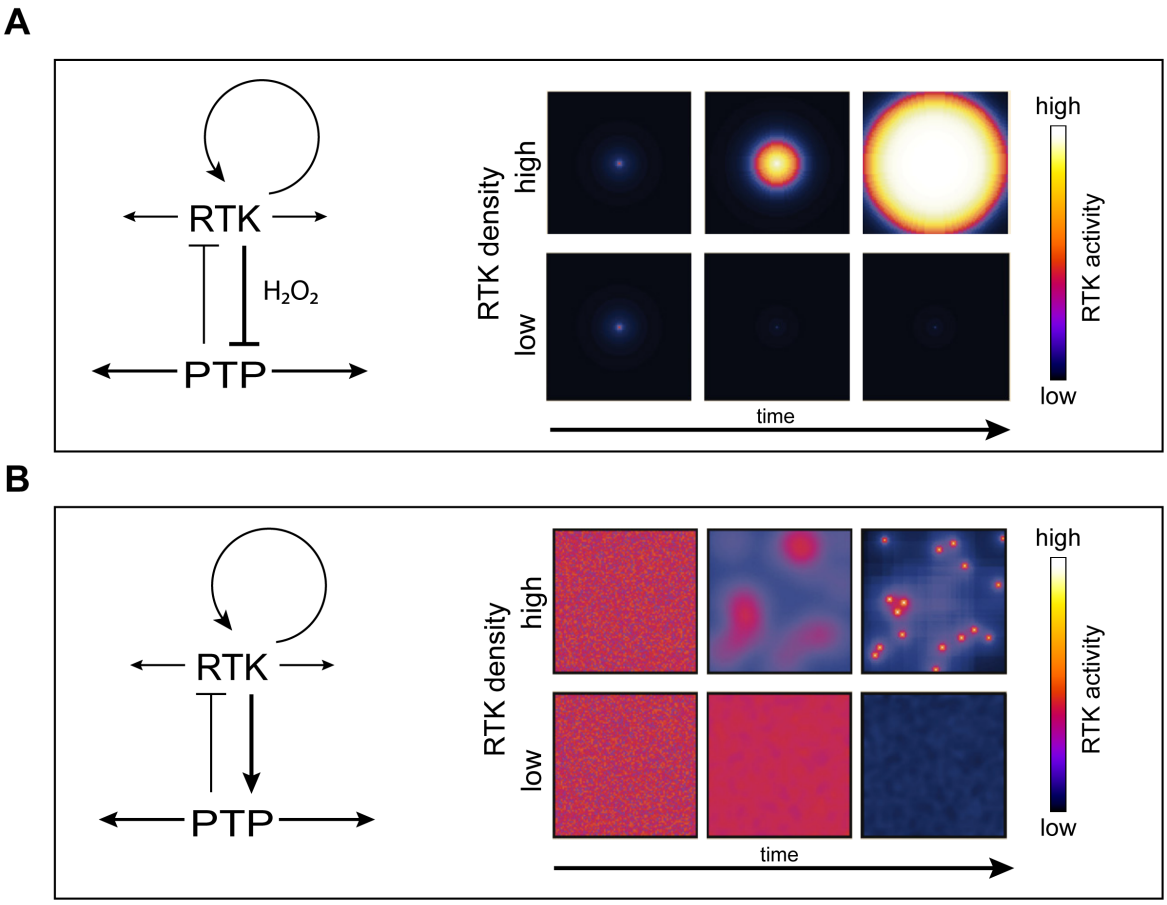

Figure 1.7: RTK-PTP network topologies determine RTK activity pattern
(A) Double negative feedback as generated by RTK-mediated H_2O_2 production leads to a bistable system. RTK density on the membrane determines spreading of RTK activity either leading to lateral signal propagation (upper case) or signal termination (lower case) after local point activation. **(B)** A Turing system as generated by a RTK that activates its own inhibitory PTP leads to RTK activity spots at high receptor density (upper case) after global stimulation. (adapted from[94])

1.3 ROS and cancer

Elevated ROS level are a common phenomenon in cancer and other pathologies. Two decades ago it was found that cancer cells generate higher levels of ROS than their non-transformed counterparts, raising the question if redox signaling has an impact in disease initiation and progression[97].

Indeed, several reports support the theory that ROS production and signaling promote transformation of malignant cells. For instance, it was shown that human cancer cells driven by oncogenic KRas require mitochondrial ROS for proliferation[98]. In addition, NOX1 itself is capable of transforming NIH3T3 cells, and when injected into nude mice these cells produce particularly aggressive tumors[9]. On the other hand, YA cell line transformation was reserved

by co-transfection with catalase, providing strong evidence for a role of H_2O_2 in cellular transformation and growth[99].

The tight coupling between ROS and cancer is also reinforced by the observation that many common oncogenes such as Ras can directly alter the redox state of a cell[100]. At the same time, it was shown that cells with increased ROS levels are dependent on a more potent antioxidant system to prevent senescence (Figure 1.8)[101]. Signaling motifs that are responsive to H_2O_2 are localized close to the sources of ROS generation, allowing activation of those despite the high overall antioxidant activity in cancer cells that protects against oxidative-stress-induced cell death[102]. A classical example of this strategy is the oxidation of the phosphatase PTEN at the PM, activating the pro-survival pathway via PI3K and AKT[54]. In turn, it was shown that PRDX1, a ROS scavenger, expression reactivates oxidized PTEN restoring its tumor suppressive function[103]. As already discussed earlier, the crosstalk between RTK activation and ROS signaling leads to the reversible inhibition of PTPs. Increased H_2O_2 levels in cancer cells can therefore lead to an enhanced inhibition of PTPs thereby promoting kinase-dependent signaling driving cancer formation[104].

The impact of ROS in malignant signaling makes it also an interesting target for the development of new anti-cancer treatments. In general, two strategies can be distinguished; either the application of drugs decreasing intracellular ROS levels or treatments, which lead to the further increase of ROS until the cellular antioxidant system is saturated provoking cell death. The former option seemed promising as inhibition of tumorigenesis was shown upon treatment with antioxidants such as n-acetylcysteine (NAC) and vitamin C[105]. But several large-scale, clinical studies have shown that dietary antioxidant supplementation with β-carotene, vitamin A or vitamin E rather increased cancer progression than preventing it[106,107]. These conflicting results illustrate the fragile nature of redox homeostasis and that perturbations of this system have in most cases an unpredictable outcome. The opposite approach of increasing ROS levels till cancer cells can no longer cope with them implies that cancer cells are more vulnerable to oxidative stress-induced cell death. Indeed, treatment of cultured human colorectal cancer (CRC) cells harbouring KRas or BRaf mutations with high levels of vitamin C leads to the depletion of the antioxidant glutathione (GSH). Thus, ROS accumulates leading to the inactivation of GAPDH resulting in an energetic crisis and cell death[108]. Moreover, administration of the small molecule piperlongumine has been shown to decrease the abundance of reduced GSH leading to a selective killing of cancer cells[109]. Several similar approaches were successful in inhibiting cancer cell growth making a combination of

ROS-producing agents with ROS-scavengers beneficial for clinical cancer therapy[110]. A better understanding of the molecular mechanisms of ROS signaling in cancer cells could help to identify pathways that are indispensable for cancer cell survival. Targeting these mechanism could help to reduce cancer cell adaptation and resistance to common chemotherapeutics[83].

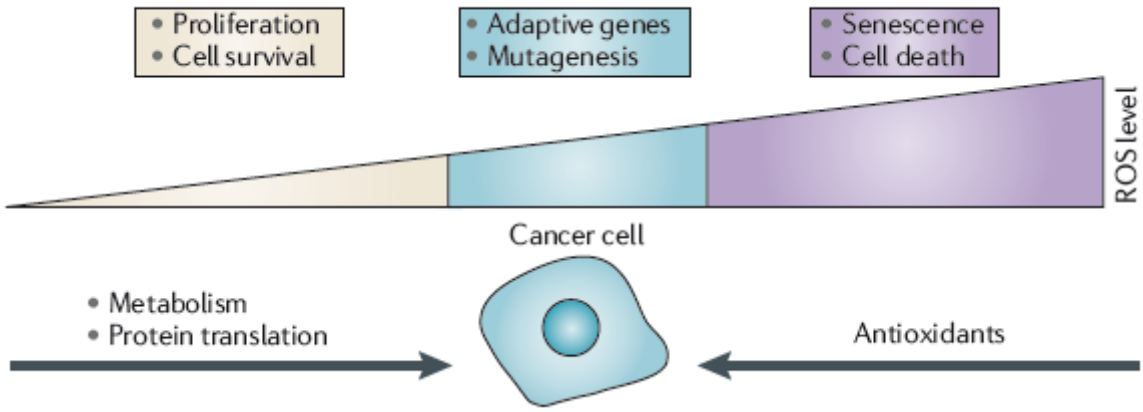

Figure 1.8: Interdependence between ROS levels and cancer
Moderate levels of ROS (yellow) can promote cell proliferation or survival pathways, whereas abnormally high concentrations result in oxidative stress causing senescence or cell death (purple). Adaptive mechanisms in cancer cells can counter oxidative stress enabling cell survival (blue). However, these adaptions make cancer cells more prone to apoptosis caused by a further increase in ROS levels. (adapted from[111])

2 Objective

The delicate balance between protein phosphorylation and dephosphorylation is a major determinant in regulating protein activity in signaling networks. Imbalances in these processes are frequently linked to malignant transformation and tumor development. In general, PTPs catalyze the dephosphorylation of signaling proteins, mostly important for shutting down signaling activity initiated by tyrosine kinases such as RTKs. The interplay between PTPs and RTKs is shaping the spatial-temporal distribution of phosphorylated proteins in cells, thereby determining cell fate.

In the last years, inactivation of PTPs by H_2O_2 has gained more interest and opened up a new field of discussion about the link between RTK activity and PTP inhibition. This coupling between RTK activation and PTP inhibition is ensured by activation of NADPH oxidases downstream of active RTKs, such as EGFR. The production of H_2O_2 and the resulting inhibition of PTPs together with the autocatalytic activity of EGFR generates a bistable system[86,112]. Thereby, receptors retain low activity in unstimulated cells and show a robust response to a certain threshold concentration of ligand.

In this work, we want to investigate if the malignant transformation of cells by HRas G12V increases intracellular H_2O_2 levels as often observed in human tumors. Furthermore, we want to investigate if oncogene-induced H_2O_2 is affecting the EGFR-PTP network by inhibiting the overall PTP activity and thus lowering the EGFR activation threshold. Therefore, we want to monitor the H_2O_2 production in transformed and non-transformed cells and how it can affect EGFR phosphorylation dynamics at basal level and upon ligand stimulation. Furthermore, it is still difficult to detect protein oxidation in living cells. By implementing a new approach, we want to reveal PTP oxidation with spatial-temporal resolution in the context of malignant transformation induced by HRas G12V. In summary, this should give new insights into the RTK-PTP reaction network, their coupling through H_2O_2 and how this network is affected upon oncogenic transformation of cells.

3 MATERIALS AND METHODS

3.1 Materials

3.1.1 Chemicals

2-Mercapto-ethanol	SERVA Electrophoresis GmbH
Acetic acid	Sigma-Aldrich
Ammonium persulfate (APS)	SERVA Electrophoresis GmbH
Ampicillin sodium salt	SERVA Electrophoresis GmbH
Bromophenolblue	Sigma-Aldrich
Catalase	Sigma-Aldrich
Copper(II) Sulfate ($CuSO_4$)	Sigma-Aldrich
DCP-Bio1	Kerafast, Inc.
DCP-Rho1	Kerafast, Inc.
Dimedone	Sigma-Aldrich
Dimethyl sulfoxide (DMSO)	SERVA Electrophoresis GmbH
Dithiothreitol (DTT)	Fluka Analytical
DYn-2	Cayman Chemical
Ethanol	J.T.Baker
Ethylenediaminetetracetic acid (EDTA)	Fluka® Analytical
Glycerol	GERBU Biotechnik GmbH
Hoechst 33342	Thermo Fisher Scientific
Isopropanol	J.T.Baker
Kanamycin sulfate	GERBU Biotechnik GmbH
Magnesium chloride ($MgCl_2$)	Merck KG/J.T.Baker
Methanol	AppliChem GmbH
Monopotassium phosphate (KH_2PO_4)	J.T.Baker
N-Ethylmaleimide (NEM)	Sigma-Aldrich
N,N,N',N'-Tetramethylene-diamine (TEMED)	Sigma-Aldrich
Sodium chloride (NaCl)	Fluka Analytical
Sodium dodecyl sulfate (SDS)	SERVA Electrophoresis GmbH
Tris-base	Carl Roth GmbH
Tris-HCl	J.T.Baker
Tris(2-carboxyethyl)phosphin (TCEP)	Sigma-Aldrich
Tris(benzyltriazolylmethyl)amine (TBTA)	Carl Roth GmbH
Tritox X-100	SERVA Electrophoresis GmbH

Tween 20	SERVA Electrophoresis GmbH
UltraPure™ Agarose	Thermo Fisher Scientific

3.1.2 Enzymes

AgeI-HF (10,000 U/ml)	New England Biolabs Inc.
Calf Intestinal Phosphatase (10,000 U/ml)	New England Biolabs Inc.
HindIII-HF (20,000 U/ml)	New England Biolabs Inc.
NheI-HF (20,000 U/ml)	New England Biolabs Inc.
T4-DNA ligase	Thermo Fisher Scientific
XhoI (20,000 U/ml)	New England Biolabs Inc.

3.1.3 Antibodies

Primary Antibodies	*Source*	*Supplier*
Actin	Mouse	Mab1522, Chemicon
Akt	Mouse	2920, Cell Signaling Technology
Akt (pThr308)	Rabbit	9271, Cell Signaling Technology
Cysteine sulfenic acid	Rabbit	07-2139, Millipore
EGFR	Goat	AF231, R&D Systems
EGFR	Rabbit	4267, Cell Signaling Technology
EGFR (pY1045)	Rabbit	2237, Cell Signaling Technology
EGFR (pY1068)	Rabbit	3777, Cell Signaling Technology
EGFR (pY845)	Mouse	558381, BD Bioscience
Erk	Mouse	ab36991, Abcam
Erk (pThr202/pThr204)	Rabbit	9101, Cell Signaling Technology
GAPDH	Mouse	Cb1001, Calbiochem
GAPDH	Rabbit	14C10, Cell Signaling Technology
GFP	Mouse	632681, Clontech
GFP	Rabbit	632593, Clontech
NOX2	Rabbit	ab31092, Abcam
NOX4	Rabbit	ab79971, Abcam
Phosphotyrosine (PY72)	Mouse	InVivo Biotech Services GMBH
PTP1B	Mouse	610139, BD Bioscience
α-tubulin	Mouse	T9026, Sigma-Aldrich

Secondary Antibodies	*Supplier*
Alexa Fluor 488 donkey anti-rabbit	Invitrogen™ Life Technologies
Alexa Fluor 546 goat anti-mouse	Invitrogen™ Life Technologies
Alexa Fluor 555 donkey anti-goat	Invitrogen™ Life Technologies
Alexa Fluor 647 chicken anti-rabbit	Invitrogen™ Life Technologies
Alexa Fluor 647 donkey anti-mouse	Invitrogen™ Life Technologies
IRdye 680 donkey anti-goat	LI-COR® Biosciences
IRdye 680 donkey anti-mouse	LI-COR® Biosciences
IRdye 680 donkey anti-rabbit	LI-COR® Biosciences
IRdye 800 donkey anti-goat	LI-COR® Biosciences
IRdye 800 donkey anti-mouse	LI-COR® Biosciences
IRdye 800 donkey anti-rabbit	LI-COR® Biosciences

3.1.4 Oligonucleotides

All oligonucleotides were purchased from MWG Eurofins as unmodified DNA Oligos.

HyPer-ER_LIC-F	GATAAAGTTTTAAAACAGGCGGTTCATGCACTGAGTTACTGG
HyPer-ER_LIC-R	GTTCAACAGCAACACAATGATGCAGTCGACGGTACCGC

3.1.5 Plasmids

cHyPer3	kind gift by Vsevolod V. Belousov (NBIC, Moscow, Russia)
EGFR-mCherry	ErbB1 with C-terminally fused mCherry (cloned by Jenny Ibach)
EGFR-mCitrine	ErbB1 with C-terminally fused mCitrine (cloned by Jenny Ibach)
HyPer3-ER	generated by fusing the ER coding sequence from PTP1B with cHyPer3
HyPer3-TK	generated by fusing the CAAX box from KRas with cHyPer3 (cloned by Lisaweta Roßmannek)
mCherry-N1	Clontech Laboratories Inc.
PTB-mCherry	PTB domain from Shc with C-terminal mCherry (cloned by Jenny Ibach)

3.1.6 Kits and Commercial Solutions

3.1.6.1 Molecular Biology

100x BSA	New England Biolabs Inc.
10x Restriction Enzyme Buffer 1-4	New England Biolabs Inc.
2-log DNA ladder	New England Biolabs Inc.
5x T4 DNA Ligation Buffer	Thermo Fisher Scientific
BigDye® Terminator v3.1 cycle sequencing kit	Applied Biosystems
DyeEx® 2.0 Spin kit	QIAGEN
NucleoBond® Xtra Maxi EF kit	Macherey-Nagel GmbH & Co. KG.
NucleoSEQ	Macherey-Nagel GmbH & Co. KG.
QIAprep® Spin Miniprep kit	QIAGEN
QIAquick® Gel Extraction kit	QIAGEN
RedSafe nucleic acid staining solution	iNtRON
Roti®-Histofix 4 %	Carl Roth GmbH
Roti®-Prep Plasmid MINI	Carl Roth GmbH

3.1.6.2 Cell Culture

Dulbecco's Modified Eagle's Medium (DMEM)	PAN™ Biotech
Dulbecco's Phosphate Buffered Saline (DPBS)	PAN™ Biotech
Fetal bovine serum (FBS)	PAN™ Biotech
FuGENE® HD Transfection Reagent	Promega
Hank's Buffered Salt Solution (HBSS)	PAN™ Biotech
L-Glutamine	PAN™ Biotech
Lipofectamine® Transfection Reagent	Thermo Fisher Scientific
Non-essential amino acids 100x	PAN™ Biotech
Trypsin/EDTA	Macherey-Nagel GmbH & Co. KG.

3.1.6.3 Biochemistry

30 % Acrylamide/Bis solution	Bio-Rad Laboratories, Inc.
30 % Hydrogen Peroxide (w/w) in H_2O	
Alexa Fluor® 594 Azide	Thermo Fisher Scientific
Amicon 30 kD cut-off Protein Desalting Spin Columns	Thermo Fisher Scientific
Bradford reagent	Sigma-Aldrich®
Chameleon Duo Pre-Stained Protein Ladder	Li-Cor® Biosciences GmbH
Complete Mini EDTA-free protease inhibitor tablets	Roche Applied Science
Fluorolink Cy3.5 Monofunctional Dye	GE Healthcare

Image-iT FX Signal Enhancer	Thermo Fisher Scientific
Novex NuPAGE LDS-Sample Buffer 4x	Thermo Fisher Scientific
NuPAGE® Antioxidant	Thermo Fisher Scientific
NuPAGE® LDS Sample Buffer (4X)	Thermo Fisher Scientific
NuPAGE® MES SDS Running Buffer (20X)	Thermo Fisher Scientific
NuPAGE® MOPS SDS Running Buffer (20X)	Thermo Fisher Scientific
Odyssey Infrared Imaging System blocking buffer	LI-COR Biosciences GmbH
PF6-AM	friendly provided by Chang lab, University of California, Berkeley, California
PG-Sepharose beads	Sigma-Aldrich®
Phos-Tag Biotin BTL-104	Wako Pure Chemicals Industries
Phosphatase Inhibitor Cocktail 2	Sigma-Aldrich®
Phosphatase Inhibitor Cocktail 3	Sigma-Aldrich®
Precision Plus ProteinTM Dual Color Prestained standards	Bio-Rad Laboratories, Inc.
Streptavidin	Sigma-Aldrich®
XT Reducing Agent 20x	Bio-Rad Laboratories, Inc.
XT Sample Buffer 4x	Bio-Rad Laboratories, Inc.
Zeba Spin Desalting Columns 40k MWCO	Thermo Fisher Scientific

3.1.7 Buffers and Solutions

3.1.7.1 Molecular Biology

1x TAE	40 mM Tris/Acetate (pH 7.5), 20 mM NaOAc, 1 mM EDTA
2-log DNA ladder	1 mg/ml 2-log DNA ladder (NEB) diluted in 1x DNA loading buffer (50 µg/ml)
DNA loading buffer	50% glycerol, 0.1% Orange G, 0.1 M EDTA
LB agar	15 g/l agar in LB medium (ZE Biotechnologie, MPI Dortmund)
LB medium	10 g/l Bacto-Trypton, 5 g/l yeast extract, 10 g/l NaCl, pH7.4
SOC medium	20 g/l Bacto-Trypton, 5 g/l Bacto yeast extract, 0.5 g/l NaCl, 2.5 mM KCl, 10 mM $MgCl_2$, 20 mM glucose (ZE Biotechnologie, MPI Dortmund)

3.1.7.2 Cell Culture

Complete Growth	DMEM + 10 % FBS, 1 % NEAA and 2 mM L-Glutamine in DMEM

Medium (CGM)	
Imaging medium	DMEM without Phenol red + 25 mM HEPES + 0.5 % FBS
Starvation Medium	DMEM + 0.5 % FBS, 1 % NEAA and 2 mM L-Glutamine in DMEM

3.1.7.3 Biochemistry

1x TBS	100 mM Tris-HCl, 150 mM NaCl
1x TBS (PhosTag)	10 mM Tris, 100 mM NaCl, pH adjusted to 7.5
1x TBS-T	100 mM Tris-HCl, 150 mM NaCl, 0.1 % Tween®-20
1x TBS/T (PhosTag)	1x TBS, 0.1 % Tween®-20
Dimedone lysis buffer	50 mM Tris (pH 8), 150 mM NaCl, 1 % IGEPAL, 0.1 mM PMSF, 20 mM NEM
Modified RIPA lysis buffer	50 mM triethanolamine hydrochloride (pH 7.4), 150 mM NaCl, 1 % IGEPAL, 1 % Na deoxycholate, 0.1 % SDS, 200 U/ml Catalase
RIPA lysis buffer	50 mM Tris (pH 7.5), 150 mM NaCl, 1 mM EGTA, 1 mM EDTA, 1% IGEPAL, 0.25% Na-deoxycholate, 2.5 mM Na pyrophosphate, 1 mM β-glycerophosphate, 0.1 mM PMSF
SDS Running buffer, 10x	25 mM Tris-base, 192mM glycine, 0,1% SDS
SDS Sample buffer, 5x	60 mM Tris-HCl (pH 6.8), 25 % glycerol, 2 % SDS, 14.4 mM 2-mercapto-ethanol, 0.1 % bromo-phenolblue
Transfer buffer, 10x	25 mM Tris-base, 192mM glycine, 20% methanol

3.1.8 Mammalian Cell Lines

3.1.9 Ligands, Proteins and Inhibitors

DPI	Sigma-Aldrich
EGF-AlexaFluor647	Kirsten Michel
EGF, human	Sigma-Aldrich
PalmB	Nachiket Vartak
PTP1Bc	Jian Hou

3.1.10 Material and Equipment

1.5 mm 10-well, 12-well, 15-well combs	Thermo Fisher Scientfic
35-mm MatTek petri dishes	MatTek Corporation
4-well LabTek chambers	Nunc by Thermo Fischer

8-well LabTek chambers	Nunc by Thermo Fischer
BioRad ChemiDoc™ XRS	Bio-Rad Laboratories, Inc.
BioRad Power Pac HC	Bio-Rad Laboratories, Inc.
Cell scraper 16cm 2-Pos.-blade	Sarstedt AG and Co.
Centrifuge 5415R	Eppendorf
Centrifuge 5810R	Eppendorf
Centrifuge RC 26 Plus	Sorvall
Cuvettes (1 ml) Ref. 67.742	Sarstedt Aktiengesellschaft & Co.
ddH_2O	Millipore
Dual Plate xCELLigence	Roche Applied Science
Empty Gel Cassettes, mini, 1.5 mm	Thermo Fisher Scientfic
Eppendorf safe lock tubes (0.5/1.5/2 ml	Eppendorf
Falcon tubes (15/50 ml)	BD Falcon™
Heatable magnetic stirrer 'IKMAG®RCT'	IKA®Labortechnik
Incubation box for western blots	LI-COR Biosciences
Mini and Midi agarose gel chamber	Carl Roth GmbH
Molecular Imager Gel Doc XR	Bio-Rad Laboratories
NALGENE® Cryo 1 °C freezing container	Nunc by Thermo Fischer
Nanodrop ND-1000 spectrophotometer	Peqlab Biotechnologie GmbH
Nuaire™ Cellgard Class II Biological Safety Cabinet	Integra Biosciences
Integra Biosciences	
NuPage 4-12% Bis-Tris Gel	Novex by Life Technologies
Odyssey Infrared Imager	Licor Biosciences
Parafilm	Pechiney Plastic Packaging
Pipetboy acu	Integra Biosciences
PVDF membrane	Bio-Rad Laboratories, Inc.
Sarstedt serological pipettes (5/10/25 ml)	Sarstedt AG & Co.
T25 tissue culture flask	Sarstedt AG and Co.
T75 tissue culture flask	Sarstedt AG and Co.
Test tube rotator 34528	Snijders
Tissue culture plates (24-well)	Sarstedt AG and Co.
Tissue culture plates (6-well)	Sarstedt AG and Co.
Vacuum centrifuge	Eppendorf
Vi-CellTM XR cell viability analyzer	Beckman Coulter, Inc.
Vortex Genie I touch mixer	Scientific Industries
XCell II™ Blot Module	Invitrogen™ Life Technologies

3.1.11 Microscopes

Cell R	Olympus
Fiber coupling unit	PicoQuant GmbH
Fluo View FV1000	Olympus
HCX PL APO (λ blue) 63x/1.4	Leica MICROSYSTEMS
HCX PL APO 40x/1.25- 0.75	Leica MICROSYSTEMS
HCX PL APO CS2 63x/1.4	Leica MICROSYSTEMS
IU-LH75XEAPO: 75W xenon APO lamp	Olympus
IX 81: inverse microscope	Olympus
IX2-UCB controlling unit	Olympus
Leica TCS SP5	Leica MICROSYSTEMS
Leica TCS SP8	Leica MICROSYSTEMS
PR-IX2 motorised stage	Olympus
Scan Stage	Olympus
Sepia II	PicoQuant GmbH
U-HSTR2: hand switch	Olympus
U-RFL-T	Olympus
UPLSAPO 40x/0.9 NA	Olympus
UPLSAPO 60x/1.2 NA	Olympus

3.1.12 Software

Adobe Illustrator CS4	Adobe Systems Inc.
CellProfiler	CellProfiler
Fiji	Schindelin et al. Nat. Meth. (2012)
FV10-ASW Fluoview Software	Olympus
Igor Pro v6.35A5	Wavemetrics
ImageJ64 v1.48i	http://imagej.nih.gov/
Leica Application Suite	Leica
MatLab	MathWorks
Microsoft Office 2011	Microsoft Corporation
Prism 6	GraphPad Software, Inc.
RTCA Software v2.0	ACEA Bioscience, Inc.
SymPhoTime v5.12	Picoquant GmbH

3.2 Methods

3.2.1 Molecular Biology

3.2.1.1 Transformation of chemically competent bacteria

For amplifying recombinant DNA, chemically competent *E.coli* cells (XL 10 Gold) were transformed with foreign plasmid DNA. For each transformation, 1.63 µl 2.25 mM DTT and either ligation product (5 µl) or plasmid DNA (~50 ng) was added to 50 µl bacteria. Cells were incubated on ice for 30 min, followed by a heat shock at 42°C for 90 sec; cells were then returned on ice for another 2 min. For expressing the antibiotic resistance, encoded on the plasmid, 250 µl SOC medium was added and cells were incubated for 1 hour at 37°C and 225 rpm. The bacteria were shortly centrifuged and supernatant was discarded by decanting. For transformation of ligation product, the whole pellet was resuspended and plated on LB agar plates containing the appropriate antibiotics (50 µg/ml Kanamycin or 100 µg/ml Ampicillin). If plasmid DNA was transformed, 20 – 50 µl of the cell suspension was plated. The plates were incubated overnight at 37°C.

On the next day, single colonies were picked and grown at 37°C and 225 rpm in 5 ml LB medium supplemented with appropriate antibiotic. Either the bacteria were grown overnight (mini cultures) or the preculture was transferred to 150 ml LB medium supplemented with antibiotic after 6 hours (midi cultures) and incubated at 37°C overnight. Mini cultures were used for further DNA manipulations and midi cultures were used to obtain endotoxin-free plasmids for transfection of mammalian cell cultures.

3.2.1.2 Agarose gel electrophoresis

To separate nucleic acids by size, agarose gel electrophoresis was used. The DNA was separated in 0.8 % to 2.0 % agarose gels depending on the size of the DNA molecules in question. Agarose gels were prepared with TAE buffer supplemented with 5 µl/100 ml RedSafe™ DNA stain. For size estimation of DNA fragments, a 2-log DNA ladder was added to one lane of the gel. Samples were diluted in either 6X loading buffer (Novagen) or 10X loading buffer based on Orange G. If a separated DNA fragment was needed for further cloning the desired band was cut out of the gel and the DNA was purified with the QIAquick® Gel Extraction Kit (Quiagen) as described in the manufacturer's manual.

3.2.1.3 Restriction Digest

Restriction Endonucleases Type II are cutting double-stranded DNA at specific nucleotide sequences, so called restriction sites. This method was used for analyzing cloning products, for creating linearized DNA vectors and DNA fragments with sticky ends for ligation.

Each restriction reaction was carried out with 1 – 2 µg DNA, 10 U of each restriction enzyme (New England Biolabs, Inc.) and the appropriate buffer. The reaction was replenished with ddH_2O to a final volume of 100 µl. For a complete digestion, reactions were incubated for 1 h up to overnight at 37°C. Linearized plasmids or PCR products were purified using the QIAquick® PCR purification kit (Quiagen) or extracted after agarose gel electrophoresis using QIAquick® Gel Extraction Kit.

3.2.1.4 Dephosphorylation of 5'-Phosphorylated DNA fragments

To prevent self-ligation of the destination vector, dephosphorylation of 5'-end of the cut vector needs to be carried out. Therefore, 0.5 U/μg DNA of alkaline phosphatase (calf intestinal phosphatase, CIP) was added directly on the restriction mix and reaction tubes were incubated for 1 h at 37 °C.

3.2.1.5 Ligation of DNA fragments

To create the desired cloning product out of a linearized vector and a specific insert, DNA ligation reaction was used. The T4 DNA ligase (New England Biolabs, Inc.) catalyzes the formation of two covalent phosphodiester bonds between the 3' hydroxyl end of one nucleotide with the 5' phosphate end of another nucleotide under consumption of ATP. Usually 50 ng of a vector were used with a threefold molar excess of insert fragments. The ratio between vector and insert has been adjusted if the insert size was much smaller in relation to the vector. The following formula was used to calculate the necessary amount of insert:

$$\text{amount insert [ng]} = \frac{\text{amount vector [ng]} \cdot \text{insert size [bp]} \cdot \text{excess insert}}{\text{vector size [bp]}}$$

The reaction was supplemented with the provided reaction buffer, T4 DNA ligase and replenished with ddH_2O to 20 µl. The incubation was carried out for 1 hour at RT or at 16°C

overnight. The ligation reaction was subsequently used for transformation into chemically competent bacteria (3.2.1.1).

3.2.1.6 Ligation independent cloning

The desired insert was amplified via PCR with AccuPrime™ *Pfx*. Next, the destination vector was linearized using appropriate digestion enzymes and 5' overhang was created with T4 DNA polymerase (NEB). The annealing was carried out with different vector/insert ratios, usually 1:1 and 1:5. Reaction was supplemented with T4 ligase buffer, filled up with ddH_2O to 10 µl and incubated for 30 min at 37 °C. The ligation reaction was subsequently used for transformation into chemically competent bacteria (3.2.1.1).

3.2.1.7 Polymerase chain reaction (PCR)

The polymerase chain reaction (PCR) was used for amplifying a particular DNA sequence. Hybridization of single stranded vector with primers will occur at a temperature dependent on the primer of choice (usually 45-60 °C). Heat-stable DNA polymerase elongates bound primers as an exact copy of the original template, doubling the target DNA sequence for every cycle resulting in an exponential amplification of the target sequence.

For standard PCR, AccuPrime™ *Pfx* was used. PCR reaction mixtures contained the equivalent of 20 ng template DNA, 5.0 μl 10x AccuPrime™ *Pfx* reaction buffer, 1.5 μl of a 2 mM dNTP mix, 1.5 μl of 10 mM forward primer, 1.5 μl of 10 mM reverse primer, 2.5 U AccuPrime™ *Pfx* DNA polymerase and total volume was adjusted to 50 μl with ddH_2O. In case of GC-rich templates, PCR reaction was supplemented with 5% DMSO. PCR was carried out as stated in Table 1.

Table 1: Reaction cycle for AccuPrime™ polymerase

Cycle:	*Temperature*	*Time*	*#Cycles*
Initial Denaturation	97 °C	5 min	1
Denaturation	97 °C	15 sec	
Annealing	Tm -3°C to 5 C°	30 sec	33
Elongation	68 °C	1 min/kb	
Final	68 °C	7 min	1
Storing	4 °C	∞	

3.2.1.8 Sequencing

Sequencing of dsDNA was performed according to the dideoxy chain terminating method, as described before[113]. Sequencing PCRs were performed using the BigDye® terminator v3.1 cycle sequencing kit (Applied Biosystems).

3.2.2 Mammalian Cell Culture

3.2.2.1 Cell lines

Cells used in this study are BJ hTERT SV40 HRas wt (BJ-ST), derived from BJ cells (human foreskin fibroblasts) by ectopic expression of telomerase catalytic subunit (hTERT), the simian virus 40 large-T oncoprotein and the HRas wt allele and the isogenic cell line, BJ hTERT SV40 HRas G12V (BJ-ELR), derived like the wt form but with the constitutively active form of HRas (HRas G12V)[114]. MCF7 (ECACC, Cat No. 86012803) cells were used for experiments when a low endogenous expression of EGFR was needed.

3.2.2.2 Cultivation of immortalized mammalian cell lines

Cells were routinely maintained in DMEM supplemented with 10 % fetal bovine serum (FBS), 2 mM L-Glutamin and 1 % non-essential amino acids (NEAA) in a humidified incubator at 37°C and 5 % CO_2. Cells were passaged at a confluency of 80-90 % by aspiration of culture medium, 1 x washing with DPBS and addition of 1 ml Trypsin/EDTA, which was incubated on cells for 3 min at 37°C. Enzymatic reaction was stopped by addition of 10 ml fresh CGM. Cells were gently triturated and cell number was determined with a Vi-CELL XR cell viability analyzer. The required cell number was replated into fresh flasks or other cell culture dishes for desired experiments.

3.2.2.3 Cryo-preservation of mammalian cell lines

For long-term storage of cell lines cryo-stocks were prepared in cryo-medium (CGM + 10 % DMSO) and kept in liquid nitrogen at –196 °C. DMSO serves as cryo-preservative preventing intracellular ice formation and thus decreased cell viability after thawing.

For cryo-stock preparation cells were collected from T75 flasks as described above and diluted in cryo-media at a concentration of 3 x 10^6 cells/ml. Afterwards, 0.5 ml of the cell suspension were applied into pre-cooled cryo vials and transferred to a NALGENE® Cryo 1 °C freezing box filled with isopropanol, which allows a controlled freezing rate of 1 °C/min. Cells were kept at -80 °C overnight and on the next day cryo-stocks were transferred to a liquid nitrogen freezer for long term storage.

To thaw cells, cryo vials were placed into a 37 °C water bath and thawed cell suspension was diluted with minimum 10 ml of prewarmed CGM and transferred to a fresh T75 flask. After reattachment of cells, medium was exchanged with fresh CGM to remove remaining DMSO.

3.2.2.4 Transient transfection with Plasmid DNA

Cell were transiently transfected with plasmid DNA with FuGENE 6 HD Transfection Reagent or Lipofectamine 2000 Transfection reagent according to manufacturer's instructions. Both transfection procedures are based on liposome transfection. Positively charged lipids enclose the negatively charged DNA forming so-called liposomes, which can easily fuse with the cellular plasma membrane.

For Transfection with FuGENE 6 HD Transfection Reagent cells were grown in the appropriate culture dish for 24 hrs to reach a confluency of 60-70 %. For Transfection with Lipofectamine 2000 Transfection Reagent cells were grown to a confluency of 80-90 % due to its higher cell toxicity. The transfection was performed with a DNA:transfection reagent ratio of 1:3. DNA and transfection reagent were diluted in serum-free medium according to Table 2. Cells were incubated with the reaction mixture for 16-24 hrs at 37 °C in a humidified incubator with 5 % CO_2 until required experiment was performed.

Table 2: Transfection protocol for FuGENE and Lipofectamine

Culture dish	**Surface area**	**No. Cells**	**Fugene 6**	**DNA**	**Medium**
48-well 8-well Labtek	1 cm^2 0.8 cm^2	1.2-3.6 x 10^4	0.3 µl	0.10 µg	25 µl
24-well 4-well Labtek	2 cm^2 1.8 cm^2	2.5-7.5 x 10^4	0.6 µl	0.20 µg	25 µl
12-well 2-well Labtek	4 cm^2	0.5-1.5 x 10^5	1.5 µl	0.50 µg	50 µl

Culture dish	**Surface area**	**No. Cells**	**Lipofectamine**	**DNA**	**Medium**
6-well 35 mm dishes	10 cm^2 9.6 cm^2	0.25-1 x 10^6	10 µl	4.0 µg	2 x 250 µl
60-mm	20 cm^2	0.5 - 2 x 10^6	20 µl	8.0 µg	2 x 500 µl
10-cm	60 cm^2	1.5 –6 x 10^6	60 µl	24 µg	2 x 1.5 ml

3.2.2.5 Real time cell analysis

The xCELLigence real-time cell analysis (RTCA) is an assay based on dynamically measuring the impedance-based cell index (CI), a dimensionless unit representing cell attachment and thereby reflecting cell growth over time. Cells are grown on specific 16-well E-plates with gold electrodes at the dish bottom to evaluate the ionic environment at the electrode/solution interface. The Dual Plate xCELLigence instrument correlates this information to the cell number over time.

For the performed RTCA assays 7.5 x 10^3 cells were seeded per well and cell growth was monitored in total for 72 hrs. Before the cells were added to the dishes 100 µl CGM was used to blank the instrument. Afterwards the cells were added in another 100 µl CGM resulting in a final volume of 200 µl per well. The plates were then placed into the RTCA instrument kept in a humidified incubator at 37 °C and 5% CO_2. The CI was monitored every 15 min for 24 hours. Afterwards, the desired treatment was performed by addition of 20 µl medium with the indicated inhibitor or ctrl solution. Measurements were continued for another 24-48 hrs. For reliable results, each condition was performed as duplicates.

3.2.2.6 Stimulation and Treatment of live cells

Before stimulation with GF or treatment with H_2O_2, cells were starved overnight in starvation medium. Indicated concentration of either ligand or H_2O_2 were diluted in starvation medium and added to cells. Incubation was carried out for the indicated time in a humidified incubator at 37 °C and 5% CO_2. If cells were treated with dimedone, DYn-2, DCP-Rho1 or DCP-Bio1 treatment was performed in CGM without FCS. All probes were incubated at an endconcentration of 5 mM and for 10 min in a humidified incubator at 37 °C and 5% CO_2, if not indicated otherwise.

3.2.2.7 Loading cells with PF6-AM

The intracellular H_2O_2 levels were detected with the dye PF6-AM (friendly provided by Chang lab, Departments of Chemistry and Molecular and Cell Biology, University of California, Berkeley, California)[115]. Cells were seeded on 4-well Lab-Tek™ dishes and grown for two days. Cells were loaded with either 1 µM (BJ cells) or 5 µM (MCF7 cells) PF6-AM in PBS supplemented with Ca^{++}/Mg^{++} for 20 min at 37 °C. The cells were then washed twice with fresh DMEM and imaged in phenol red free DMEM supplemented with 25 mM HEPES. For inhibitor experiments 10 µM DPI or equal amount of DMSO was incubated 10 min before PF6-AM was added and together with the dye for 20 min. PalmB or the equal amount of

DMSO was incubated at a concentration of 50 µM overnight. When stimulated with EGF, 320 ng/ml EGF-Alexa647 was incubated simultaneously with PF6-AM.

3.2.3 Biochemistry

3.2.3.1 Preparation of whole cell lysates

Whole cell lysates were prepared from mammalian cells grown in 35-mm or 60-mm tissue culture dishes. Before cell lysis, culture medium was aspirated and cells were washed once with ice-cold PBS. For cell lysis, 70 µl ice-cold lysis buffer supplemented with protease and phosphatase inhibitor cocktail tablet was added and incubated for 10 min on ice. Cells were scratched of the dish and transferred to a cold reaction tube. Lysates were cleared by centrifugation for 15 min at 15000 x g, at 4°C. Supernatant was transferred to a fresh precooled tube and pellet was discarded. Same steps were performed for cells treated with dimedone except that PBS was supplemented with 50 mM NEM and for lysis, and dimedone lysis buffer was supplemented only with protease inhibitor cocktail tablet.

3.2.3.2 Determination of Protein Concentration with Bradford Assay

The Bradford assay is a colorimetric protein assay used to determine the protein concentration of proteins in solution. It is based on the absorbance shift of the dye Coomassie brilliant blue G-250 from 465 nm to 595 nm when bound to hydrophobic amino acids. Therefore, the absorbance measurement at 595 nm is proportional to the protein concentration in the investigated solution.

The protein concentration of all cell lysates was determined with the Bradford assay according to the manufacturer's protocol. Protein standard was prepared by a serial dilution of a 1 mg/ml BSA stock solution obtaining concentrations ranging from 1-16 µg/ml in a total volume of 500 µl ddH_2O. Accordingly, 1 µl of each sample of interest was also diluted in 500 µl ddH_2O in separate plastic cuvettes. For calibrating the spectrophotometer, 1 µl lysis buffer was diluted in 500 µl ddH_2O and used as a blank sample. Finally, to each cuvette 500 µl Bradford reagent was added to receive a total volume of 1 ml. All samples were mixed and absorption was measured at 595 nm. Protein concentration of all lysates was determined by plotting the measured absorption values against the standard curve obtained by the prepared BSA standard.

3.2.3.3 Sample preparation for SDS-PAGE

Protein concentration of whole cell lysates was adjusted to 20 µg per sample and 5x SDS loading buffer was added. For denaturation samples were boiled for 5 min at 95°C followed by centrifugation at max speed for 1min. For dimedone samples 4X XT Sample buffer supplemented with XT Reducing Agent was used and for 10 min at 70°C.

3.2.3.4 Denaturating SDS-Polyacrylamid Gel Electrophoresis (SDS-PAGE)

Denaturating SDS-Polyacrylamide Gel Electrophoresis (Sodium-dodecylsulfate-polyacrylamid-gelelectrophoresis) is used to separate proteins according to their size and charge. The anionic detergent SDS prevents the formation of secondary and tertiary structures of polypeptide chains once denatured in the presence of a reducing agent. Additionally, the binding of SDS leads to an equalized distribution of charge per size of proteins, ensuring an evenly migration through a polyacrylamide matrix of proteins when an electric field is applied. Depending on the pore size of the gel, smaller polypeptide chains can migrate faster than bigger polypeptides and a separation is possible.

All SDS-PAGEs were prepared in 1.5 mm thick empty gel cassettes compatible with the XCell *SureLock*™ Mini-Cell system. Depending on the sample volume and number of samples either 10-, 12- or 15-well combs were used. First the separating gel was poured in the cassette and after polymerization the stacking gel was added. The acrylamide concentration of the separating gel was adjusted to the molecular weight of the protein of interest and prepared according to the following recipe:

Table 3: Recipe for SDS-PAGE (volumes indicated in ml)

	Separating gel 8 %	**Separating gel 12 %**	**Stacking gel**
ddH_2O	7.0	5.0	4.1
30 % Acrylamide mix	4.0	6.0	1.0
1.5 M Tris (pH 8.8)	3.8	3.8	-
1.0 M Tris (pH 6.8)	-	-	0.75
10 % SDS	0.15	0.15	0.06
10 % APS	0.15	0.15	0.06
TEMED	0.009	0.009	0.006

For electrophoresis, the gels were locked into a XCell *SureLock*™ Mini-Cell gel chamber that was filled with 1x Running Buffer. The comb was carefully removed, each sample pocket was washed with 1x running buffer and loaded with the protein samples. For size determination 2 µl of Odyssey Two-Color Protein Molecular Weight Marker was applied to the first pocket. Electrophoresis was performed with constant voltage of 80 V till samples entered the separating gel and the voltage was increased to 130 V for approximately 90 min.

3.2.3.5 Western Blot

Western blot is a technique to detect specific proteins, which were electrophoretically separated and transferred to a nitrocellulose or PVDF membrane. Membranes can be stained with respective antibodies binding to the protein of interest.

All Western Blots were performed with the XCell II™ Blot Module according to manufacturer's instructions. To transfer the separated proteins from the polyacrylamide gel to the PVDF membrane, the separation gel was placed under a methanol-activated membrane. One Whatman filter paper and two sponges, equilibrated in ice-cold transfer buffer, were placed both under and above the blotting sandwich, respectively. The blotting module was placed in an XCell SureLock Mini-Cell, filled up with ice-cold transfer buffer and transfer was carried out with constant voltage of 40 V for 70 min.

After the transfer, PVDF membranes were incubated with gentle shaking for 1 hour at RT with Li-Cor Odyssey Blocking Buffer in a Li-Cor incubation box. For labeling of the proteins of interest, the membranes were incubated on a shaker at 4 °C overnight with the respective primary antibodies diluted in Li-Cor Odyssey Blocking Buffer. On the next day, membranes were incubated with IRDye secondary antibodies diluted in Odyssey Blocking Buffer for 40 min at RT. IRDye labeled Straptavidin was used for DCP-Bio1 detection. After incubation of both primary and secondary antibodies, the membranes were washed 3 x with TBTS/T for 10 min at RT. Finally, membranes were scanned with the Li-Cor Odyssey imaging system.

3.2.3.6 Immunoprecipitation

Cell lysis and determination of protein concentration for Immunoprecipitation (IP) were carried out as described in 3.2.3.1 and 3.2.3.2. For isolating the protein of interest, the respective antibody was immobilized on Protein-G-Sepharose beads (PG-beads) and the whole protein lysate was incubated with the antibody-bound beads. All mentioned

centrifugation steps were carried out at a speed of 850 x g to avoid protein damage caused by added beads.

Agarose PG beads were washed 4 x with ice cold PBS by repeated steps of centrifugation for 2 min at 4 °C, aspiration of the supernatant and addition of fresh PBS. After the last centrifugation, beads were diluted in the same amount of PBS to obtain a 50 % PG-bead solution. To get rid of proteins binding unspecific to PG-beads, 500 µl protein lysate (0.2-1 mg protein) was precleared with 20 µl beads for 1 hr at 4 °C on a wheel-over-wheel-shaker. After centrifugation for 2 min at 4 °C, supernatant was collected in a fresh tube and the respective antibody was added and incubated overnight at 4 °C on a wheel-over-wheel-shaker. On the next day, 30 µl PG-beads were added to each sample and rotated for yet another 2 hr. Samples were washed 4 x with ice cold lysis buffer. After the last washing step, proteins bound to beads were eluted by adding 20 µl Laemmli buffer (1X), shortly vortexed and boiled for 5 min at 95 °C. Afterwards, samples were centrifuged for 1 min at max speed and loaded on SDS-gels. Following steps were carried out as described in 3.2.3.4 and 3.2.3.5.

3.2.3.7 In vitro oxidation of PTP1Bc

Recombinant PTP1Bc (in 25 mM Tris, 150 mM NaCl, 5 % Glycerol) was loaded on Microcon 3 kD YM-3 membrane and centrifuged at 4 °C, 13000 x g for roughly 60 min till most of the buffer was separated from the protein. For recovery, sample reservoir was placed upside down in a fresh tube and centrifuged for 3 min at 1000 x g, 4 °C. Protein concentration was determined via Bradford assay (3.2.3.2) and concentration was adjusted with degassed PBS to 4 mg/ml (108 mM). PTP1Bc was fully reduced by treatment with 1 mM DTT for 20 min at 0 °C. DTT was removed by using again an Microcon 3 kD YM-3 membrane and protein concentration was determined via Bradford. For each sample 10 mM protein was either treated with 5 mM dimedone or the equivalent amount of DMSO and different concentrations of H_2O_2 for 30 min at RT while gently shaking. Reaction was stopped by addition of 20 mM NEM and 4X reducing XT sample buffer. Samples were denatured at 70 °C for 5 min. Detection was carried out as described in 3.2.3.5.

3.2.3.8 Denaturating Bis-Tris-Polyacrylamid Gel Electrophoresis for dimedone detection

The biochemical detection of oxidized proteins derivatized with dimedone was performed similarly to normal gel electrophoresis (3.2.3.4). For electrophoresis, precast NuPAGE 4-12 % Bis-Tris-Gels together with NuPAGE MOPS SDS Running buffer for whole protein lysates or NuPAGE MES SDS Running buffer for PTP1Bc *in vitro* samples. Running

buffer in the inner chamber was supplemented with NuPAGE Antioxidant. After loading of samples, electrophoresis was performed at constant voltage of 200 V for 45-50 min. Afterwards, western blot was performed as described in 3.2.3.5.

3.2.3.9 Labeling of DYn-2 via cupper-catalyzed click chemistry

Cell were washed once with PBS + 20 mM NEM and subsequently fixed with Roti®-Histofix 4 % supplemented also with 20 mM NEM for 10 min at RT. Fixative was removed by washing cells 3 x for 5 min with TBS and cells were permeabilized with PBS + 0.1 % Triton X-100 for 5 min at RT. Afterwards, cells were washed 3 x for 5 min with PBS and unspecific binding was prevented by incubation of cells with Image-iT FX Signal Enhancer for 60 min at RT. For the click-chemistry reaction the following mixture was prepared:

Table 4: Click-Chemistry reaction mix

	Stock concentration	**Final concentration**
Alexa594-Azide	5 mM in DMSO	100 µM
$CuSO_4$	50 mM in H_2O	1 mM
TCEP	50 mM in H_2O	1 mM
TBTA	10 mM in DMSO	100 µM

The components were added in the above-mentioned order and after every step the reaction was shortly vortexed. Before addition of TBTA the reaction was incubated for 2 min at RT. After addition of TBTA, PBS was added to obtain the final concentration stated in Table 4. Afterwards, mixture was diluted again 3x with PBS and 145 µl were added on each well and incubated for 1 hr at RT in the dark. To stop the reaction, click-chemistry mixture was removed and cells were washed 2 x 5min with PBS + 1% Tween-20 and 0.5 mM EDTA and 2 x 5 min with PBS. Finally, cells were directly imaged in PBS.

3.2.3.10 Immunocytochemistry

Cells were treated as indicated, once washed with PBS and fixed with Roti®-Histofix 4 % for 10 min at RT. Fixative was removed by washing 3 x with TBS for 5 min at RT. Permeabilization was carried out with TBS supplemented with 0.1% TritonX-100 for 5 min at RT, followed by three wash steps with TBS for 5 min at RT. To prevent unspecific antibody-binding, cells were blocked with Li-COR Odysseys blocking buffer for min 30 min at RT and then incubated with primary antibodies for 60 min at RT. Cells were washed 3 x with TBS and

secondary antibodies were incubated for 30 min at RT. Excess antibody was removed by three further washing steps with TBS. When needed, cell nuclei were stained with Hoechst-reagent diluted in TBS (1:10000) for 15 min at RT and then washed once with PBS. Finally, cells were imaged in PBS with the appropriate microscope.

3.2.3.11 PhosTag preparation and labeling of fixed cells

Streptavidin (STV) was dissolved in PBS and washed twice with PBS using an Amicon 30 kDa cut-off. Absorption was measured at 280 nm and concentration was adjusted to 100 µM (calculated according to Lambert-Beer; extinction coefficient: 165000 $M^{-1}cm^{-1}$). Bicine (pH 9.3) was added to the STV solution resulting in 0.1 M. Monofunctional Cy3.5 was dissolved in 10 µl DMF and dye concentration was determined by measuring the absorption at 581 nm. For labeling, a 10-fold excess of dye was added to the STV solution and incubated for 45 min at RT and afterwards purified twice by gel exclusion chromatography using protein desalting spin columns. Phos-Tag-Biotin was added in a 200-fold excess to STV-Cy3.5 in TBS/T supplemented with 0.4 mM $Zn(NO_3)_2$ and incubated for 30 min at RT. Mixture was cleared using gel exclusion chromatography with Zebra Spin Desalting Columns 40 kDa cut-off. Cells were plated and transfected as described earlier (3.2.2.4). After overnight starvation with medium containing 0.5 % FCS, cells were treated as described, once washed with PBS and fixed with Roti-Histofix 4 % for 10 min at RT. To remove PFA, cells were washed 3 times with TBS and afterwards permeabilized with TBS containing 0.1 % Triton X-100 for 5 min at RT. Cells were washed 3 x with TBS/T and 170 nM Phos-Tag-Cy3.5 complex in TBS/T was incubated for 1 hr at RT. Finally, cells were washed once with TBS/T and imaged in PBS.

3.2.3.12 Staining of DCP-Bio1 with STV-Cy3.5

STV-Cy3.5 was prepared as described in 3.2.3.11. After incubation of DCP-Bio1, cells were fixed with Roti®-Histofix 4 % for 10 min at RT. Permeabilization was carried out with TBS supplemented with 0.1% TritonX-100 for 5 min at RT, followed by three wash steps with TBS for 5 min at RT. To prevent unspecific staining, cells were blocked with Image-iT FX Signal Enhancer for min 60 min at RT. STV-Cy3.5 was incubated overnight at a concentration of 300 nM at 4 °C and subsequently removed by washing 3 x 5 min with PBS. Finally, cells were directly imaged in PBS.

3.2.4 Microscopy

3.2.4.1 Confocal laser-scanning microscopy (LSM)

Olympus FV1000

Confocal images at the Olympus FV1000 equipped with a 60x/1.35 NA oil objective and a temperature controlled incubation chamber were acquired in sequential mode frame by frame. mTagBFP/DAPI were excited with a 405 nm diode laser, mCitrine/Alexa488 with a 488 nm Argon laser, mCherry/Alexa594 with a 561 nm DPSS laser and Alexa647 with a 633 nm Helium-Neon laser using the DM405/488/561/633 dichroic mirror. Detection of blue fluorescence emission was restricted to a bandwidth of 425-478 nm and was collected using a bandwidth of and through a SDM490 emission beam splitter. Yellow fluorescence was detected between 498-551 nm using the SDM560 beam splitter. Red fluorescence was detected in the bandwidth of 575-623/675 nm depending on the presence of a far red fluorophore and separated from the far red emission using a SDM640 beam splitter. All images were 2x averaged and acquired with a pinhole size of 250 µm or 400 µm. Live cells were imaged in imaging medium, whereas fixed cells were imaged in PBS. All images were acquired at 37 °C and 0 % CO_2.

LeicaSP8

The LeicaSP8 was equipped with a HC PL APO CS2 60x/1.4 NA oil objective and an environmental-controlled chamber at 37°C. mCitrine and mCherry were excited at 488 nm and 561 nm, respectively using a 470-670 nm white light laser. Detection of fluorescence emission was restricted with an Acousto-Optical Beam Splitter (AOBS) to the following bandwidth – mCitrine (498-551 nm) and mCherry (575-675 nm). Images were obtained in sequential mode and the pinhole was set to 3 airy units. Live cells were imaged in imaging media at 37 °C.

3.2.4.2 Fluorescence lifetime imaging microscopy (FLIM)

Fluorescence lifetime imaging microscopy (FLIM) is a method to quantitatively analyze Förster resonance energy transfer (FRET) in a biochemical context[116]. FRET is the non-radiative transfer of energy by dipole-dipole coupling between two fluorophores that are within a few nanometers of each other and can only occur under the condition that the emission spectrum of the donor fluorophore sufficiently overlaps with the excitation spectrum of the acceptor[117].

Confocal FLIM experiments were performed using a time-correlated single-photon counting module on an Olympus FV1000 confocal microscope. The pulsed laser was controlled with the Sepia II software at a pulse repetition rate of 40 MHz. In each sample mCitrine served as donor molecule and was excited with a 507 nm diode laser. Fluorescence emission was spectrally filtered using a bandpass emission filter (537/25). Photons were detected using a single-photon counting avalanche photodiode and timed using a single-photon counting module using the SymPhoTime software V5.13. Images were collected after an integration time of ~ 3 min.

3.2.5 Image analysis

3.2.5.1 FLIM analysis with global analysis

FLIM analysis using global analysis[118] implemented into MatLab based on frequency domain analysis of TCSPC data[119]. All data from the same experiment using the same donor molecule were pooled together and jointly analyzed. For each pixel, the single photon arrival times of the TCSPC measurement were used to calculate the complex Fourier coefficients of the first harmonic. In a second step, the Fourier coefficients were corrected by the Fourier coefficient of a calculated reference[119]. The corrected Fourier coefficients are then plotted into a phasor plot, so that the Fourier coefficients from each pixel of the image are represented by one point in the phasor plot. By fitting a straight line through all points in the phasor plot, the "global lifetimes" τ_D and τ_{DA} are determined at the intersections with the half-circle. The half-circle represents all possible values of mono-exponential lifetimes, wheras all points within the half-circle represent all possible mixtures od two mono-exponential species. τ_{DA} is the donor fluorescence lifetime in presence of the acceptor and τ_D the donor-only lifetime. Finally, the projection of each point in the phasor plot into the fitted segment between τ_D and τ_{DA} can be used to calculate the relative fraction of donor-only and donor-acceptor pairs (α) in each pixel.

3.2.5.2 Single cell segmentation

Cells were segmented in CellProfiler[120] using the image of the nuclear stain (PhosTag) and EGFR-mCitrine. All images were corrected for background and bleed through, and mean values per cell (excluding the nuclear region) from all channels were obtained.

3.2.5.3 HyPer image analysis

Images were processed with Fiji ImageJ software. First, images were converted into 32-bot and background corrected. Either images excited with 405 nm or 561 nm were thresholded to set background pixels to 'Not a number' (NaN). Afterwards the ratio between 488/405 or 488/561 was calculated and mean values for each cell were measured. Values for each cell were normalized to images taken before stimulation to obtain the fold increase upon treatment.

3.2.6 Statistical Analysis

Results are expressed as the mean ± SEM, unless otherwise stated. Statistical significance of ungrouped data was estimated by Student's t-test. Statistical significance of grouped data was estimated by two-way ANOVA. For two-way ANOVA a Bonferroni correction was performed and adjusted p-values were calculated and indicated in the corresponding figures.

4 RESULTS

4.1 Intracellular H_2O_2 production

4.1.1 Ras- and EGFR-dependent regulation of intracellular H_2O_2 levels

Gain of function mutations such as the frequently found G12V substitution in the Ras oncogene, are common drivers of tumor formation and progression. Malignant transformation is often associated with higher ROS levels either caused by enhanced cellular stress, higher cellular metabolism or direct activation of ROS producing enzymes by the oncogene. In this study, we used immortalized normal human BJ fibroblasts (BJ-ST; here wt cells) and compared them with an isogenic cell line stably infected with the oncogenic form of HRas (HRas G12V; BJ-ELR cells; here G12V cells)[114]. To test whether HRas G12V leads to higher H_2O_2 levels, the cell permeable dye PF6-AM was used, which increases in fluorescence when H_2O_2 is present due to a boronate chemical switch[115]. Indeed, we could show that the basal intracellular H_2O_2 level was nearly twofold higher in G12V cells as compared to wt cells (Figure 4.1 A).

To identify if the measured H_2O_2 production was caused by an activation of NOX proteins, both cell lines were treated with the common NOX inhibitor DPI[121], and H_2O_2 levels were monitored again with PF6-AM. Incubation with DPI led to a dramatic decrease in H_2O_2 levels in both cell types indicating active NOX enzymes as the main source of intracellular H_2O_2 production in resting BJ cells (Figure 4.1 B). To uncouple NOX activation and subsequent H_2O_2 production from active Ras signaling, we blocked depalmitoylation of palmitoylated Ras by inhibiting the acyl protein thioesterase 1 (APT1) with palmostatin B (PalmB). Inhibition of APT1 by PalmB disturbs the steady-state localization of Ras by randomizing its localization to all membranes and thus leading to a perturbation of Ras signaling activity[122]. When BJ cells were pre-incubated with PalmB and H_2O_2 levels were detected with PF6-AM, a significant decrease in fluorescence was detected for both cell types implicating low H_2O_2 levels (Figure 4.1 C). This indicates that NOX activation and thus H_2O_2 production is dependent on active Ras signaling, in untransformed and oncogenic cells. However, treatment with PalmB led to a more significant decrease of H_2O_2 levels in G12V cells showing that Ras transformation has a high impact on intracellular ROS production.

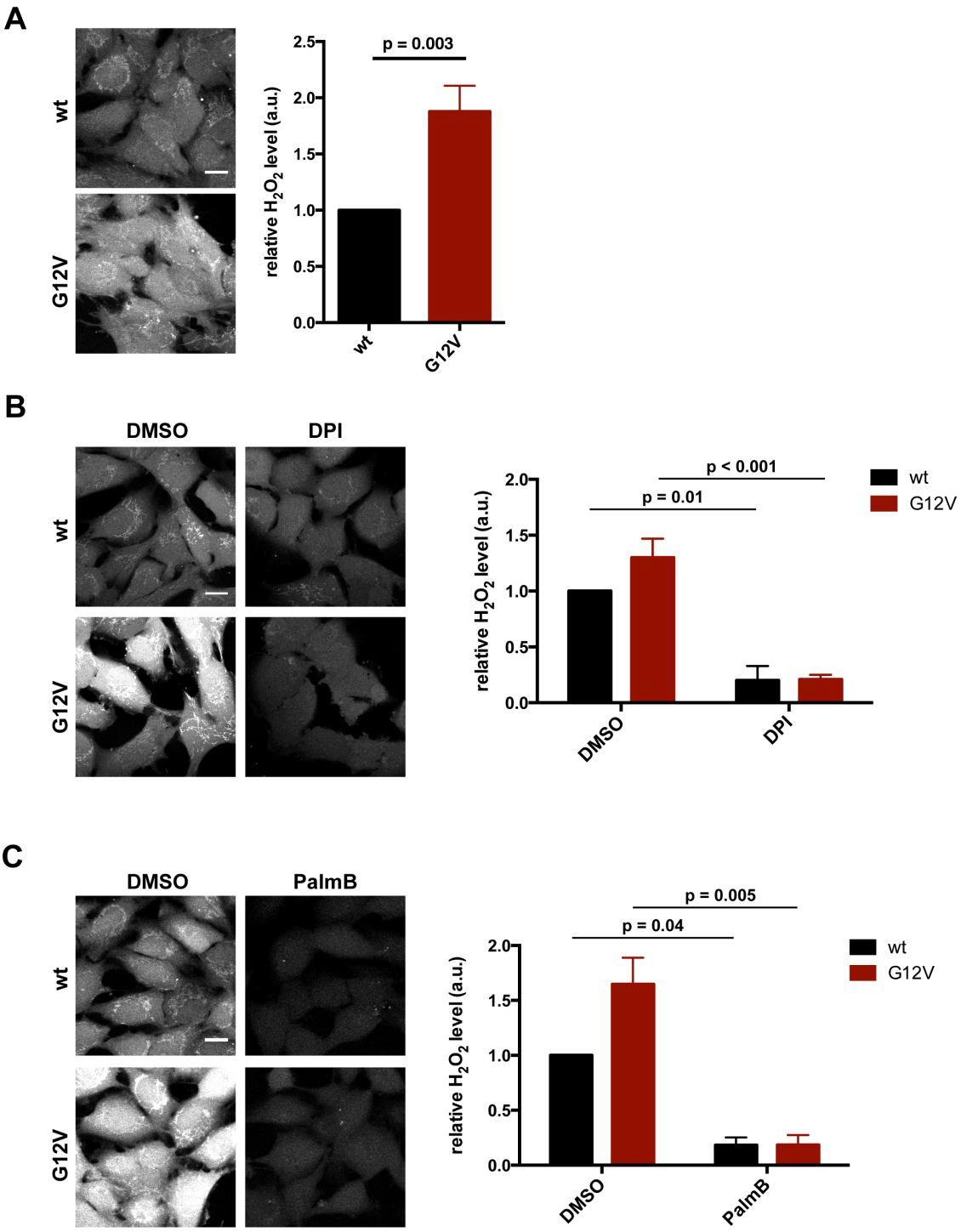

Figure 4.1: HRas G12V increases H_2O_2 production by activation of NOX enzymes
(A) Representative fluorescence images of unstimulated wt and G12V cells incubated with the H_2O_2 sensitive probe PF6-AM. Graph shows average ± SEM of mean fluorescence intensity of three independent experiments each with 5-7 fields of view (confluent layer of cells). P values were calculated by Student's t test. Scale bar: 10 µm **(B)** Representative fluorescence images of unstimulated wt and G12V cells pre-incubated either with 10 µM DPI or DMSO and then loaded with PF6-AM. Plot on the right shows average ± SEM of mean fluorescence intensity of three independent experiments each with 5-7 fields of view (confluent layer of cells). P values were calculated by two-way ANOVA. Scale bar: 10 µm **(C)** Representative fluorescence images of cells treated either with 50 µM PalmB or DMSO overnight and then loaded with PF6-AM. Plot on the right shows average ± SEM of mean fluorescence intensity of two independent experiments each with 5-7 fields of view (confluent layer of cells). P values were calculated by two-way ANOVA. Scale bar: 10 µm

To check if the production of H_2O_2 is mediating normal cell growth, we performed real-time cell analyzer (RTCA) assays of wt and G12V cells with increasing concentrations of DPI. Cells were first grown in complete growth medium without the inhibitor, which was added after 24 hrs when cells were fully attached. In wt cells, addition of 3 and 5 µM did not have any significant effect on cell growth and first addition of 10 µM DPI led to increased apoptosis indicated by a decreasing cell index (Figure 4.2 A). In contrast, G12V cells already showed impaired cell growth after treatment with 3 µM DPI getting more pronounced with higher DPI concentrations (Figure 4.2 A). By comparing the relative growth rates, we could show that the growth of G12V cells is highly dependent on intracellular H_2O_2 production whereas wt cells continued to proliferate even in the presence of DPI (Figure 4.2 B).

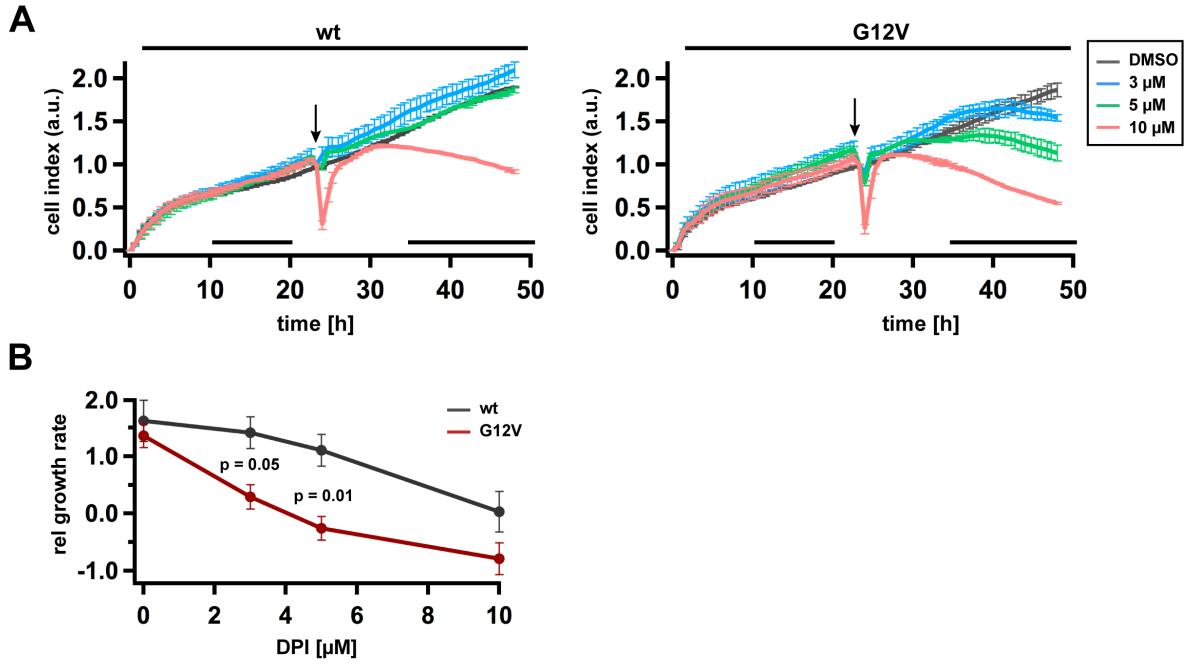

Figure 4.2: Dependency of cell growth on NOX activity
(A) Growth curves of wt (left) and G12V cells (right) recorded by RTCA measurements. Both cell types were treated with indicated concentrations of DPI or DMSO. Curves were normalized to the cell index value before inhibitor was added. Lines under curves represent the values used for calculating the relative growth rate **(B)** Relative growth rates of three independent experiments showing mean values ± SEM obtained by calculating the quotient before and after inhibitor addition. P values were calculated by Student's t-test.

Ras usually acts downstream of RTKs linking the production of H_2O_2 to active growth factor signaling. One of the most studied RTKs is EGFR, a receptor that has been shown to evoke H_2O_2 production and is like Ras often hyperactivated in human cancers[26,123]. To study if not only Ras but also the upstream EGFR can enhance the intracellular H_2O_2 production, we overexpressed EGFR-mCherry in MCF7 cells, a cell line with a low endogenous EGFR

expression level[124]. When incubated with PF6-AM, cells with higher EGFR-mCherry expression showed a tendency for higher intracellular H_2O_2 concentrations (Figure 4.3 A). This correlation became even more distinct when cells were stimulated with EGF provoking full receptor activation (Figure 4.3 B). In contrast, pre-incubation with DPI led to an overall decrease in H_2O_2 levels, showing that activation of NOX enzymes is also necessary for EGFR-dependent H_2O_2 production (Figure 4.3 C, D).

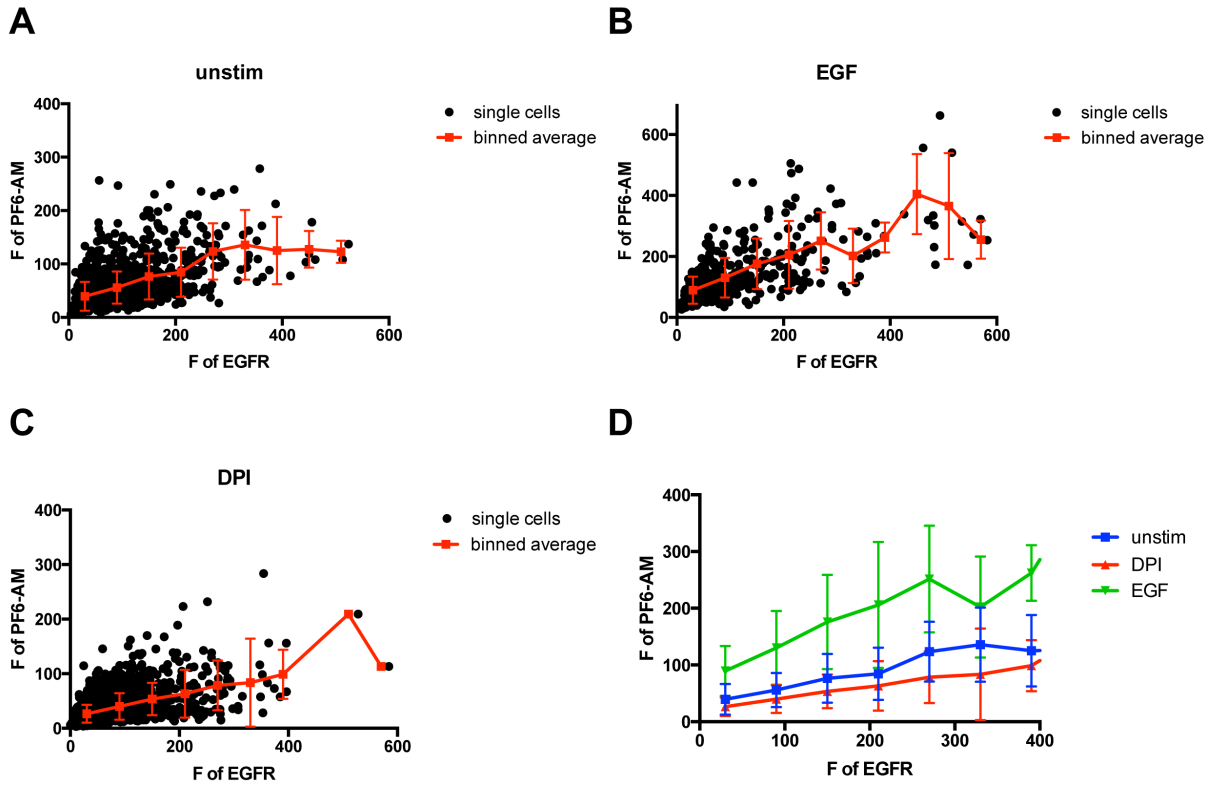

Figure 4.3: H_2O_2 production in dependence to EGFR expression in MCF7 cells
(A) Dependence of H_2O_2 levels (F of PF6-AM) on EGFR-mCherry expression level (F of EGFR) obtained for unstimulated MCF7 cells. Black dots represent fluorescence intensities (F) for EGFR-mCherry and PF6-AM per cell and red line represents binned average ± SEM. **(B)** Dependence of H_2O_2 levels as measured by PF6-AM fluorescence on EGFR-mCherry expression level obtained for MCF7 cells stimulated with 100 ng/ml EGF. **(C)** Dependence of H_2O_2 levels as measured by PF6-AM fluorescence on EGFR-mCherry expression level obtained for MCF7 cells pre-treated with 10 µM DPI. Black dots represent fluorescence intensities for EGFR-mCherry and PF6-AM per cell and red line represents binned average ± SEM. **(D)** Binned averages for all three conditions showed in (A), (B) and (C).

4.1.2 Spatial-temporal dynamics of H_2O_2 production upon EGF stimulation

Sine we could show that H_2O_2 production is dependent on both active Ras signaling and EGFR activation, we continued with detecting the temporal dynamics of H_2O_2 production upon EGF stimulation. Therefore, we used the genetically encoded sensor HyPer3[125] in BJ cells with endogenous EGFR levels and in MCF7 cells, where we ectopically expressed the receptor. HyPer3 consists of a circularly permutated YFP (cpYFP) flanked by the OxyR domains from

E.coli. Upon exposure to H_2O_2 a disulfide is formed between Cys199 and Cys208 leading to an increased fluorescence emission (500-530 nm) when excited at 488 nm and a decreased fluorescence emission when excited at 405 nm, enabling a ratiometric readout, which is insensitive to random fluctuations caused, for instance, by cell shape changes or focus drift[126]. Additionally, HyPer can be reduced by the cellular antioxidant system making it suitable for the detection of dynamic changes of intracellular H_2O_2 concentrations.

First, we used the originally published cytoplasmic form of HyPer3 (cHyPer3) expressed in BJ wt and G12V cells. To test the dynamic range and reversibility of the sensor, a high concentration of exogenous H_2O_2 was added to both cell types, followed by addition of the reducing agent DTT. As expected, an increased fluorescence was detectable when excited at 488 nm and a corresponding decrease was detectable when excited at 405 nm upon addition of H_2O_2 (Figure 4.4 A). In contrast, addition of DTT induced the opposite effect in both cell types, verifying the reversibility and ratiometric readout of cHyPer3. Interestingly, fold increase upon H_2O_2 of cHyPer3 was higher in wt cells compared to G12V cells and accordingly, fold decrease was upon DTT administration faster in G12V cells (Figure 4.4 B).

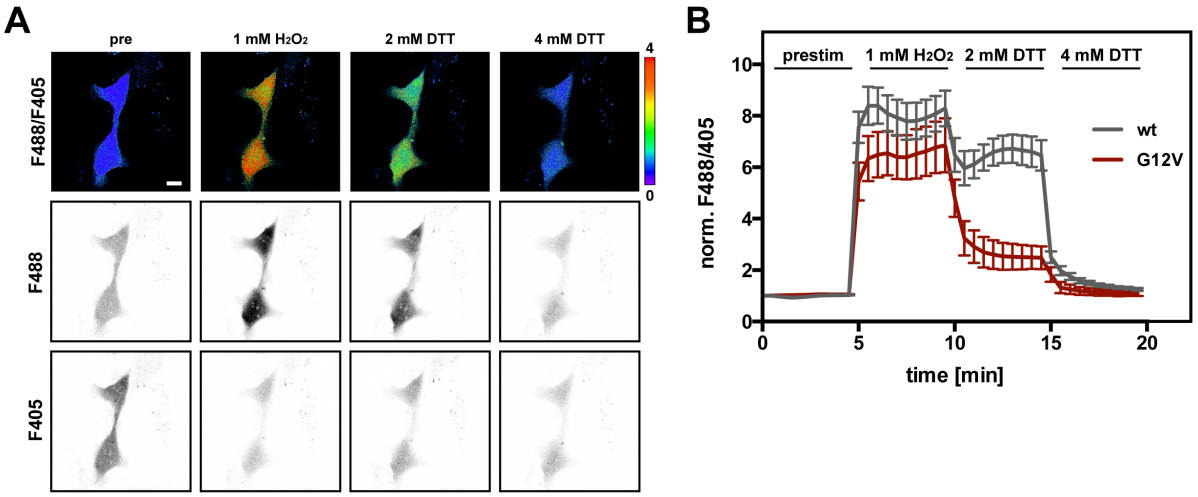

Figure 4.4: Oxidation/reduction cycle of cHyPer3
(A) First row shows pseudocolored images of the 488/405 fluorescence ratio of cHyPer3 expressed in BJ cells treated as indicated. Middle row shows fluorescence images of cHyPer3 excited with the 488 nm laser line (F488) and lower row shows excitation at 405 nm (F405). Scale bar: 20 µm **(B)** Plot shows average ± SEM of 488/405 ratio upon treatment with H_2O_2 or DTT as indicated for 6-8 cells per cell type.

In addition to the cytoplasmic HyPer3 version, a membrane anchored (HyPer3-TK) and an ER-anchored (HyPer3-ER) version were tested to map the spatial-temporal production of H_2O_2 upon EGF stimulation. HyPer3-TK consists of the truncated C-terminal

HVR of KRas fused to cHyPer3 and HyPer3-ER is a fusion of the ER-anchor from PTP1B and cHyPer3. When expressed in BJ cells both constructs showed a correct localization, a clear fluorescence at the PM for HyPer3-TK and ER staining HyPer3-ER (Figure 4.5). To test if trapping the sensor to an intracellular compartment hinders its reversible ratiometric readout, the same controls were performed as for cHyPer3 (Figure 4.5). HyPer3-TK shows a slightly lower fold increase of the F488/F405 ratio compared to the cHyPer3 construct upon treatment with the same concentration of H_2O_2. Interestingly, addition of 2 mM DTT was not sufficient to reduce HyPer3-TK and an addition of 4 mM DTT was required to significantly decrease the F488/F405 ratio in both cell types (Figure 4.5 A). This could indicate that the cytoplasm has a higher reduction potential than the PM. Similar to cHyPer3, HyPer3-TK shows less oxidation and a faster reduction when expressed in G12V cells.

The oxidation dynamics of HyPer3-ER were similar in both cell types upon addition of H_2O_2 (Figure 4.5 B). Reduction of the construct was not detectable upon treatment with 2 mM DTT as already observed for HyPer3-TK. Upon addition of 4 mM DTT a decrease in the F488/F405 ratio was detectable for both cell types, although wt cells showed a slower reduction than G12V cells.

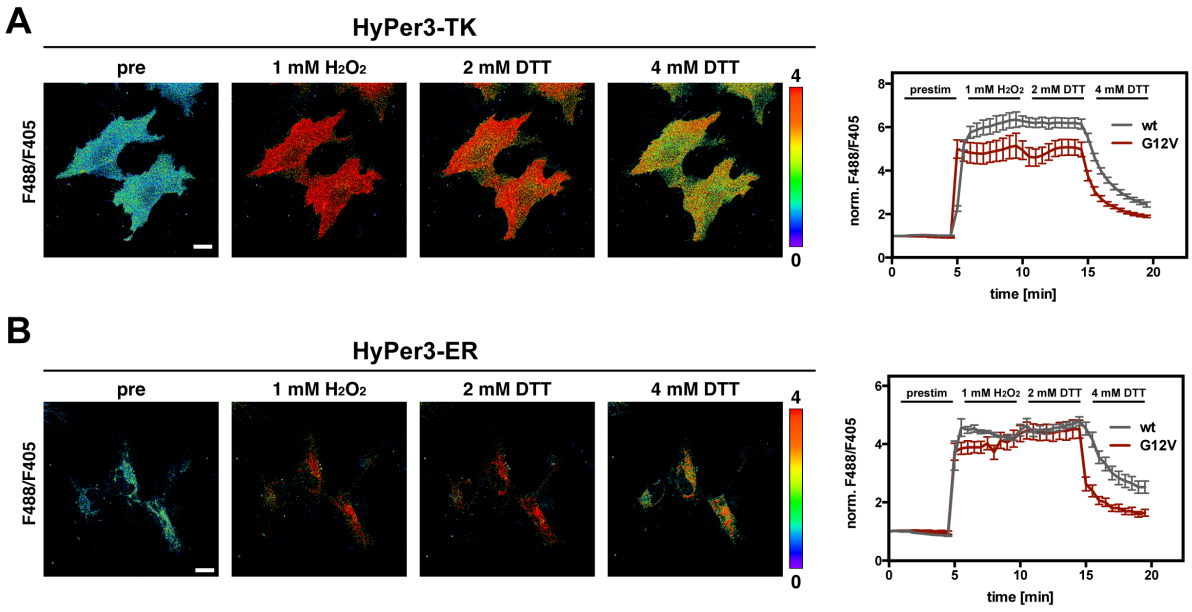

Figure 4.5: Oxidation/reduction cycle of HyPer3-TK and HyPer3-ER
(A) Left panel shows pseudocolored images of the 488/405 fluorescence ratio of cells treated as indicated and expressing HyPer3-TK. Plot on the right panel shows average ± SEM of 488/405 ratio per time point upon treatment with H_2O_2 or DTT as indicated for 6-8 cells per cell type. Scale bar: 20 µm (B) Left panel shows pseudocolored images of the 488/405 fluorescence ratio of cells treated as indicated and expressing HyPer3-ER. Plot on the right panel shows average ± SEM of 488/405 ratio per time point upon treatment with H_2O_2 or DTT as indicated for 6-8 cells per cell type. Scale bar: 20 µm

Further on, all three constructs were used to map compartment-specific H_2O_2 production upon EGF-Alexa647 (320 ng/ml) stimulation in BJ cells. Only cHyPer3 showed an increase in the F488/F405 ratio in G12V cells (Figure 4.6 A) whereas all other constructs didn't change upon EGF stimulation or even decreased (Figure 4.6 B, C). This indicates that H_2O_2 production upon EGF stimulation is only detectable in the cytoplasm of G12V cells when stimulated with EGF.

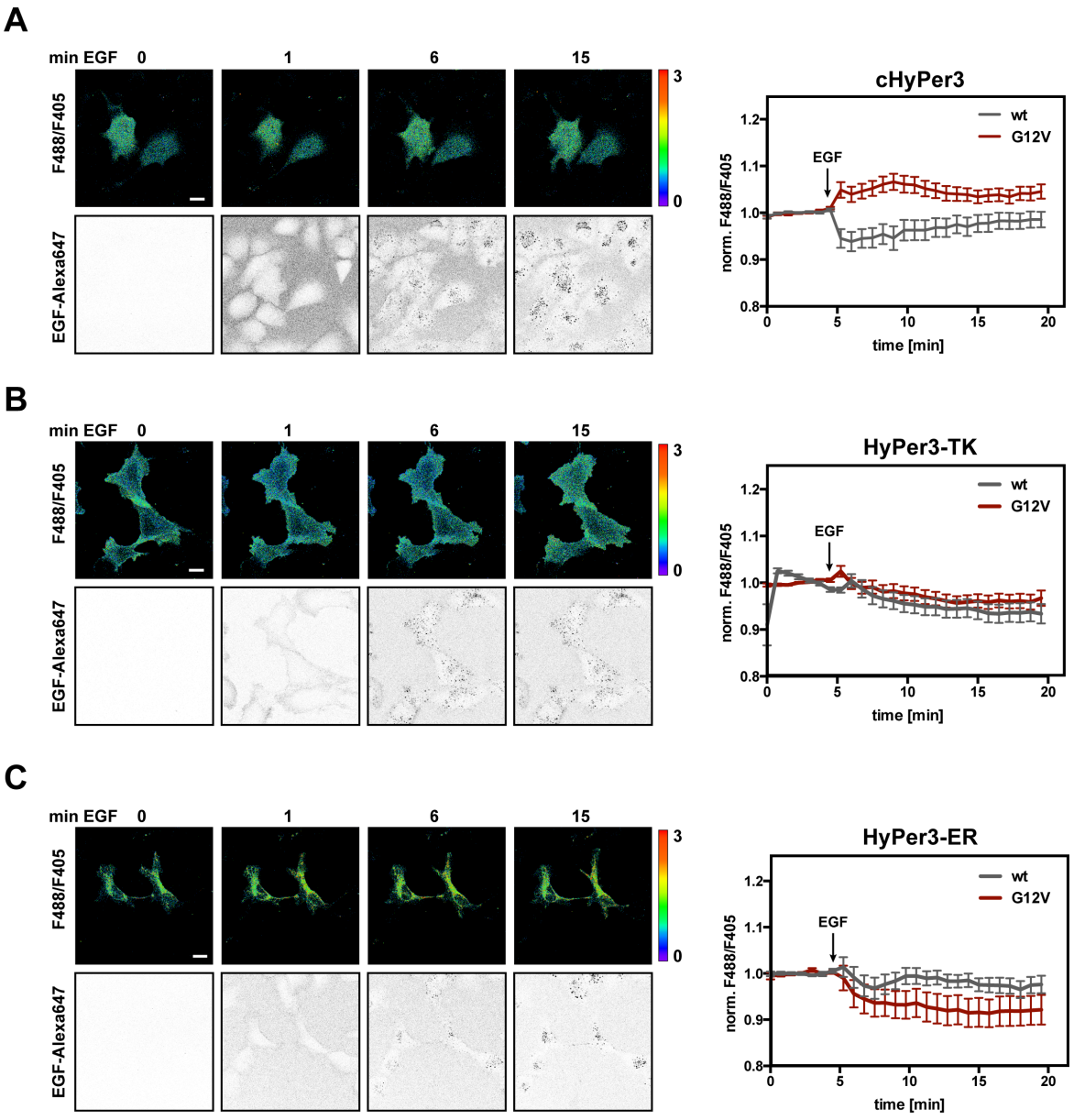

Figure 4.6: H_2O_2 production in different cellular compartments upon EGF stimulation
(A) Pseudocolored images on the left represent the 488/405 fluorescence ratio (upper row) of wt cells expressing cHyPer3 at different time points after stimulation with EGF-Alexa647 (lower row). Graph on the right shows temporal dynamics of H_2O_2 production upon EGF-Alexa647 stimulation in wt and G12V cells detected by 488/405 fluorescence ratio of cHyPer3. Every time point represents average ± SEM of 488/405 fluorescence ratio of minimum 30 different cells. Arrow indicates addition of EGF-Alexa647 (320 ng/ml); images were taken every 1 min. Scale bar: 20 µm **(B)** Pseudocolored images on the left represent the 488/405 fluorescence ratio (upper row) of wt cells expressing HyPer3-TK at different time points after stimulation with EGF-Alexa647 (lower row). Graph on the right shows temporal dynamics of H_2O_2 production upon EGF-Alexa647 stimulation in wt and G12V cells detected by 488/405 fluorescence ratio of HyPer3-TK. Every time point represents average ± SEM of

488/405 fluorescence ratio of minimum 30 different cells. Arrow indicates addition of EGF-Alexa647 (320 ng/ml); images were taken every 1 min. Scale bar: 20 µm **(C)** Pseudocolored images on the left represent the 488/405 fluorescence ratio (upper row) of wt cells expressing HyPer3-ER at different time points after stimulation with EGF-Alexa647 (lower row). Graph on the right shows temporal dynamics of H_2O_2 production upon EGF-Alexa647 stimulation in wt and G12V cells detected by 488/405 fluorescence ratio of HyPer3-ER. Every time point represents average ± SEM of 488/405 fluorescence ratio of minimum 30 different cells. Arrow indicates addition of EGF-Alexa647 (320 ng/ml); images were taken every 1 min. Scale bar: 20 µm

It was surprising that all HyPer constructs when expressed in BJ cells just showed a minor or no increase upon EGF stimulation, whereas a clear increase in H_2O_2 levels was detectable in MCF7 cells when measured with PF6-AM (Figure 4.3). Therefore, we tried to optimize the detection of the HyPer construct since the direct ratiometric readout displays some drawbacks. For instance, the excitation at 405 nm is likely to bleach fluorophores or could induce to the production of ROS that oxidizes HyPer prior to EGF stimulation.

As an alternative, we tested a two-fluorophore system consisting of cHyPer3 and co-expression of mCherry as reference. In this case, HyPer was just excited with the 488 nm laser line and mCherry fluorescence intensity excited at 561 nm should correct for H_2O_2 independent changes, which are for example caused by changes upon cell movement or focus drift. This system was first tested in EGFR-expressing MCF7 cells as in those cells a clear H_2O_2 increase upon EGF stimulation was detectable with measured with PF6-AM (Figure 4.3). Labeled EGF (EGF-Alexa647) was used to visualize EGFR overexpression. Upon EGF stimulation the F488/F561 ratio increased fast and plateaued after 3 min reflecting production of H_2O_2 (Figure 4.7). For the control measurement, where just medium was added to the cells, no change was detectable indicating a specific increase of H_2O_2 upon EGF stimulation. In general, the two-fluorophore system is less noisy and more sensitive making it preferable for measuring the temporal dynamics of H_2O_2 production upon GF stimulation.

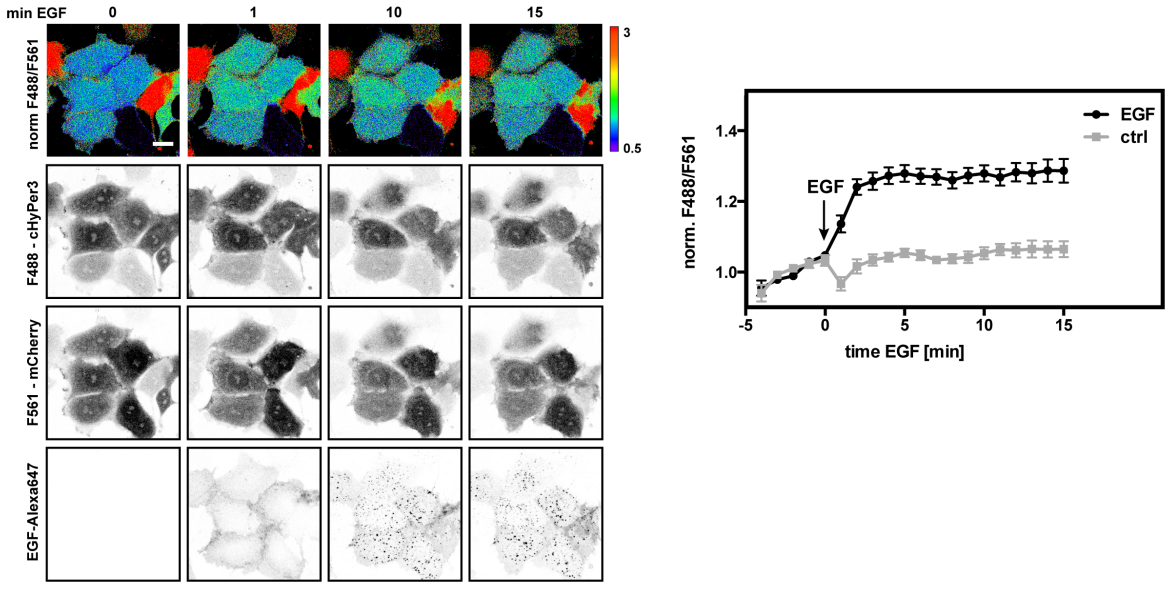

Figure 4.7: Detection of EGF induced H_2O_2 production in MCF7 cells with cHyper3-mCherry system
Pseudocolored images of the normalized 488/561 fluorescence ratio (upper row) of MCF7 cells expressing cHyPer3 (second row) and mCherry (third row) at different time points after stimulation with EGF-Alexa647 (320 ng/ml; lower row) Scale bar: 20 µm. Graph on the right shows temporal dynamics of H_2O_2 production upon EGF-Alexa647 stimulation (n = 11 cells) and for the ctrl case (n = 9 cells). Every time point represents average ± SEM of 488/561 fluorescence ratio normalized to the mean intensity of 5 images taken before EGF/medium addition as indicated by the arrow.

The same method was used to measure H_2O_2 production in BJ cells upon EGF stimulation without overexpressing the receptor (Figure 4.8 A). Consistent with data from MCF7 cells, the F488/F561 ratio showed a significant increase after EGF addition in both cell types. However, G12V cells showed a higher increase than wt cells concordant with the previous obtained H_2O_2 measurements at basal level (Figure 4.6, Figure 4.8 B). Comparable to the results in MCF7 cells, H_2O_2 production plateaued around 5 min after stimulation and did not decrease further. Although reversibility was tested before (Figure 4.4), it is possible that the endogenous antioxidant system is not sufficient for reducing overexpressed HyPer3 once oxidized. These results proof that EGF stimulation leads to an increase in H_2O_2 levels and that the presence of constitutively active HRas even further increases the production.

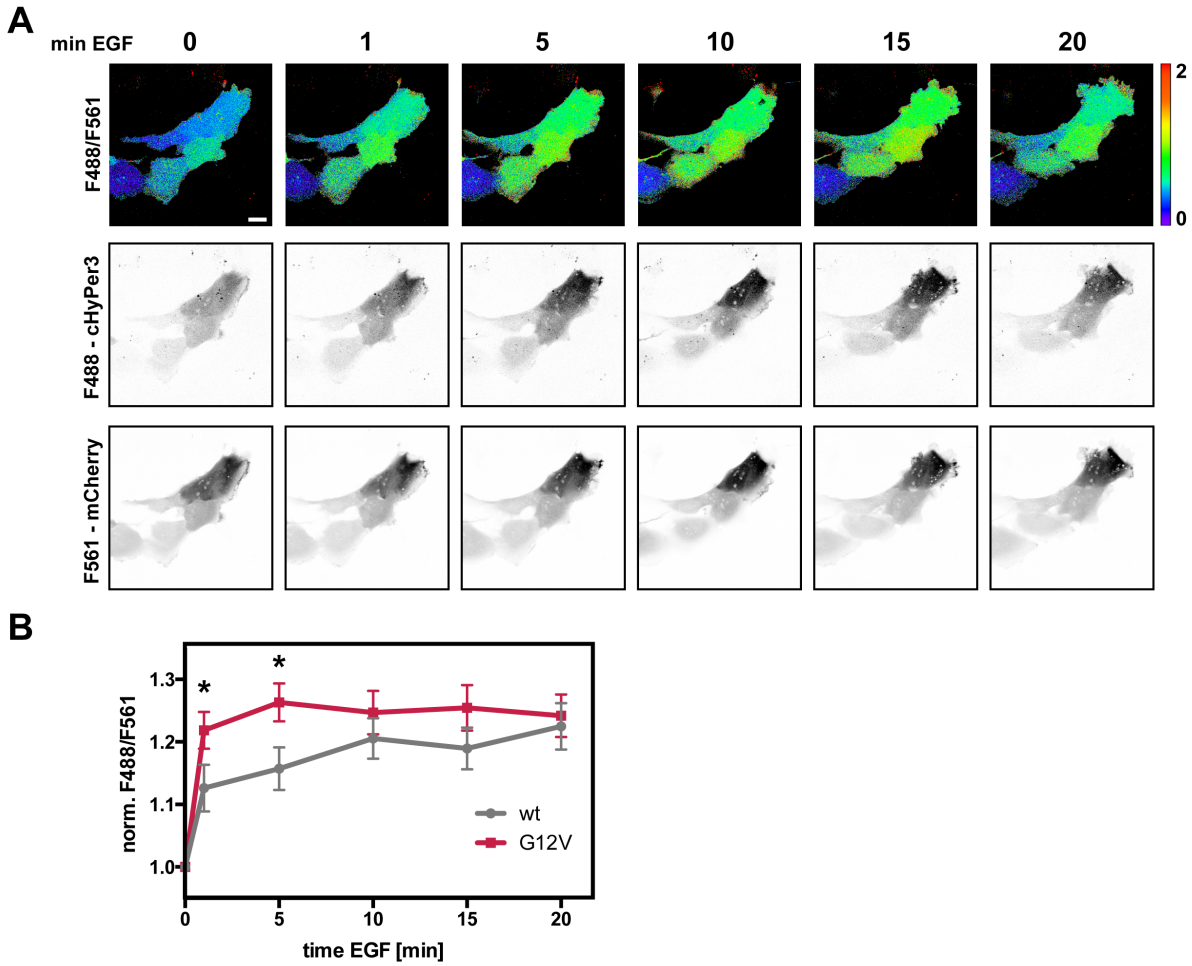

Figure 4.8: Detection of EGF induced H_2O_2 production in BJ cells with cHyper3-mCherry system
(A) Pseudocolored images of the 488/561 fluorescence ratio (upper row) of BJ G12V cells expressing cHyPer3 (middle row) and mCherry (lower row) at different time points after stimulation with EGF (100 ng/ml). Scale bar: 20 µm. **(B)** Graph shows temporal dynamics of H_2O_2 production upon EGF stimulation for wt (n = 29) and G12V cells (n = 29). Every time point represents average ± SEM of 488/561 fluorescence ratio normalized to the image taken before stimulation. P values were obtained by Student's t-test; significance as shown by (*) represents $p < 0.05$.

4.1.3 Detection of NOX enzymes

We could show that inhibition of NOX enzymes by DPI led to a decreased intracellular H_2O_2 production and that the presence of constitutively active HRas increases the intracellular H_2O_2 production. For a better understanding of the molecular mechanism of H_2O_2 production in BJ cells, we investigated two members of the NOX family. On the one hand we checked for NOX2 expression, which is GF-regulated and PM-located. On the other hand, we focused on NOX4, which is expressed on the ER and in contrary to NOX2 constitutively active[3]. First, we checked for total protein expression level of these proteins via western blot analysis of whole cell lysates of BJ cells (Figure 4.1 A, B). Although H_2O_2 production was higher in G12V cells, NOX2 and NOX4 levels are comparable in both cell types (Figure 4.9 A, B). Since NOX4 is

constitutively active a similar expression level in both cells indicates that this NOX enzyme is not responsible for higher H_2O_2 levels in G12V cells. Therefore, we continued with immunostainings of NOX2 revealing an accumulation of the protein at the PM in G12V, which even increases upon EGF stimulation (Figure 4.9 C). This distinct staining pattern was not detected in wt cells. This indicates that constitutively active HRas triggers NOX2 assembly and activation in resting cells leading to higher H_2O_2 levels in unstimulated and EGF stimulated cells. In addition, EGF stimulation in G12V cells can even increase NOX2 activation leading to elevated H_2O_2 levels.

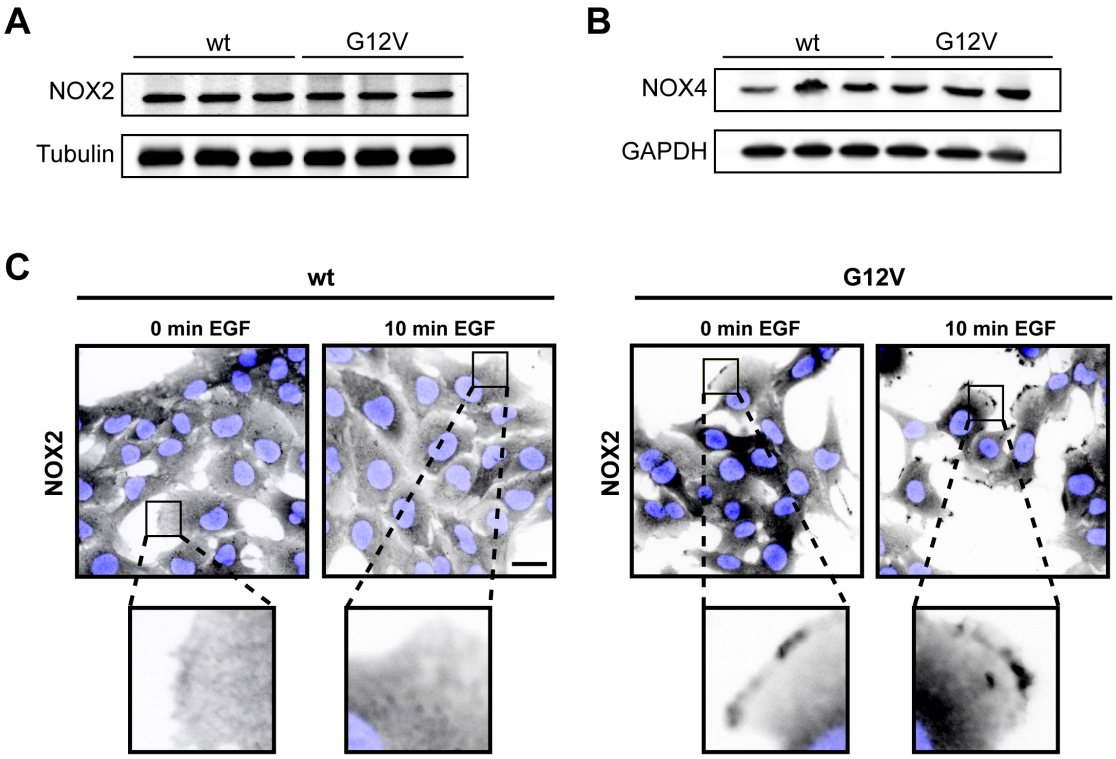

Figure 4.9: Expression level and spatial distribution of NOX enzymes in BJ cells
(A) Western blot of whole cell lysates detecting NOX2 levels in BJ wt and G12V cells in triplicates. Tubulin serves as loading control. **(B)** Western blot of whole cell lysates detecting NOX4 levels in BJ wt and G12V cells in triplicates. GAPDH serves as loading control. **(C)** Representative images of NOX2 immunostaining in untreated and EGF treated (50 ng/ml) BJ cells. Boxes indicate regions of interest that are blown up below the original image showing NOX2 staining in the periphery of the cell. Scale bar: 50 µm

Taken together, we could show that EGF stimulation induces H_2O_2 production via activation of NOX enzymes and that constitutively active HRas leads to an increase of intracellular H_2O_2, at basal level and upon EGF stimulation.

4.2 Effect of H_2O_2 production on EGFR phosphorylation dynamics

Inhibition of PTPs by EGF-induced H_2O_2 production together with the autocatalytic activation mechanism of EGFR exemplifies a double negative feedback ensuring robust threshold-activated receptor phosphorylation[94]. Thus, we hypothesized that increased H_2O_2 levels as caused by gain of function mutations of oncogenes as shown here for HRas, can influence this delicate balance between RTK activation and PTP inhibition.

4.2.1 Ligand dependent EGFR activation in BJ cells

In the previous experiments, EGF stimulation has been shown to trigger H_2O_2 production but receptor activation itself and how it could be affected by H_2O_2 was not considered. The classical EGFR activation scheme follows ligand binding, receptor dimerization, auto-phosphorylation *in trans* and recruitment of adaptor proteins resulting in signal transduction[64]. To examine, if higher H_2O_2 levels caused by HRas G12V promote EGFR activity, BJ cells were stimulated with 50 ng/ml EGF for different time points and receptor phosphorylation was analyzed from whole cell lysates via western blot. For both cell lines, EGFR phosphorylation, as probed with the generic phospho-tyrosine antibody PY72, peaked 5 min after stimulation and declined to basal level within 60 min (Figure 4.10). The overall phosphorylation profile of EGFR is highly similar in both cell lines and apart of non-significant differences at later time points, HRas G12V cells did not show an enhanced receptor activation.

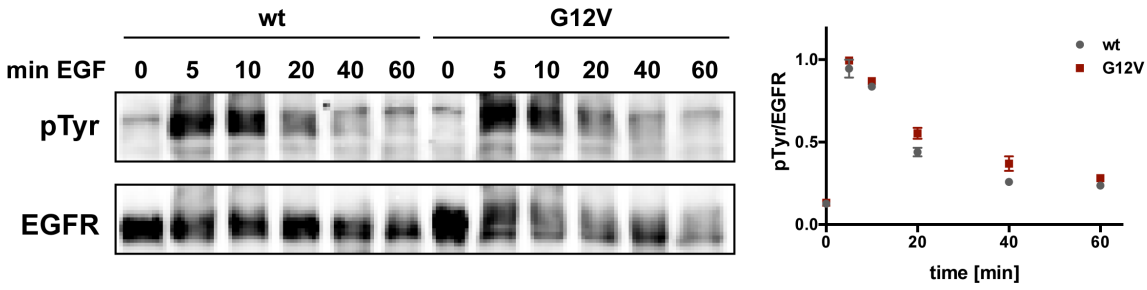

Figure 4.10: Temporal phosphorylation profile of EGFR upon EGF stimulation in BJ cells
Left panel shows representative western blot images of phosphorylated EGFR at different time points upon EGF stimulation (50 ng/ml) in BJ wt and G12V cells. Plot on the right shows mean ratio ± SEM of phospho-tyrosine signal over total EGFR signal at indicated time points after EGF stimulation (n=2).

Since population means as obtained by western blotting often miss out phenotypic differences among individual cells and do not provide any information about cell-to-cell variance or spatial regulation of protein activities, we analyzed EGFR phosphorylation in BJ

cells via single live-cell imaging using FLIM. For detection of activated EGFR, EGFR-mCitrine, serving as donor molecule, and PTB-mCherry, serving as acceptor molecule, were overexpressed in BJ cells. Binding of PTB to the phosphorylated receptor results in FRET between both fluorophores enabling the computation of the fraction of phosphorylated EGFR (α). Upon stimulation with EGF (100 ng/ml), α quickly increased in both cell types and stayed relatively stable over the measured time course (Figure 4.11). EGFR phosphorylation peaked at the PM forming a gradient, which declined towards the cell interior. PTB-mCherry was not imaged to prevent bleaching of the acceptor, which could result in an artificial increase in α. Imaging of several cells revealed that EGF stimulation leads to a sustained activation profile of EGFR-mCitrine already peaking 2 min after EGF addition (Figure 4.11 B). This is contrary to the transient phosphorylation profile obtained by western blot analysis of endogenous EGFR in BJ cells (Figure 4.10). A possible explanation for this can be a limited access of PTPs to its specific EGFR phosphorylation site or ectopic expression of the receptor overcomes the endogenous PTP activity upon EGF stimulation and the receptor stays phosphorylated for a longer time course. However, no significant difference between wt and G12V cells was detectable upon EGF stimulation as already observed before (Figure 4.10, Figure 4.11 B). Interestingly, HRas G12V transformed cells showed a detectable but non-significant increase in EGFR activation at basal state before addition of EGF when compared to wt cells.

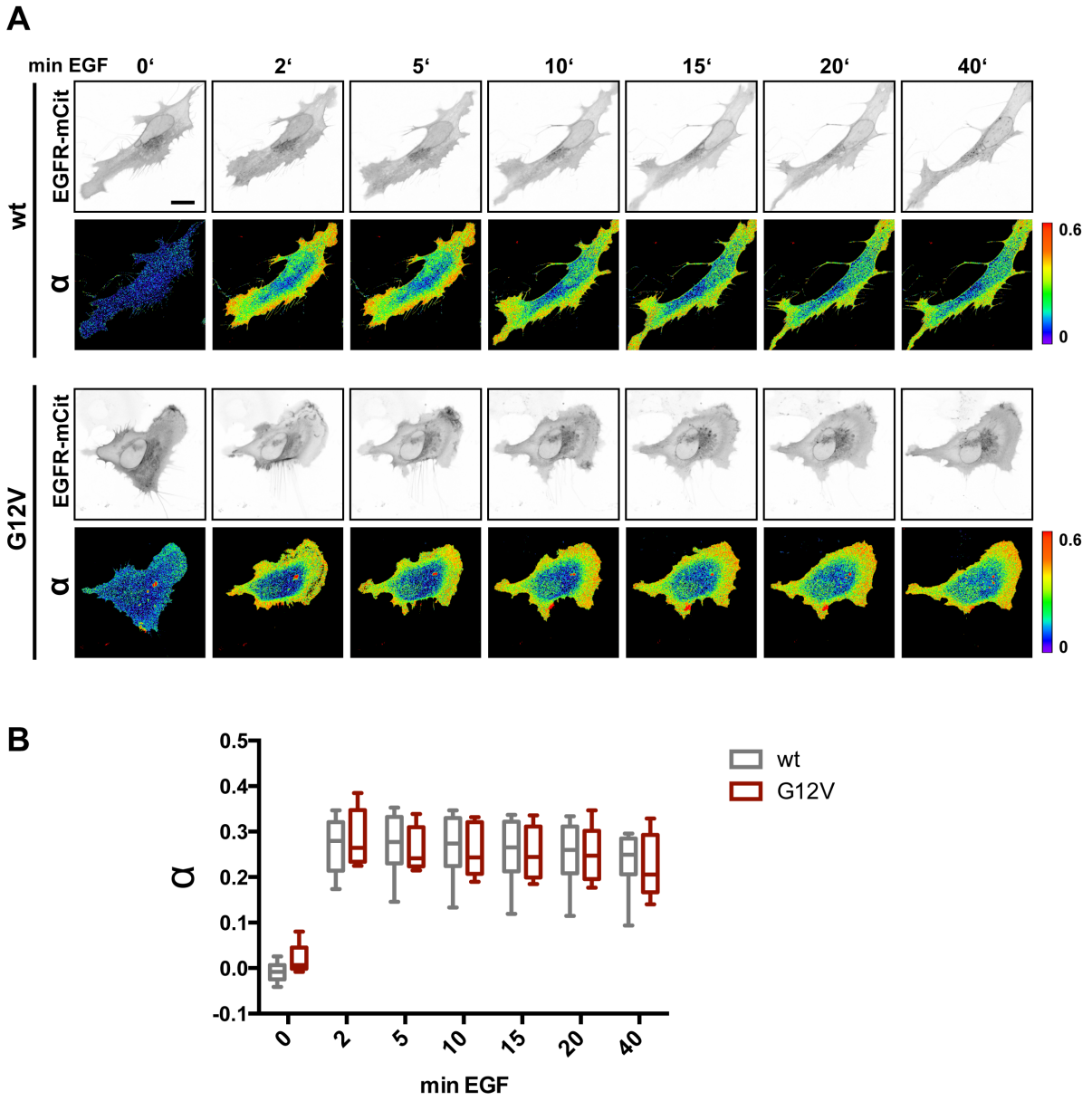

Figure 4.11: Mapping EGFR phosphorylation upon EGF stimulation
(A) FRET-FLIM measurement of the interaction between EGFR-mCitrine (upper row) and PTB-mCherry (not shown) shows spatial activation of the receptor upon EGF stimulation (100 ng/ml) in wt and G12V cells. The fraction of interacting molecules (α) indicates EGFR activity as shown in spatial maps (lower row) Scale bar: 20 µm. **(B)** Box and whiskers graph of data represented in (A); middle line of the box represents median and box extends from the 25th to the 75th percentiles, whiskers indicate min and max values (n_{wt} = 8; n_{G12V} = 6).

Besides higher H_2O_2 level in G12V cells, no significant effect on EGFR phosphorylation was detectable. This raises the question if the production of H_2O_2 upon EGF stimulation is indeed crucial for proper EGFR activation. To test this, we performed the same experiment with inhibition of NOX enzymes by pre-incubation with 10 µM DPI. Again, the receptor gets quickly phosphorylated with the highest activation at the PM decreasing towards the cell nucleus as shown before (Figure 4.12 A). Interestingly, wt cells still show a robust increase in α, whereas EGFR-mCitrine in G12V cells is significantly less phosphorylated when

treated with DPI (Figure 4.12 B). By comparing α from untreated to DPI treated cells, it was even more obvious that NOX inhibition and thus blocking the endogenous H_2O_2 production only decreases EGFR phosphorylation in G12V and not in wt cells (Figure 4.12 C). At all measured time points after EGF stimulation, EGFR-mCitrine was significantly more phosphorylated in untreated G12V cells as in DPI treated cells showing that EGFR activation in these cells is more dependent on H_2O_2 production as in untransformed wt cells.

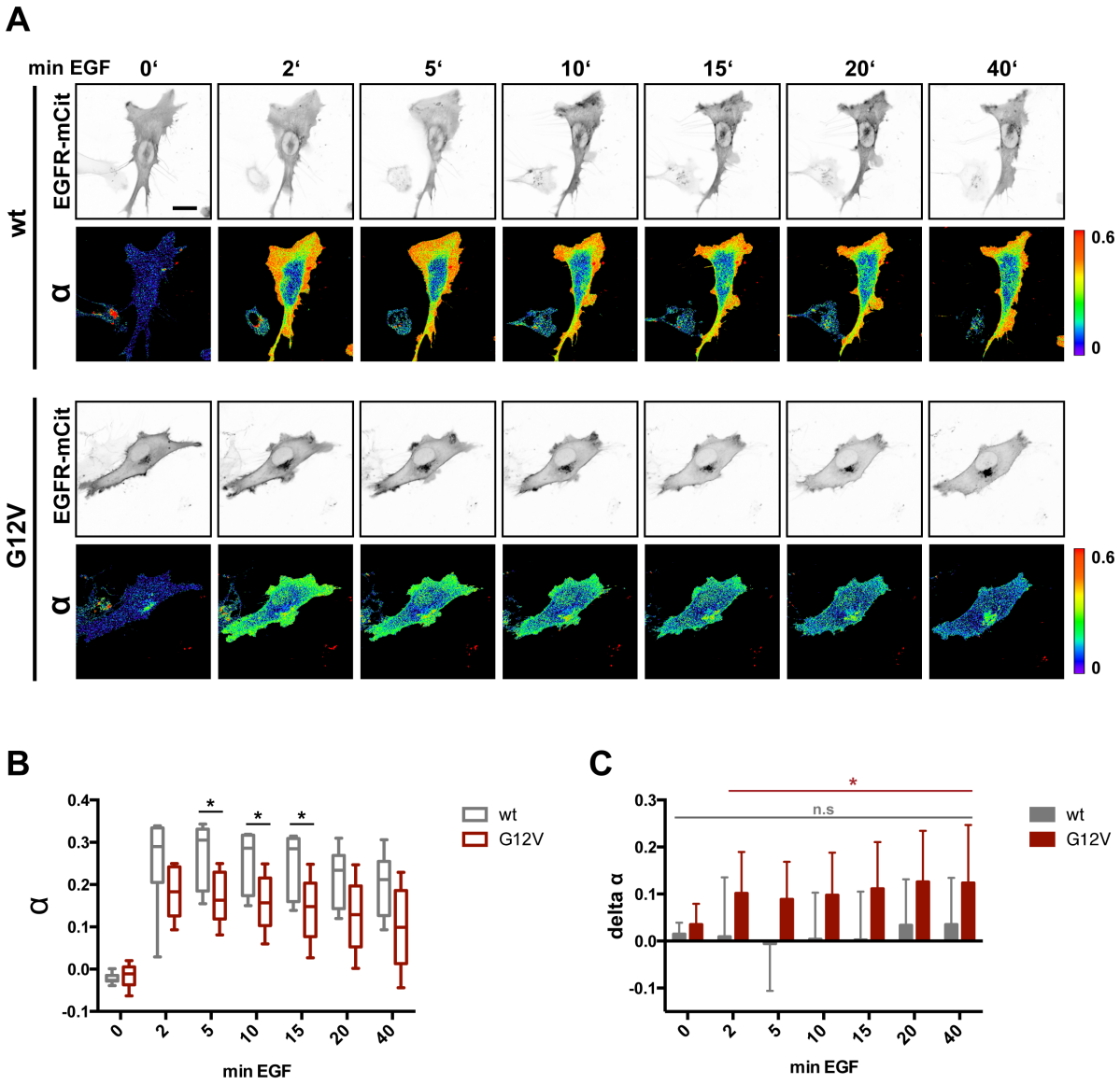

Figure 4.12: EGFR phosphorylation dynamics upon treatment with DPI
(A) FRET-FLIM measurement of the interaction between EGFR-mCitrine (upper row) and PTB-mCherry (not shown) shows spatial activation of the receptor upon EGF stimulation (100 ng/ml) in wt and G12V cells pre-treated with 10 µM DPI. The fraction of interacting molecules (α) indicates EGFR activity as shown in spatial maps (lower row) Scale bar: 20 µm. **(B)** Box and whiskers graph of data represented in (A); middle line of the box represents median and box extends from the 25th to the 75th percentiles, whiskers indicate min and max values (n_{wt} = 7; n_{G12V} = 5). P values obtained by student's t-test; significance level is indicated as follows: $p < 0.05$ (*) **(C)** Bar diagram shows difference between α mean from untreated cells minus α mean from DPI treated cells. Error bars represent SEM; p values obtained by student's t-test; significance level is indicated as follows: $p < 0.05$ (*); n.s. = not significant

To sample more cells and to get a more detailed picture about the spatial regulation of EGFR phosphorylation, we performed FRET-FLIM experiments in fixed cells using PhosTag labeled with Cy3.5 serving as acceptor molecule and again ectopic expression of EGFR-mCitrine as donor molecule. In contrast to PTB, PhosTag binds to all phosphorylated amino acid residues including tyrosines, serines and threonines[127].

BJ cells were again stimulated with 100 ng/ml EGF and α was obtained for pre-stimulated cells and 1 min and 5 min after stimulation (Figure 4.13 A). In line with the live cell experiments, EGFR-mCitrine gets quickly phosphorylated upon EGF stimulation with high activity at the PM that declines towards the cell interior (Figure 4.13 A). To spatially resolve the fraction of phosphorylated EGFR, all cells were segmented into 8 radial profiles by normalizing the distances between the PM and the nuclear membrane (Figure 4.13 B). By plotting the mean α of each radial bin for all measured cells, we could show that EGFR phosphorylation is always highest close to the PM and declines drastically towards the nucleus (Figure 4.13 C). Even in unstimulated cells, in which the overall phosphorylation was relatively low, a weak phosphorylation gradient was detectable for both cell types. Comparison of the spatial EGFR phosphorylation profile of both cell types revealed no difference at early time points after EGF stimulation. Only at basal state, EGFR showed a weak pre-activation in G12V cells that was not apparent in wt cells (Figure 4.13 C). The same trend was detected in the live cell experiments when comparing α values at basal state (Figure 4.11).

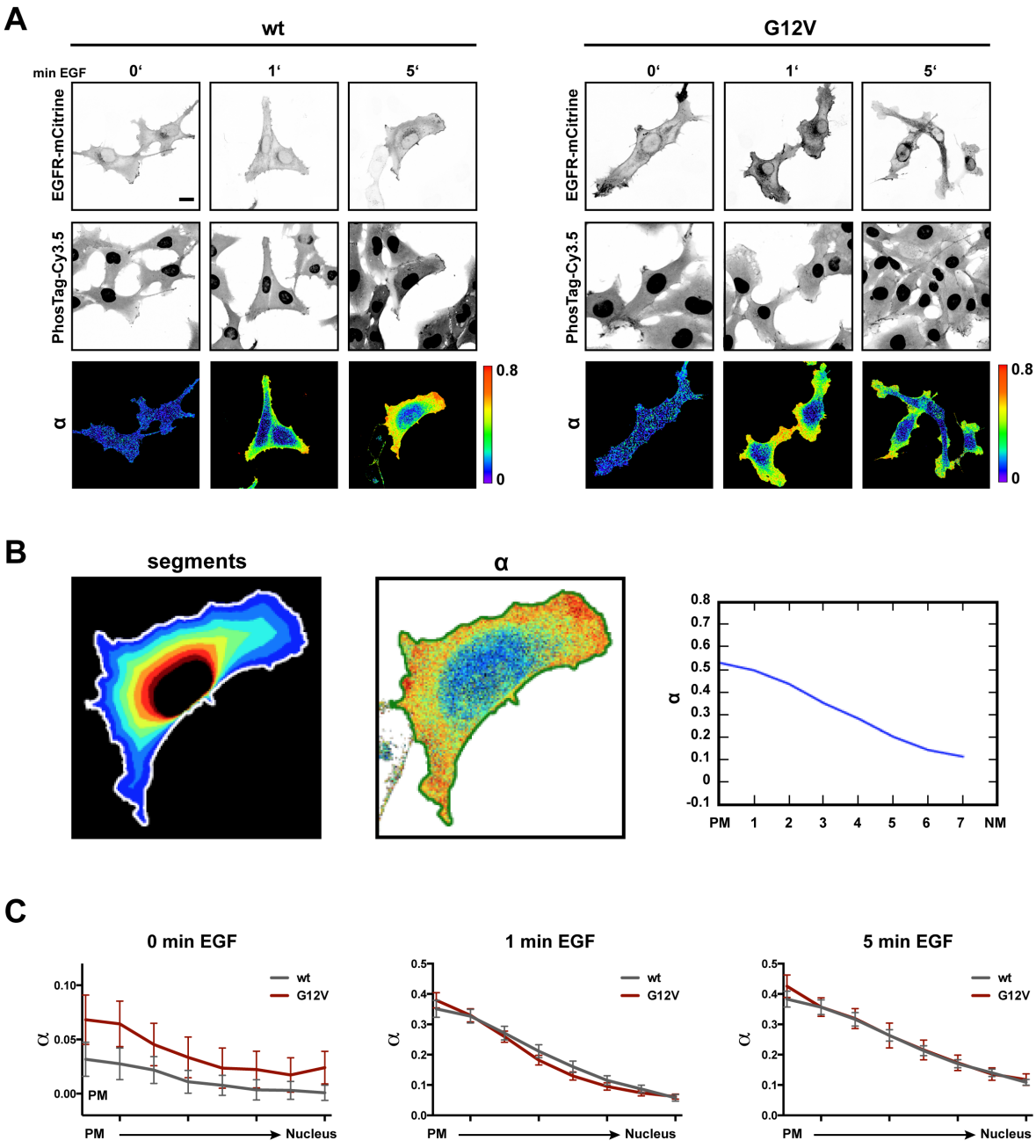

Figure 4.13: Spatial-temporal detection of EGFR-mCitrine phosphorylation
(A) FRET-FLIM measurement of the interaction between EGFR-mCitrine and PhosTag-Cy3.5 detecting EGFR phosphorylation upon EGF stimulation (100 ng/ml) for indicated time points in fixed BJ cells. Left panel shows representative images for wt cells and right panel for G12V cells; upper row: EGFR-mCitrine, middle row: PhosTag-Cy3.5, lower row: spatial distribution of interacting fraction (α). Scale bar: 20 µm **(B)** Presentation of extracting 8 normalized radial profiles from the PM to the nuclear membrane for each cell. Mean α from each bin can then be plotted resulting in a histogram representing α in space per cell **(C)** Graphs show spatial distribution of EGFR phosphorylation for indicated time points after EGF administration for wt and G12V cells. Each point represents mean α ± SEM for at least 17 cells per time point and cell type obtained from 4 independent experiments.

In summary, we could show that the temporal phosphorylation profiles of EGFR are very similar between wt and G12V cells after EGF stimulation. However, EGFR phosphorylation at basal state seems to be increased in G12V cells. In addition, full EGFR activation in G12V cells is more dependent on functional H_2O_2 production as in wt cells.

4.2.2 Autonomous EGFR activation in BJ cells

In addition to ligand-induced EGFR activation, it was also shown that EGFR can be activated in an autonomously, ligand-independent way[86,128]. When EGFR gets activated in the absence of ligand, it is mostly in a monomeric state and fails to form active, asymmetric dimers[80]. This also illustrates that the phosphorylated monomer represents a different signaling entity than the ligand-activated dimer. Since we observed an elevated basal EGFR activation in G12V cells, we investigated ligand-independent, autonomous receptor phosphorylation. Therefore we treated BJ cells with exogenous H_2O_2, which leads to a global oxidation and thus transient inhibition of PTPs resulting in EGFR phosphorylation[86]. EGFR activation was mapped by western blot analysis either by detection of phosphorylated Y1068 (Figure 4.14 B), the binding site for the adaptor protein Grb2, or by detection of the total tyrosine phosphorylation of immunoprecipitated EGFR (Figure 4.14 A). Interestingly, low H_2O_2 doses led to EGFR phosphorylation in G12V cells whereas EGFR phosphorylation in wt cells still remained at basal level. In general, this shows that basal kinase activity of EGFR is sufficient for receptor activation upon PTP inhibition. The threshold for autonomous EGFR activation is lower in G12V cells, possibly provoked by the higher endogenous H_2O_2 level, which are adding up with the extracellular applied H_2O_2 concentrations.

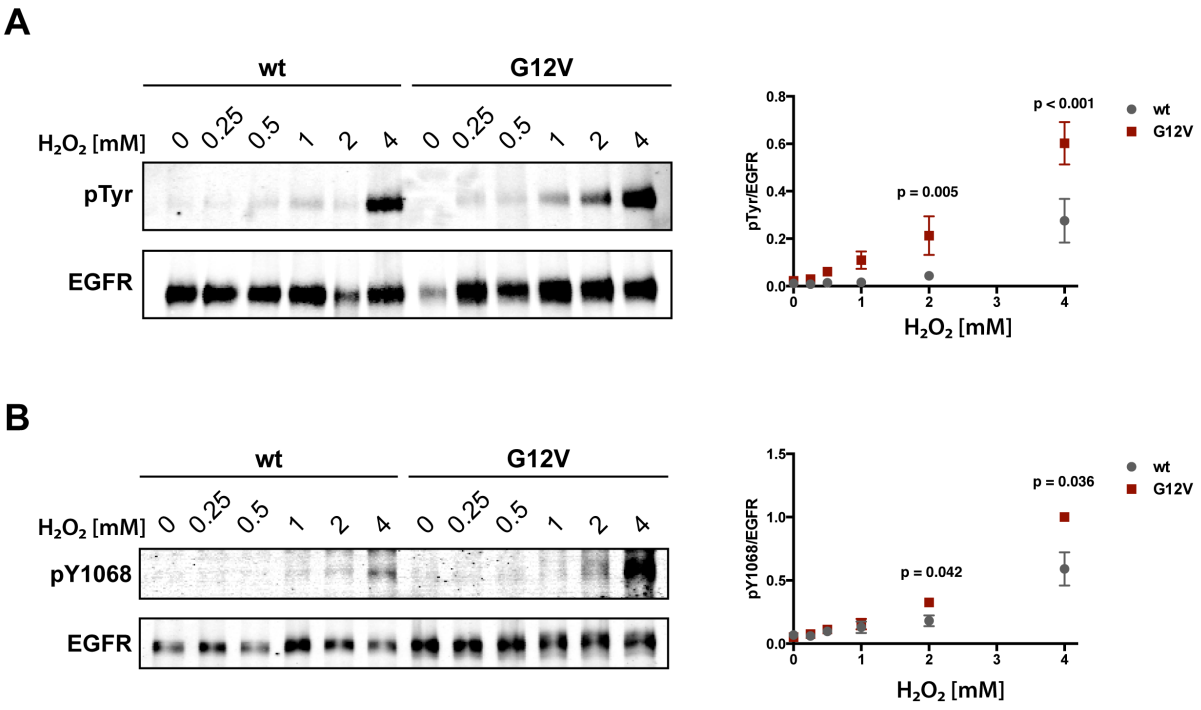

Figure 4.14: Autonomous EGFR activation induced by extracellular H_2O_2
(A) Detection of phosphorylated EGFR by western blot analysis upon treatment with indicated H_2O_2 doses for 5 min. Endogenous EGFR was immunoprecipitated from wt and G12V cell lysates with anti-EGFR antibody and IP was probed with a generic phospho-tyrosine antibody (pY72) and anti-EGFR. Graph on the right shows mean ± SEM of pTyr/EGFR ratio plotted against H_2O_2 dose from three independent experiments. P values were calculated by Student's t test. **(B)** Detection of EGFR's pY1068 by western blot analysis upon treatment with indicated H_2O_2 doses for 5 min. Graph on the right shows mean ± SEM of pY1068/EGFR ratio plotted against H_2O_2 dose from three independent experiments. P values were calculated by Student's t test.

EGFR activation coupled to PTP inhibition by H_2O_2 creates a reaction network that responds in a switch-like manner when treated with a certain threshold concentration of ligand[86]. Stimulation with a saturating EGF concentration did not amplify EGFR phosphorylation in G12V cells, despite higher H_2O_2 levels at basal state (Figure 4.1) and upon EGF stimulation (Figure 4.8). To test if a higher endogenous H_2O_2 concentration in G12V cells decreases PTP activity and thus lowers the activation threshold for EGFR, we performed EGF dose response experiments and analyzed them via western blots (Figure 4.15). In addition to the total tyrosine phosphorylation of EGFR as probed with PY72 antibody, phosphorylation of the binding sites for the E3 ligase c-Cbl (Y1045) and for Grb2 (Y1068) were detected.

Comparison between wt and G12V cells revealed that EGFR phosphorylation as detected by PY72 and pY1045 seems to respond at a lower EGF threshold in wt cells but with a more gradual response (Figure 4.15 A, B). The EGF dose response in G12V cells acts more in switch-like manner as shown by a steeper slope compared to wt cells, both for PY72 and pY0145. Phosphorylation of Y1068 is slightly higher at low doses in G12V cells but activation threshold and phosphorylation level at high doses are nearly the same between both cell types (Figure 4.15 C).

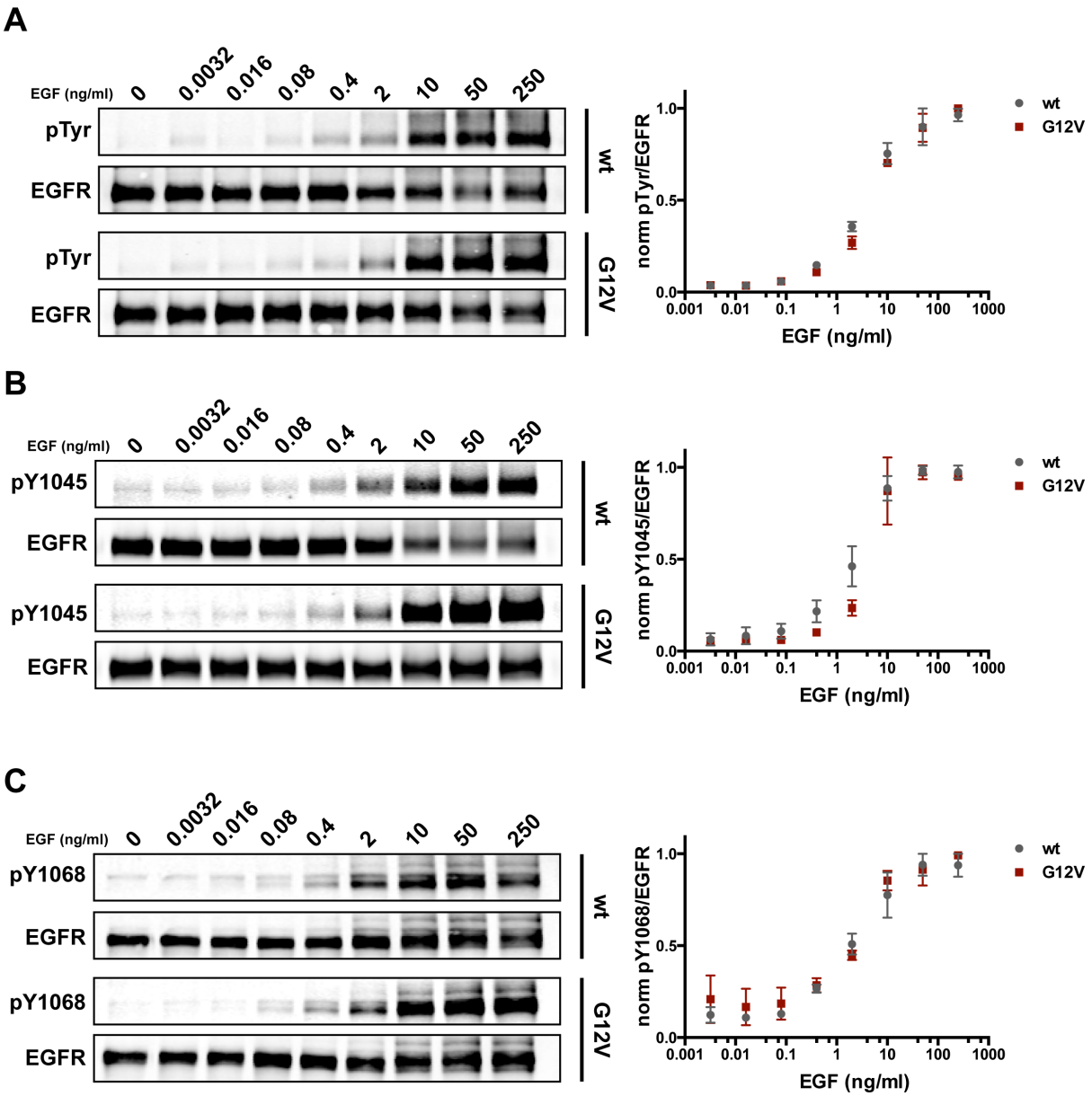

Figure 4.15: EGFR phosphorylation dose response curves in BJ cells
(A) Detection of phosphorylated EGFR by Western blot analysis upon addition of indicated EGF doses for 5 min. Endogenous EGFR was immunoprecipitated from wt and G12V cell lysates with anti-EGFR and IP was probed with a generic phospho-tyrosine antibody (pY72) and anti-EGFR. Graph on the right shows mean ± SEM of pTyr/EGFR ratio plotted against EGF dose from three independent experiments. **(B)** Detection of pY1045 by Western blot analysis upon addition of indicated EGF doses for 5 min. Graph on the right shows mean ± SEM of pY1045/EGFR ratio plotted against EGF dose from two independent experiments. **(C)** Detection of pY1068 by Western blot analysis upon addition of indicated EGF doses for 5 min. Graph on the right shows mean ± SEM of pY1068/EGFR ratio plotted against EGF dose from three independent experiments.

In addition to the biochemical detection of EGFR activation at endogenous level, single cell phosphorylation was analyzed in dependence of the EGFR expression level using immunocytochemistry. Therefore, EGFR-mCitrine was overexpressed in wt and G12V cells and phosphorylation of Y845, Y1045 and Y1068 was visualized with specific antibodies. Both

ligand-independent and EGF-induced receptor activation was investigated and compared between both cell types.

By ectopic expression of EGFR-mCitrine, a wide range of receptor expression levels was generated for both cell types (Figure 4.16 A). Plotting the pY845/EGFRmCitrine fluorescence ratio against EGFR-mCitrine fluorescence intensity showed that a broad range of different EGFR expression levels triggered ligand-independent receptor activation in both cell types with a high cell-to-cell variance (Figure 4.16 B). Upon stimulation with 100 ng/ml EGF for 5 min, relative phosphorylation of Y845 increased, in particular for cells with lower expression levels (Figure 4.16 B). In order to enable a better comparison of these data, values of single cells were binned and averaged for all conditions (Figure 4.16 C). Ligand-independent phosphorylation of Y845 occurred at high receptor expression for wt and G12V cells indicating that at high density EGFR activity overcomes endogenous PTP activity. The correlation of EGFR expression to Y845 phosphorylation was nearly linear and at high receptor expression phosphorylation levels were comparable to that of EGF stimulated cells (Figure 4.16 C). In addition, the relative phosphorylation of Y845 was always elevated in G12V cells when compared to wt cells indicating a lower threshold for autonomous EGFR activation as shown before when cells were treated with exogenous H_2O_2 (Figure 4.14). Upon EGF stimulation, phosphorylation of Y845 was independent of the EGFR expression level for both cell types, showing that ligand stimulation leads to full receptor activation even at low receptor density. Again, the relative phosphorylation was increased in G12V cells compared to wt cells, indicating that autocatalytic activation of EGFR is higher upon EGF stimulation.

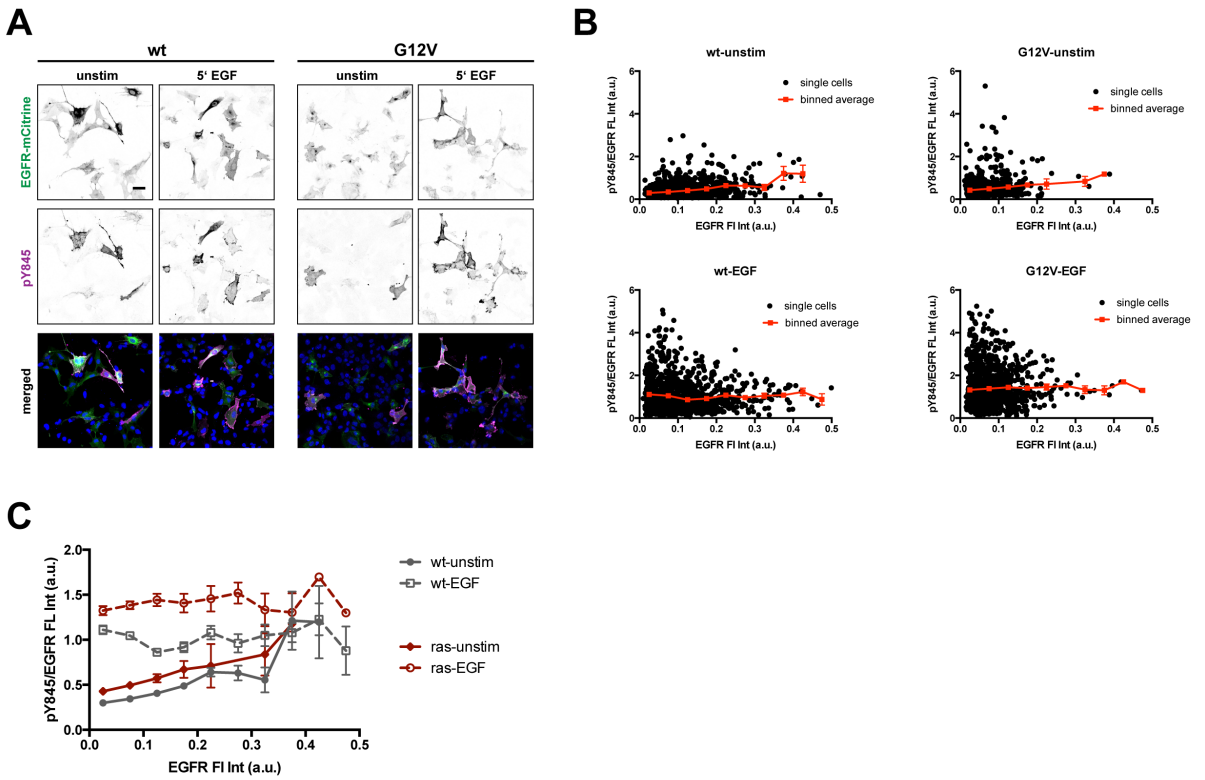

Figure 4.16: Spontaneous and EGF-induced Y845 phosphorylation in response to EGFR expression
(A) Representative images of ligand-independent and ligand-induced Y845 phosphorylation in response to EGFR-mCitrine expression in wt and G12V cells. Upper row shows EGFR-mCitrine fluorescence, middle row pY845 as detected by immunostaining with anti-pY845 antibody and lower row shows merged images. Scale bar: 50 µm **(B)** Single cell data (black dots) and binned averages ± SEM (red line) of immunostaining showed in (A). **(C)** Plot shows binned means ± SEM of single cell data representing relative phosphorylation (mean FI intensity of pY845-antibody/EGFR-mCitrine) of pY845 versus EGFR-mCitrine expression (solid lines: pre-; dashed lines: 5 min post-stimulation with 100 ng/ml EGF)

Autophosphorylation of the tyrosine 1045 triggers c-Cbl binding und thus indicates EGFR ubiquitination, which initiates receptor internalization and degradation[129]. In contrast to Y845 phosphorylation, pY1045 seems to be much more dependent on ligand stimulation. Phosphorylation was clearly higher in EGF treated cells, as obtained from the performed immunostainings (Figure 4.17 A) and single cells analysis (Figure 4.17 B). Even at high receptor expression level, no clear increase in phosphorylation was detectable for unstimulated cells. Upon EGF stimulation, a clear increase of Y1045 phosphorylation was detectable, which is not increasing with higher receptor expression levels (Figure 4.17 B). In addition, relative phosphorylation upon EGF stimulation was again higher in G12V cells as in wt cells. In summary, this indicates that the site Y1045 is not efficiently phosphorylated in the autonomously activated monomer and that EGF stimulation and dimer formation are necessary. Once activated with EGF, Y1045 is more sufficiently phosphorylated in G12V transformed cells.

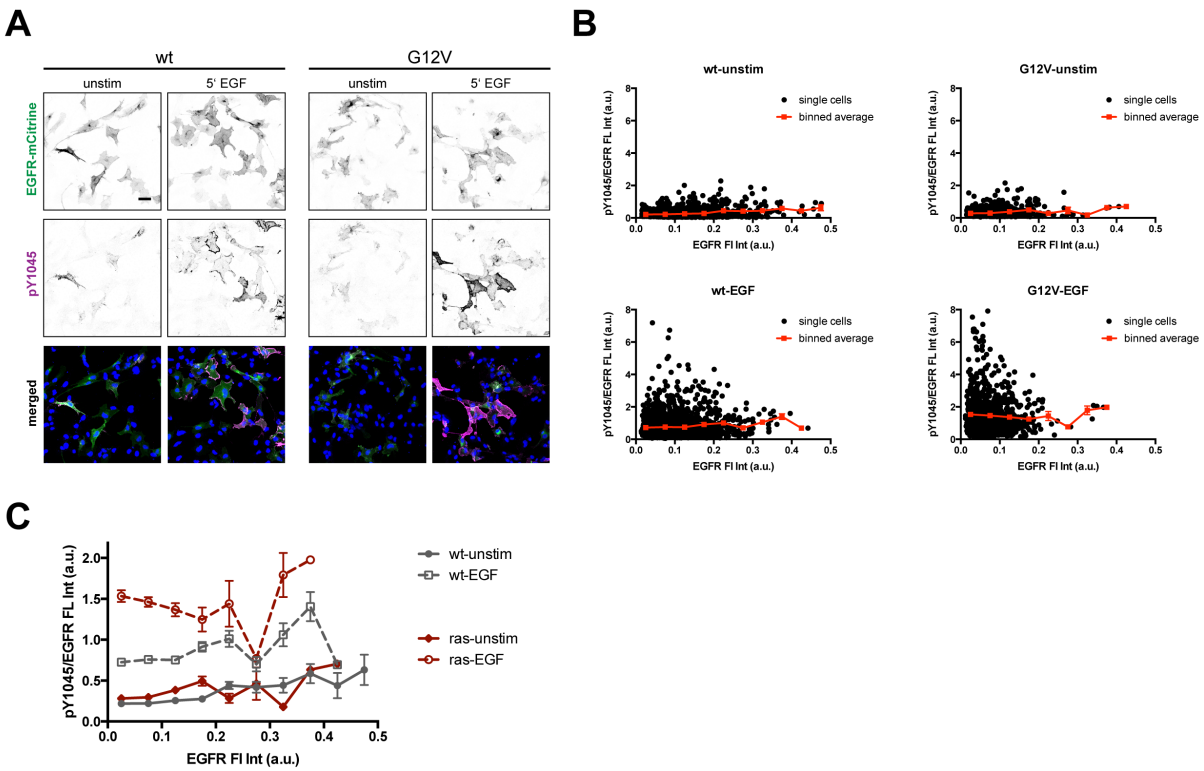

Figure 4.17: Spontaneous and EGF-induced Y1045 phosphorylation in response to EGFR expression
(A) Representative images of ligand-independent and ligand-induced Y1045 phosphorylation in response to EGFR-mCitrine expression in wt and G12V cells. Upper row shows EGFR-mCitrine fluorescence, middle row pY1045 as detected by immunostaining with anti-pY1045 antibody and lower row shows merged images. Scale bar: 50 µm **(B)** Single cell data (black dots) and binned averages ± SEM (red line) of immunostaining showed in (A). **(C)** Plot shows binned means ± SEM of single cell data representing relative phosphorylation (mean Fl intensity of pY1045-antibody/EGFR-mCitrine) of pY1045 versus EGFR-mCitrine expression (solid lines: pre-; dashed lines: 5 min post-stimulation with 100 ng/ml EGF)

Phosphorylation of the EGFR site Y1068 serves as docking site for the adaptor protein Grb2, which transduces the signal from the activated receptor to several downstream molecules such as Ras[91]. In unstimulated cells, the phosphorylation level of Y1068 increased in dependence of the EGFR expression level in both cell types but more pronounced in G12V cells (Figure 4.18 B). Unfortunately, the number of cells with high expression level was low so that data became noisy. Anyways, G12V cells showed clearly a higher Y1068 phosphorylation than wt cells at low EGFR expression levels in the absence of ligand (Figure 4.18 C). When stimulated with EGF, Y1068 was more efficiently phosphorylated at low EGFR expression levels in G12V cells. In contrast, both cell types showed a similar phosphorylation ratio at higher receptor expression levels indicating saturation.

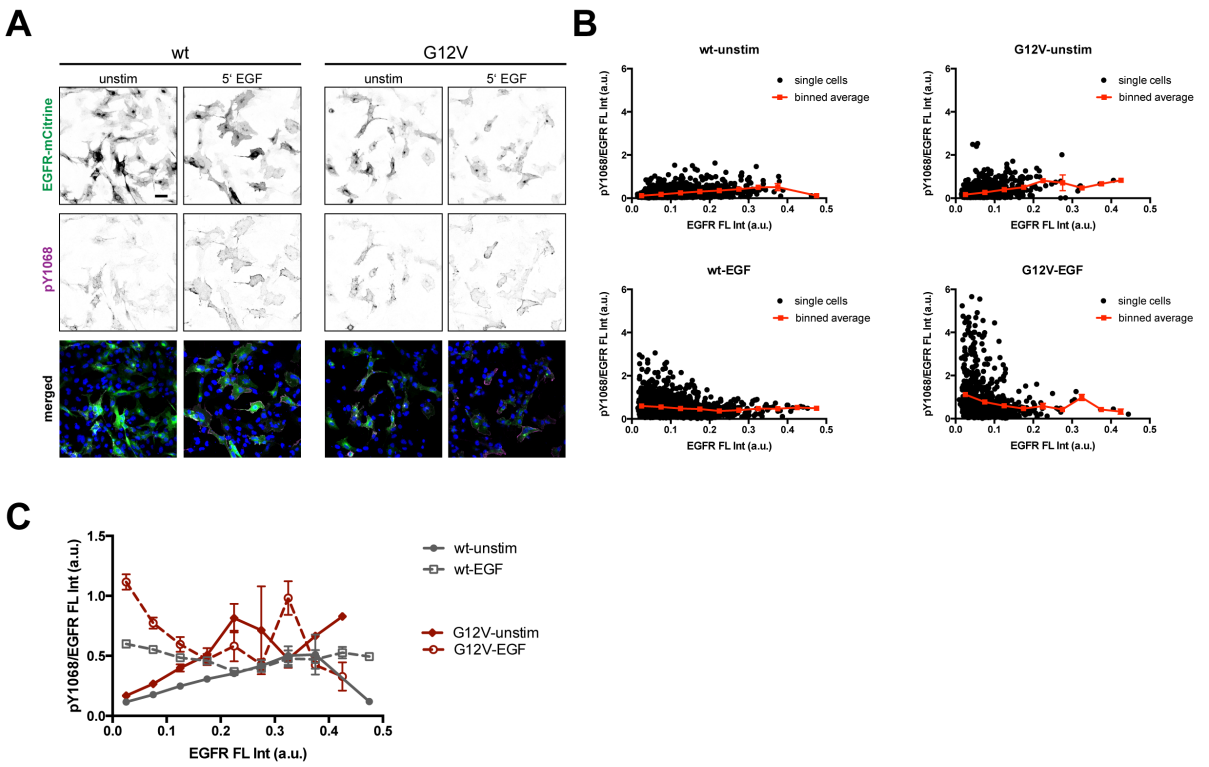

Figure 4.18: Spontaneous and EGF-induced Y1068 phosphorylation in response to EGFR expression
(A) Representative images of ligand-independent and ligand-induced Y1068 phosphorylation in response to EGFR-mCitrine expression in wt and G12V cells. Upper row shows EGFR-mCitrine fluorescence, middle row pY1068 as detected by immunostaining with anti-pY1068 antibody and lower row shows merged images. Scale bar: 50 µm **(B)** Single cell data (black dots) and binned averages ± SEM (red line) of immunostaining showed in (A). **(C)** Plot shows binned means ± SEM of single cell data representing relative phosphorylation (mean Fl intensity of pY1068-antibody/EGFR-mCitrine) of pY1068 versus EGFR-mCitrine expression (solid lines: pre-; dashed lines: 5 min post-stimulation with 100 ng/ml EGF)

In summary, we could show that the activation threshold for EGF-independent receptor activation is lower in HRas G12V transformed cells when compared to wt cells when treated with H_2O_2 or by ectopic expression of EGFR-mCitrine. Interestingly, phosphorylation of different tyrosine residues varied in their ability to get phosphorylated in the absence of ligand indicating the distinct regulation of phosphorylation and dephosphorylation of those sites. When stimulated with increasing concentrations of EGF both cell types showed an ultrasensitive phosphorylation response for all investigated tyrosine residues.

4.2.3 Activation of downstream effector molecules

It has been shown that autonomously activated EGFR represents a different signaling entity than ligand activated EGFR. In general, EGFR signal transduction mainly activates the PI3K-AKT and Ras-ERK signaling cascades, whereby ligand-activated receptors activate both pathways and monomeric EGFR was shown to only signal via AKT[80]. Thus, we detected

activation of ERK and AKT in BJ cells at basal state and upon EGF stimulation with a saturating EGF dose (50 ng/ml) in whole cell lysates via western blot analysis. In unstimulated cells phospho-ERK was slightly higher in G12V cells, which is rather evoked through oncogenic Ras signaling itself than activated EGFR[130] (Figure 4.19 A). When stimulated with EGF, both cell types showed nearly the same activation level of ERK consistent with similar Y1068 phosphorylation, the GRB2-binding site initiating ERK activation (Figure 4.10). Activation of AKT did not differ between wt and G12V cells at basal state. But G12V cells showed an elevated AKT phosphorylation in comparison to wt cells when stimulated with EGF (Figure 4.19 B).

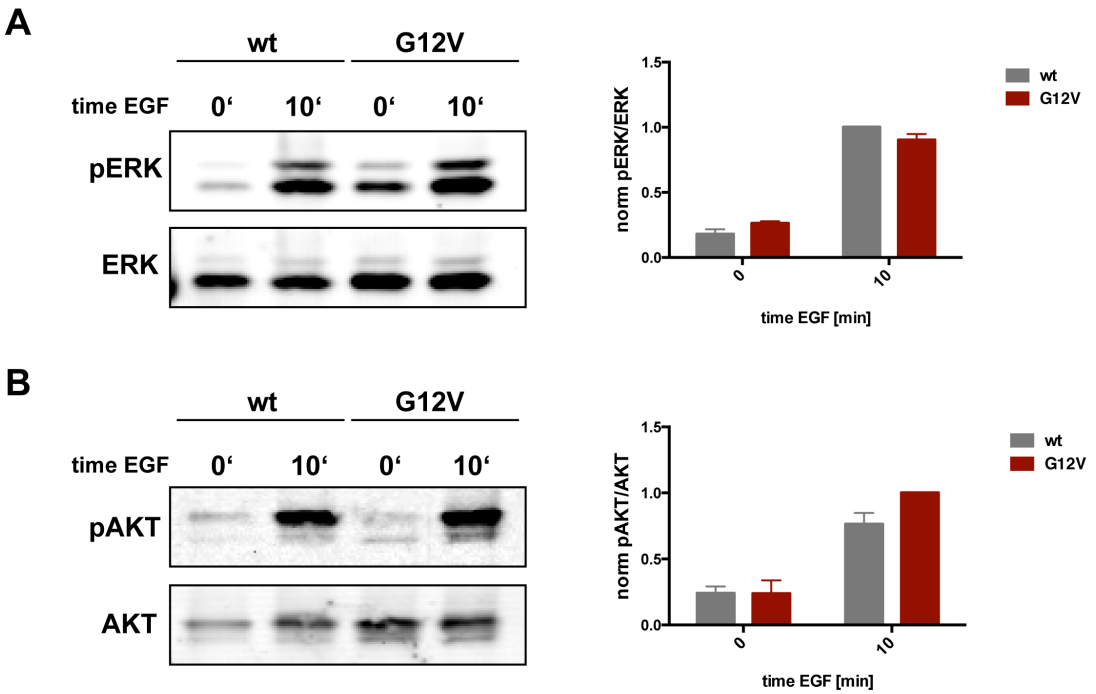

Figure 4.19: Basal and EGF-evoked phosphorylation of EGFR downstream effectors
(A) Left panel shows representative western blot images of ERK phosphorylation detected at basal level and upon EGF stimulation (50 ng/ml) for 10 min in BJ whole cell lysates. Right panel shows mean of pERK over total ERK ± SEM for two independent experiments. **(B)** Left panel shows representative western blot images of AKT phosphorylation detected at basal level and upon EGF stimulation (50 ng/ml) for 10 min in BJ whole cell lysates. Right panel shows mean of pAKT over total AKT ± SEM for two independent experiments.

Since AKT activation is important for intracellular ROS activation and is thought to only occur at the plasma membrane[131-133], we performed EGF dose response experiments and monitored downstream phospho-AKT. Interestingly, the activation profile of AKT differed significantly from the corresponding phospho-EGFR profile in both wt and G12V cells (Figure 4.20). AKT activation in wt cells peaked already at an EGF concentration of 2 ng/ml and decreased at higher doses by following rather an unsymmetrical Gaussian than a

sigmoidal curve as obtained for phospho-EGFR. In contrast, AKT activation in G12V cells plateaued between 2 and 10 ng/ml EGF and did not show a significant decrease at higher EGF concentrations (Figure 4.20). This is in line with the before performed experiment, where AKT phosphorylation was higher in G12V cells as in wt cells when stimulated with a saturating EGF concentration (Figure 4.19). In summary, AKT activation in wt cells was higher at low doses of EGF when mainly monomers are activated at the PM and internalization is not accelerated by ubiquitination. At higher EGF doses, AKT activation decreased possibly through increased internalization of phospho-EGFR dimers and a shift to ERK activation. This is contrary to AKT activation in G12V cells. Here, we found that AKT phosphorylation stays relatively low until the threshold EGF concentration of 2-10 ng/ml is reached, where AKT reaches full activation. Higher EGF concentrations did not lead to a decreased AKT activation as shown for wt cells.

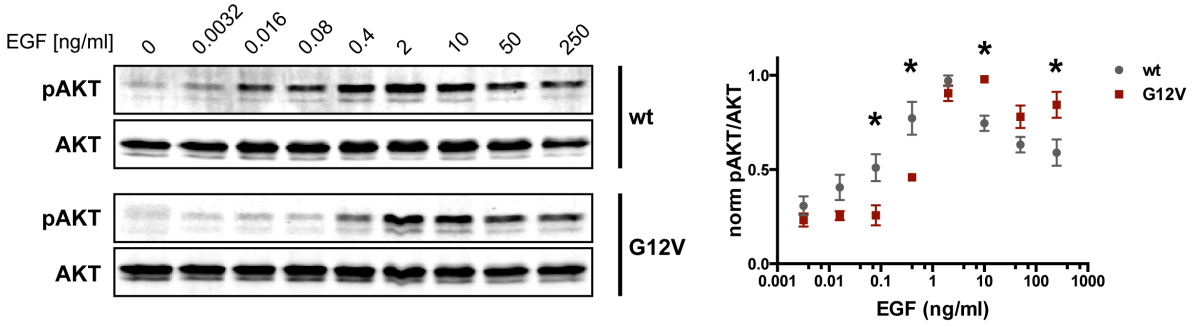

Figure 4.20: AKT phosphorylation profile upon stimulation with different EGF doses
Detection of phosphorylated AKT by Western blot analysis upon addition of different EGF doses for 5 min in BJ cells. Graph on the right shows mean ± SEM of pAKT/AKT ratio plotted against EGF dose from four independent experiments. Significance level is indicated as follows: $p < 0.05$ (*)

4.3 Oxidation of PTPs

In summary, we could show that oncogenic HRas G12V leads to an increased production of H_2O_2 at basal level and upon EGF stimulation. This leads to an increased autonomous EGFR activation in HRas G12V transformed cells and is necessary for cellular survival/proliferation and full receptor activation in EGF stimulated cells. EGF time and dose response experiments upon EGF stimulation were similar between both cell types but G12V cells were more susceptible for autonomous EGFR activation as on the one hand shown by H_2O_2 treatment and on the other hand by the dependency of phospho-EGFR on the EGFR expression level. Since high levels of H_2O_2 can affect EGFR activation mainly through the

double negative feedback created by PTP oxidation, we wanted to assess this coupling more in detail and how it can influence the responsiveness of the EGFR system.

4.3.1 Detection of PTP oxidation

Generation of H_2O_2 leads to changes in signaling events by chemoselective oxidation of cysteine residues in proteins thereby altering their activity status. It is well established that classical PTPs, as counterparts of RTK signaling, are one of the major targets of H_2O_2 signaling[134]. Oxidation of the catalytic cysteine in the PTPs active site leads to the inhibition of protein activity[42]. Here we used dimedone-derivatization of sulfenic acid, the first intermediate generated by H_2O_2, to monitor protein oxidation. First, we treated the catalytic domain of PTP1B (PTP1Bc) *in vitro* with increasing H_2O_2 concentrations either in the presence of dimedone or DMSO. Subsequent visualization by western blots and incubation with anti-dimedone antibody[62] showed that PTP1B indeed can be oxidized and that oxidation increases significantly with higher H_2O_2 concentrations (Figure 4.21). In contrast to dimedone, DMSO incubation didn't give a significant signal proving that dimedone binds to oxidized PTP1Bc and can be visualized with the anti-dimedone antibody.

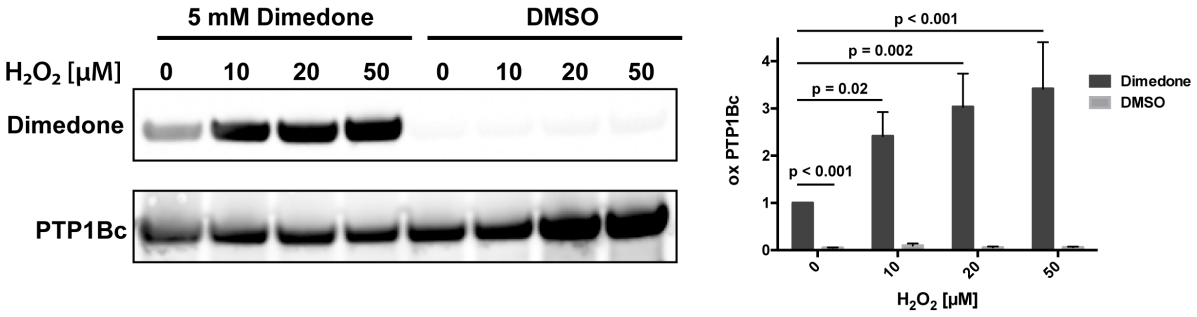

Figure 4.21: Oxidation of the catalytic domain of PTP1B *in vitro*
Catalytic domain of PTP1B (PTP1Bc) was treated with indicated concentrations of H_2O_2 in the presence of 5 mM dimedone or the equivalent volume DMSO. Fractions of oxidized PTP1Bc (right graph) were analyzed by western blot with the α-dimedone antibody. Graph shows mean ± SEM of dimedone/PTP1B ratio from three independent experiments. P values for comparison between dimedone and DMSO were calculated by Student's t test otherwise with two-way ANOVA.

Next, we sought to test if this approach is also suitable for the detection of oxidized proteins in cells. Therefore, BJ wt cells were treated with 1mM H_2O_2 either in the presence of dimedone or DMSO. To test how efficient Dimedone enters the cells and binds sulfenic acid, we used an incubation time of 10 min and 30 min and detected oxidation subsequently via western blot. As shown before in the *in vitro* assay, DMSO incubation just gave a minor

background signal, which indicates a low unspecific binding of the antibody and only incubation with dimedone led to a detectable signal (Figure 4.22 A). Incubation of 30 min and stimulation with 1 mM H_2O_2 gave a higher signal, due to the accumulation of oxidized proteins by the irreversible reaction with dimedone. Equal loading of protein was confirmed by detection of the housekeeping protein GAPDH (Figure 4.22 A). Since detection of sulfenic acid in whole cell lysates gives a signal for all oxidized proteins in the cell, we performed immunoprecipitation experiments for endogenous PTP1B and checked for its oxidation. Treatment with H_2O_2 led to a recognizable band shift when incubated with an antibody against PTP1B and incubation with dimedone gave a detectable band for sulfenic acid (Figure 4.22 B). Dimedone was incubated for either 10 min or 30 min on cells but for PTP1B oxidation no significant difference was detectable. Therefore, dimedone was incubated on living cells for 10 min in all further experiments since the shorter incubation time matches also better with the quick accumulation of EGF-evoked H_2O_2 (Figure 4.7, Figure 4.8).

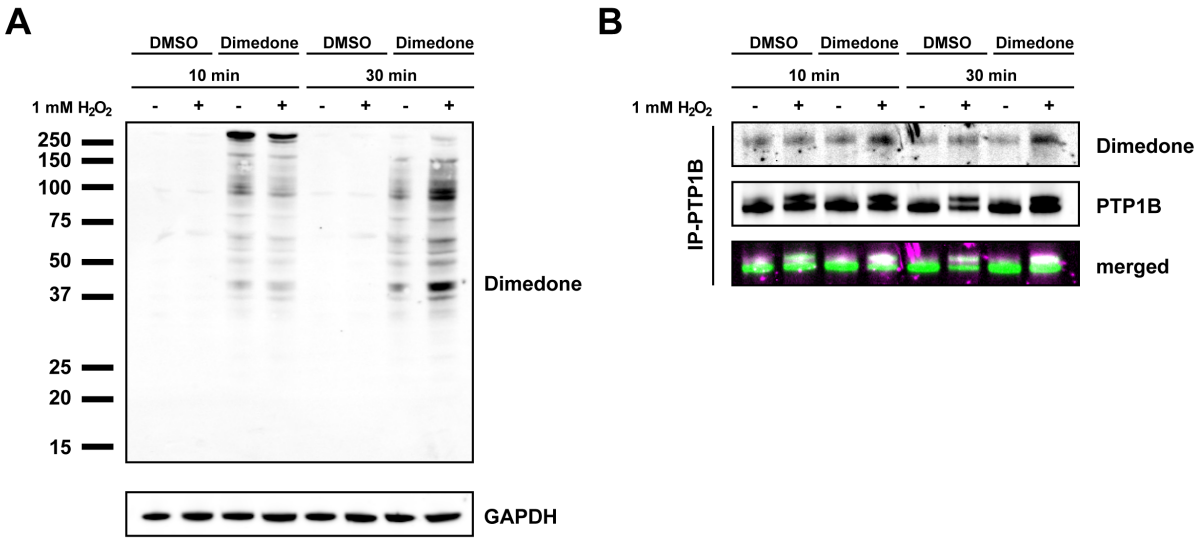

Figure 4.22: Detection of dimedone-derivatized proteins in BJ cells
(**A**) Detection of oxidized proteins in whole cell lysates of BJ cells treated as indicated. Oxidation of proteins was determined by western blot and incubation with the anti-dimedone antibody. Equal loading of proteins was confirmed with anti-GAPDH antibody. **(B)** IP of endogenous PTP1B from BJ cell lysates treated as indicated and probed with anti-dimedone and anti-PTP1B antibody.

We continued to investigate overexpressed PTP1B-mCitrine and SHP2-mCitrine, two PTPs that are known to be oxidized[40], and used dimedone for detection of sulfenic acid formation in BJ wt and G12V cells. Ectopic phosphatase expression has the advantage to be more independent in choosing antibodies due to the possibility of detecting both PTPs with

an anti-GFP antibody. In addition, a high expression level of each PTP increases substrate availability for oxidation, optimizing the signal-to-noise ratio.

First, PTP1B-mCitrine was investigated since we detected PTP1B oxidation already *in vitro* and *in vivo*. As before, treatment with H_2O_2 induced an increase in the appearing dimedone bands indicating the formation of sulfenic acid for several proteins. GAPDH, a protein highly susceptible for non-GF evoked oxidation[135], shows a high increase in oxidation for both cell types independently of PTP1B-mCitrine or SHP2-mCitrine overexpression (Figure 4.23). This proves that the here-used assay works for the detection of protein oxidation in general. The dimedone signal for PTP1B-mCitrine is lower than for GAPDH but the ratio of total over oxidized protein revealed a robust increase upon H_2O_2 treatment in both cells with a lower threshold in G12V cells (Figure 4.23 A). Detection of SHP2-mCitrine oxidation showed a similar trend but a higher fold-increase when compared to PTP1B-mCitrine oxidation (Figure 4.23 B).

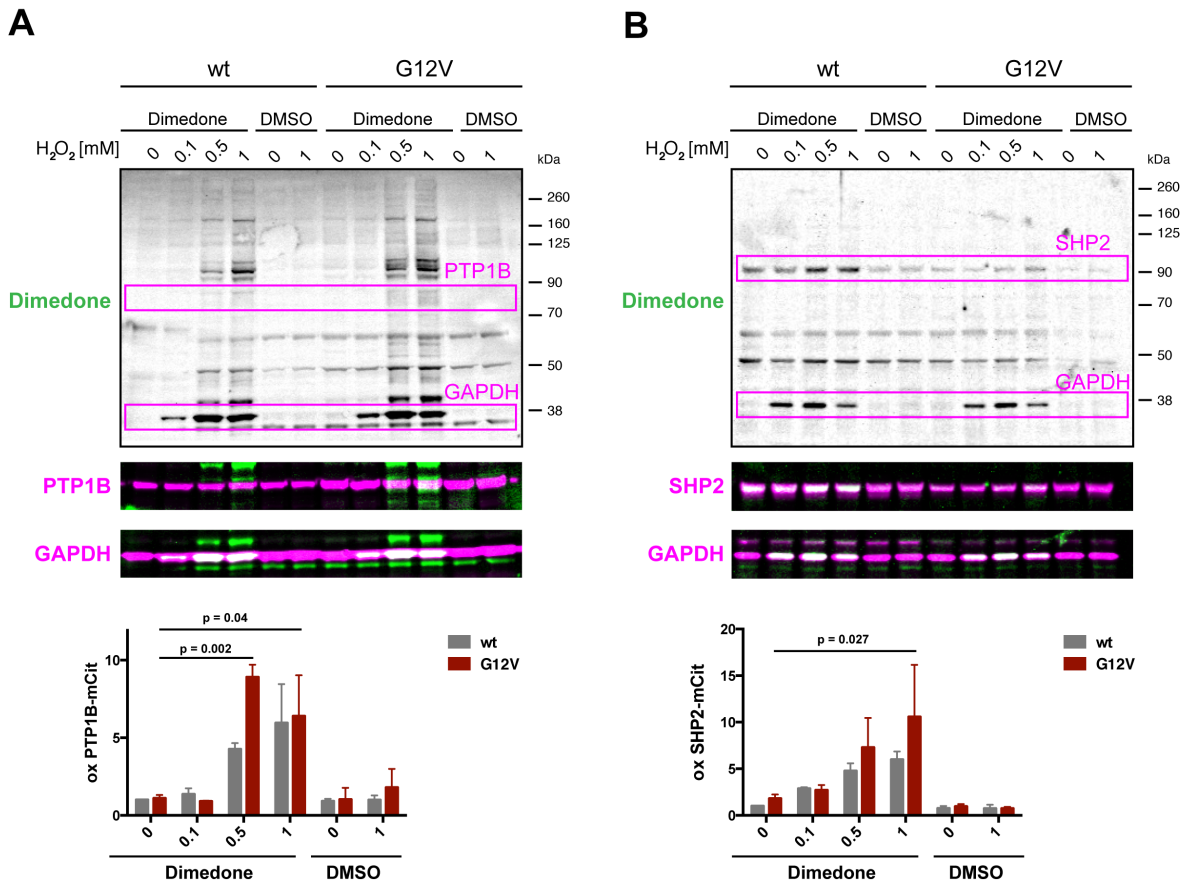

Figure 4.23: Oxidation of ectopically expressed PTPs in BJ cells
(A) Western blot analysis of oxidized proteins in BJ whole cell lysates overexpressing PTP1B-mCitrine. Upper image shows total oxidation as detected by incubation with anti-dimedone antibody; a pink box marks PTP1B-mCitrine and GAPDH bands. Middle and lower image shows merged bands of anti-dimedone overlaid with anti-GFP detecting PTP1B-mCitrine and anti-GAPDH, respectively. Lower panel shows means ± SEM of relative

increase of PTP1B-mCitrine oxidation for two independent experiments. P values were calculated via two-way ANOVA. **(B)** Western blot analysis of oxidized proteins in BJ whole cell lysates overexpressing SHP2-mCitrine. Upper image shows total oxidation as detected by incubation with anti-dimedone antibody; a pink box marks SHP2-mCitrine and GAPDH bands. Middle and lower image shows merged bands of anti-dimedone overlaid with anti-GFP detecting SHP2-mCitrine and anti-GAPDH, respectively. Lower panel shows means ± SEM of relative increase of SHP2-mCitrine oxidation for two independent experiments. P values were calculated via two-way ANOVA.

However, detection of oxidized PTPs in blots with the anti-dimedone antibody gave quite noisy signals, most likely caused by different expression levels, variations in the dimedone reaction and the unspecificity of antibody binding. In order to improve detection of oxidized proteins, we tested dimedone analogues, which are linked to different functional groups that allow alternative detection methods. First, we tested DCP-Bio1, a biotinylated derivative of Dimedone[60]. As before, recombinant PTP1Bc was used for *in vitro* oxidation and subsequent labeling with DCP-Bio1. The labeling reaction was quantified via western blot by coupling to IR-labeled Streptavidin (STV), which is comparable to immunodetection with IR-labeled secondary antibodies used before. In contrast to the reaction with unmodified dimedone, DCP-Bio1 did not show an increase in signal when PTP1Bc was incubated with increasing H_2O_2 concentrations (Figure 4.24 A). We speculated that increased affinity of the biotin-streptavidin binding saturated the signal already without addition of H_2O_2 so that a further increase upon oxidation was not detectable. Therefore, DCP-Bio1 concentration was lowered to 1 mM and 0.5 mM and oxidation was again detected via labeled-Streptavidin. However, even the lower DCP-Bio1 concentrations gave a high background signal and no increase was measured upon treatment with H_2O_2 (Figure 4.24 B).

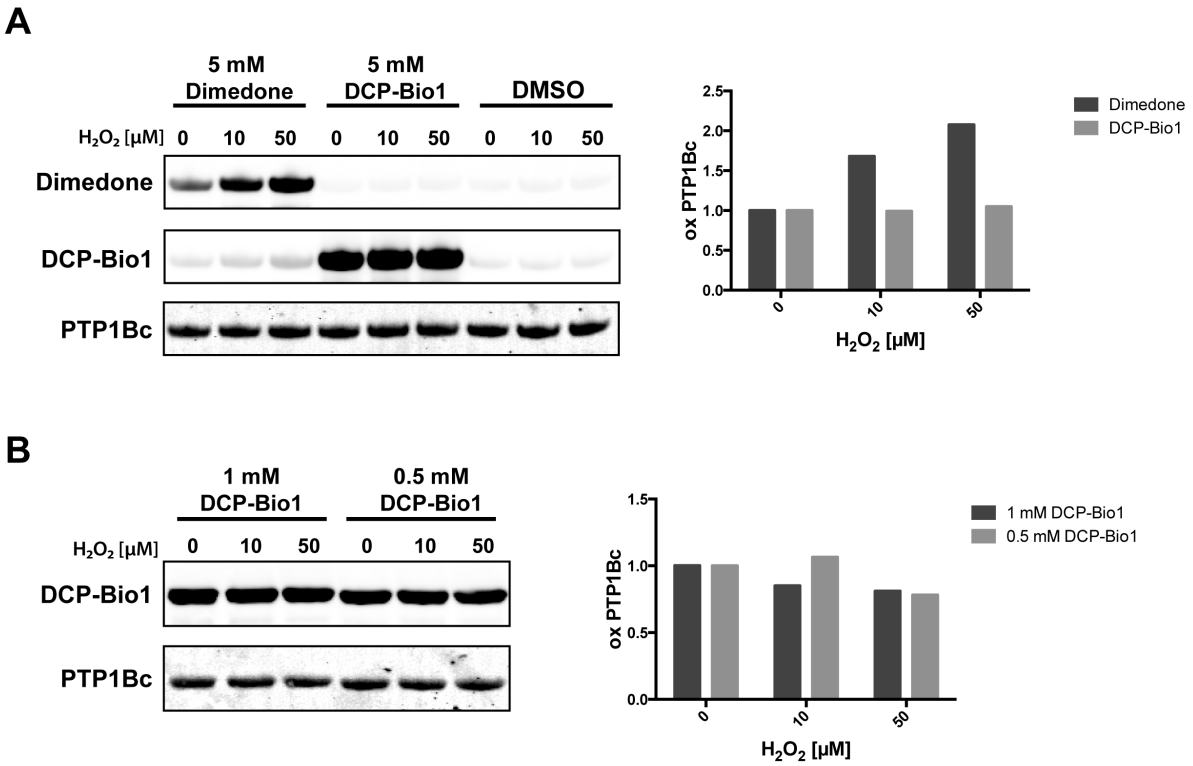

Figure 4.24: Testing different dimedone variants for protein oxidation *in vitro*
(A) PTP1Bc was treated with indicated concentrations of H_2O_2 in presence of 5 mM dimedone, 5 mM DCP-Bio1 or the equivalent volume DMSO. Fractions of oxidized PTP1Bc (right graph) were analyzed by Western blot with the anti-dimedone antibody or IRDye-800 STV. Graph on the right shows mean ± SEM of dimedone/PTP1Bc ratio from one experiment. **(B)** Western blot of PTP1Bc treated as indicated and incubated with different DCP-Bio1 concentrations for detection of oxidation. Labeling of DCP-Bio1 was detected with IRDye-800 STV. Graph on the right shows mean ± SEM of DCP-Bio1/PTP1Bc ratio from one experiment.

Since *in vitro* oxidation of PTP1Bc is really fast and the required H_2O_2 concentration and reaction time are not comparable to oxidation dynamics in cells, we repeated the DCP-Bio1 experiment in BJ cells. Unmodified dimedone and detection with anti-dimedone antibody was used as positive control to ensure that protein oxidation has worked. As for PTP1Bc, again no increase in the DCP-Bio1-STV signal was detectable upon treatment with 1 mM H_2O_2 in both cell lines (Figure 4.25 A). In contrast, the anti-dimedone signal and in particular the 37 kDa band corresponding to GAPDH increased upon treatment with H_2O_2 indicating that protein oxidation upon administration of H_2O_2 took place. Since we wanted to investigate oxidation of proteins in a spatial-temporal manner, we continued with *in situ* experiments. Therefore, BJ cells were incubated with 10 µM DCP-Bio1, followed by staining of the compound after fixation with Cy3.5-labeled STV. We speculated that Cy3.5 intensity increases upon treatment with H_2O_2 or EGF but high background staining of the nucleus and intracellular membranes made a comparison based on fluorescence intensity infeasible (Figure 4.25 B). For a quantitative analysis, we moved to a FRET-FLIM approach based on

overexpression of PTP1B-mCitrine in BJ wt cells. Although we could detect a lifetime decrease upon incubation with STV-Cy3.5 in comparison to the donor only control, this effect seems to be independent of protein oxidation since incubation with STV-Cy3.5 in the absence of DCP-Bio1 gave the same staining pattern and comparable lifetime values (Figure 4.25 C). Thus, we concluded that DCP-Bio1 is not working for the detection of oxidized PTPs and in addition, in-cell staining with labeled STV is not suitable for further experiments due to high background staining.

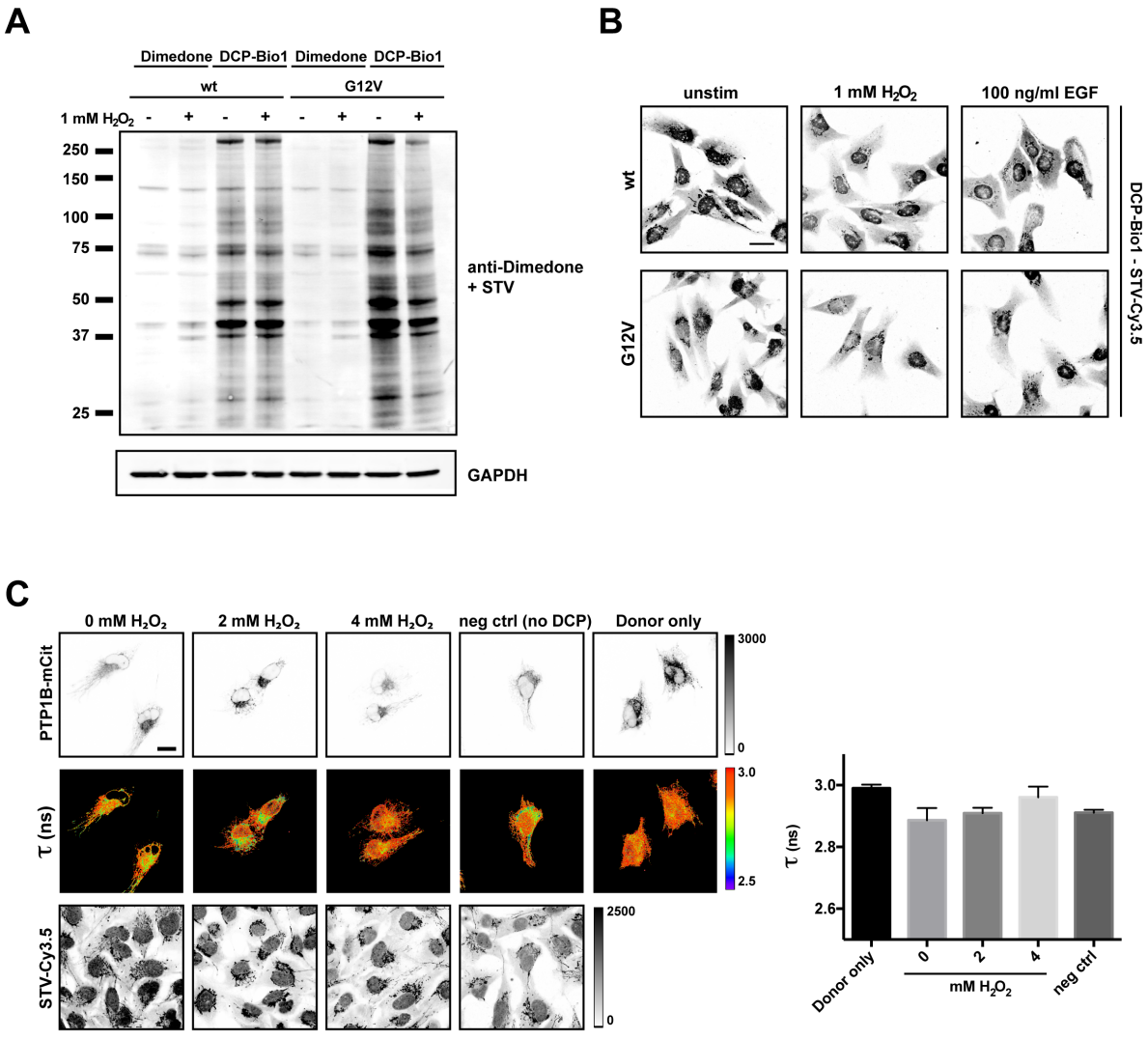

Figure 4.25: Testing DCP-Bio1 for detection of protein oxidation
(A) Western blot of BJ total cell lysates comparing detection of oxidized proteins with either dimedone (5 mM) or DCP-Bio1 (5 mM) in cells treated as indicated. Dimedone-derivatized proteins were detected with anti-dimedone antibody and DCP-Bio1-derivatized proteins with IRDye800-labeled STV. Equal protein loading was ensured with anti-GAPDH detection. **(B)** Staining of BJ cells treated as indicated with Cy3.5 labeled STV upon incubation with DCP-Bio1. Scale bar 30 µm **(C)** FRET-FLIM of PTP1B-mCitrine and DCP-Bio1 labeled with Cy3.5 tagged STV in BJ wt cells treated as indicated. Left panel shows means ± SEM for 4-5 cells per condition. Scale bar: 30 µm

To overcome the problem of unspecific STV-Cy3.5 binding to endogenous proteins and membranes, we tested a dimedone analogue, which is directly labeled with the fluorescent dye Rhodamine called DCP-Rho1[60]. This probe is cell-permeable and thus incubation on living cells without prior fixation or permeabilization, which would disrupt the cellular redox state, can be retained. Moreover, Rhodamine has a similar fluorescence spectrum as Cy3.5, which makes it also suitable as acceptor molecule for mCitrine-tagged proteins. First, we tested DCP-Rho1 in a simple staining experiment, in which BJ wt cells were treated with different H_2O_2 concentrations or pre-treated with DPI (Figure 4.26 A). Incubation of cells with DCP-Rho1 still led to a distinct staining of endomembranes but unlike to DCP-Bio1 labeled with STV-Cy3.5 staining intensity increased with H_2O_2 treatment indicating a higher abundance of oxidized proteins (Figure 4.25 B). For quantification, we tested DCP-Rho1 in a FRET-FLIM approach in H_2O_2 treated cells. The cytoplasmic PTP SHP2-mCitrine was used as donor molecule, which did not co-localize with the DCP-Rho1 on endomembranes like PTP1B lowering the chance of unspecific FRET. Since cells were fixed, we performed acceptor-photobleaching to reveal the possible FRET between DCP-Rho1 and SHP2-mCitrine (Figure 4.26 B). However, SHP2-mCitrine lifetime was around 3 ns even before acceptor-photobleaching and did not change after bleaching indicating no interaction between both fluorophores.

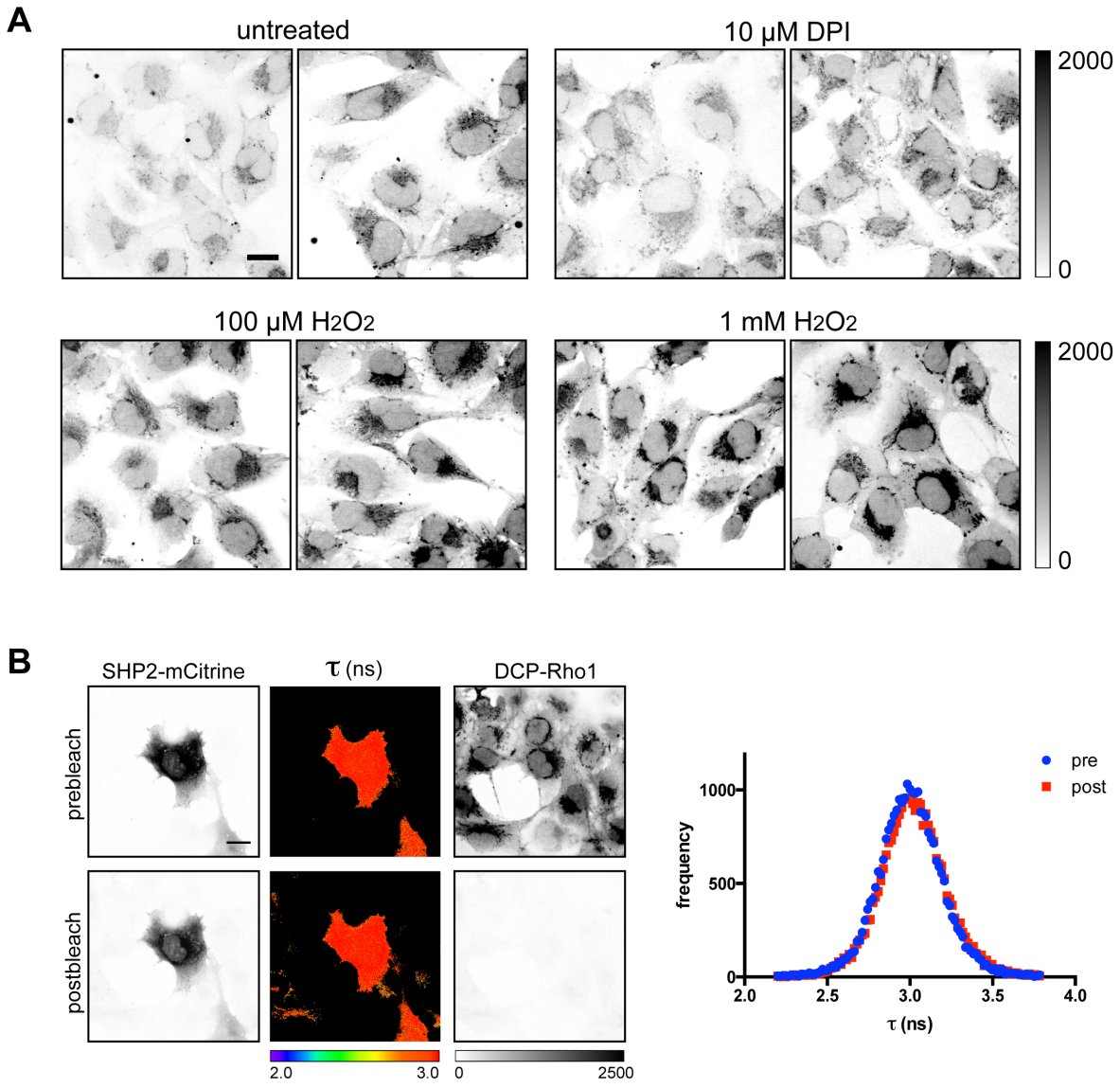

Figure 4.26: Imaging of DCP-Rho1 to reveal protein oxidation *in situ*
(A) Representative images of BJ wt cells treated as indicated and then incubated with 5 µM DCP-Rho1 for another 10 min followed by fixation with PFA. Scale bar 20 µm **(B)** FRET-FLIM of wt cells expressing SHP2-mCitrine and stained with DCP-Rho1 treated with 1 mM H_2O_2. Left panel shows representative fluorescence images of SHP2-mCitrine (first column), fluorescence lifetime (τ; second column) and DCP-Rho1 (third column) prebleach (first row) and after 30 min of acceptor-photobleaching (second row). Right panel shows τ-histogram pre- and postbleach for cell represented in images on the left. Scale bar 20 µm

4.3.2 Spatial-temporal detection of SHP2-oxidation

Since unmodified dimedone was suitable for the detection of oxidized PTP1Bc *in vitro* and also showed promising results in biochemical assays *in vivo*, we continued with a different probe called DYn-2 that is alkyne-modified and suitable for click-chemistry[40]. In contrast to DCP-Bio1 and DCP-Rho1, DYn-2 does not bear a bulky detection tag that can limit cell permeability and access to the catalytic cleft of PTPs, which is the main protein group we want to investigate here. In addition, an alkynyl-chemical reporter can be labeled with any azide-

modified detection tag in fixed cells, making DYn-2 suitable for both - biochemical and imaging-based assays.

For the RTK-PTP reaction network it has been shown that spatial partitioning of active signaling molecules is important to allow robust RTK activation while preventing autonomous activation in the absence of ligand[80,81]. Therefore, PTP oxidation is thought to be confined to compartments where EGFR gets phosphorylated. To investigate this spatially controlled PTP oxidation by GF-evoked H_2O_2, we want to set up an imaging approach to detect PTP oxidation via FLIM. The ectopic expression of a specific PTP tagged to mCitrine combined with the labeling of DYn-2 with a red fluorescent dye should result in FRET when the observed PTP is oxidized (Figure 4.27 A). First, we tested the labeling of DYn-2 with different acceptor molecules via cupper-catalyzed click-chemistry and checked by comparing these cells with just DMSO treated cells for the lowest background fluorescence (Figure 4.27 B). We decided to continue with Alexa594-Azide, which showed nearly no background in the DMSO control but gave a strong signal when DYn-2 was pre-incubated on live cells (Figure 4.27 B). In comparison to the previous two staining approaches with DCP-Bio1 and DCP-Rho1, DYn-2 labeled via click chemistry showed far less background staining of endomembranes indicating less unspecific binding of the probe and the dye itself.

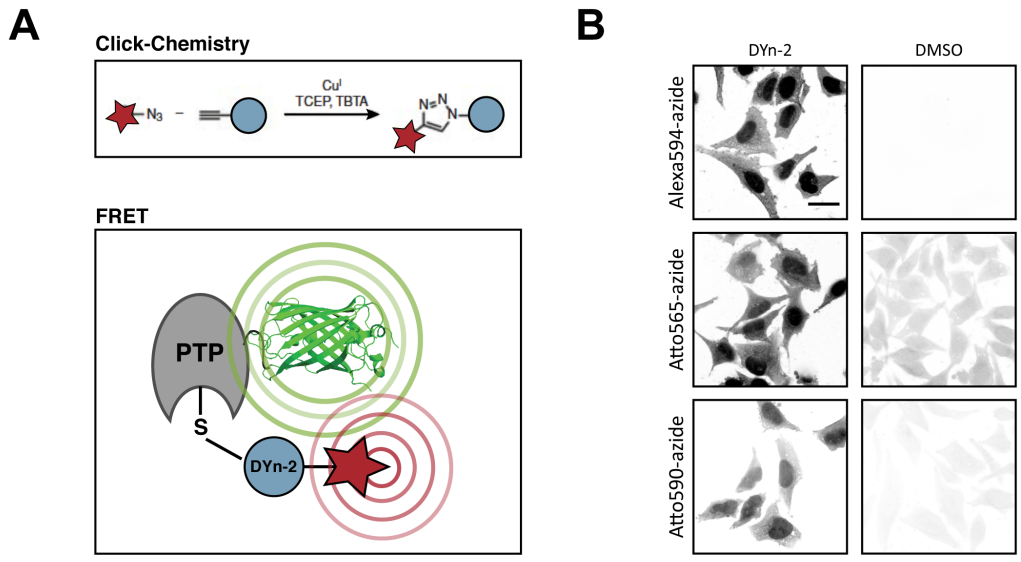

Figure 4.27: Development of a DYn-2 based approach for imaging protein oxidation
(A) Upper diagram illustrates the labeling of DYn-2 via cupper-catalyzed click-chemistry reaction with a red fluorescent dye serving as acceptor molecule. Lower panel shows binding of DYn-2 to oxidized PTPs tagged with a yellow fluorescent protein serving as donor fluorophore. Close proximity of donor and acceptor leads to FRET between both molecules and a lifetime drop of the donor detectable via FLIM. **(B)** Testing of different azide-modified acceptor molecules for the click-chemistry reaction with DYn-2. Live cells were incubated with either DYn-2 or the equivalent amount of DMSO, fixed and stained with the indicated dyes. Scale bar: 30 µm

Next, we tested if the combination of DYn-2 – Alexa594Az with mCitrine tagged PTPs is suitable for FRET-FLIM experiments. We started with SHP2 since we could show before that this PTP is susceptible to oxidation and also previous studies reported oxidation upon EGF treatment[40]. In BJ wt cells, incubation with only the dye without pre-treatment with DYn-2 did not show any significant staining and the mCitrine lifetime was not changed (Figure 4.28 A). When cells were pre-incubated with DYn-2 but unstimulated, the mCitrine lifetime decreased slightly compared to the DMSO treated cells. A clear lifetime reduction was detected when cells were treated with 0.5 mM H_2O_2, showing that this approach is suitable to detect SHP2 oxidation in cells (Figure 4.28 A). Next, we just compared the DYn-2 – Alexa594Az fluorescence intensity (Fl Int) to check if conventional imaging of DYn-2 binding itself is sufficient for the quantification of protein oxidation in general. However, DYn-2 – Alexa594Az intensity did not increase upon H_2O_2 treatment indicating that FRET-FLIM is necessary to untangle oxidation of a specific protein from global protein oxidation (Figure 4.28 B). To exclude nonspecific FRET arising from random collisions and/or unspecific associations of donor (D) and acceptor (A) molecules, we plotted mCitrine lifetime (τ) against the ratio of A over D fluorescence intensity (Figure 4.28 C). Both for unstimulated and H_2O_2 treated cells no correlation between τ and A/D Fl intensity was detectable indicating that the measured drop in τ is induced by a specific interaction between A and D molecules. In addition, treatment with H_2O_2 decreased τ to significant lower levels when compared to unstimulated cells proving that we indeed detected SHP2 oxidation (Figure 4.28 C).

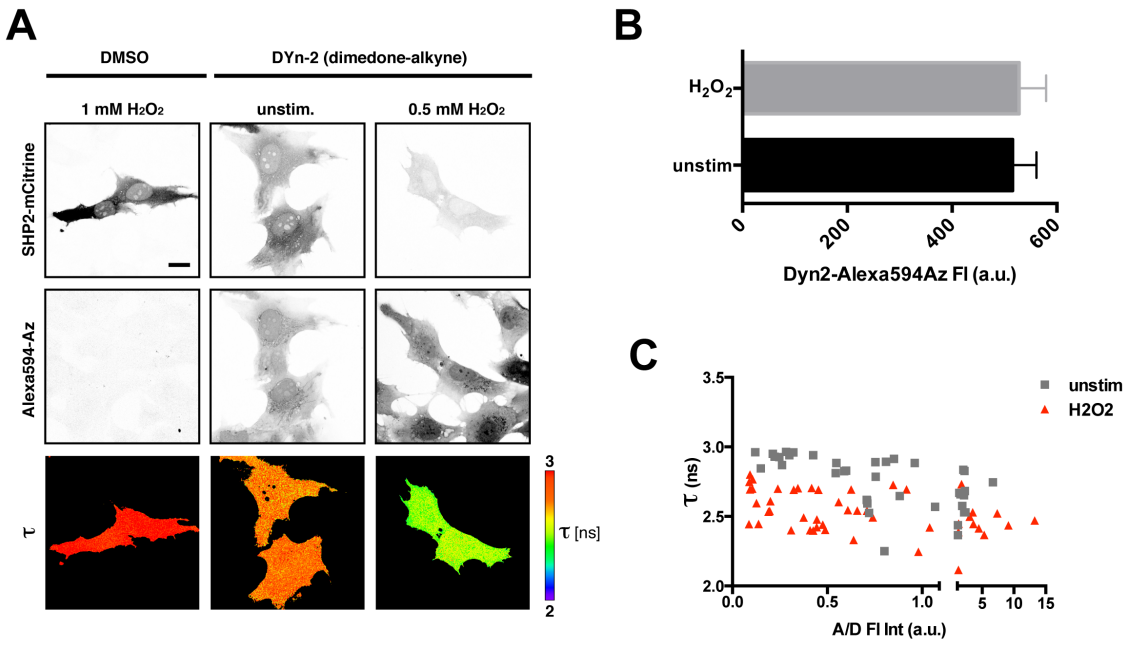

Figure 4.28: Specific detection of SHP2 oxidation with DYn-2
(A) FRET-FLIM of BJ wt cells expressing SHP2-mCitrine incubated either with DYn-2 or DMSO and subsequently stained with Alexa594Az. Representative fluorescence images of SHP2-mCitrine (first row), Alexa594Az (second row), and fluorescence lifetime (τ) of SHP2-mCitrine (third row) of cells treated as indicated. Scale bar: 20 µm **(B)** Plot shows mean ± SEM of fluorescence intensity (Fl Int) of Alexa594Az of either unstimulated cells or cells treated with 0.5 mM H_2O_2. **(C)** Graph shows τ versus Alexa594Az/mCitrine ratio of single cells that were either unstimulated or treated with 0.5 mM H_2O_2 in the presence of DYn-2.

To investigate if increased endogenous H_2O_2 level as caused by constitutively active HRas G12V (Figure 4.1, Figure 4.8) influence PTP oxidation and thus increase autonomous EGFR activation, we detected SHP2 oxidation in BJ wt and G12V cells with the above described method. In both cell types treatment with 0.1 mM and 0.5 mM H_2O_2 led to a significant decrease in τ when compared to untreated cells (Figure 4.29 A, B). When 2.5 mM H_2O_2, a concentration high above the physiological level, was applied to cells τ increased again and reached levels comparable to untreated cells. This might be caused by the overoxidation of the thiol of the catalytic cysteine to sulfinic or sulfonic acid, which both do not react with DYn-2 or any other dimedone derivative[136]. G12V cells showed in total a higher heterogeneity in SHP2 oxidation as wt cells pointing to a wider range of endogenous H_2O_2 levels (Figure 4.29 B). In addition, 0.5 mM H_2O_2 still led to a decrease of τ in G12V cells, whereas the same concentration led to an increase of τ in wt cells when compared to 0.1 mM H_2O_2 (Figure 4.29 B). This observation is in agreement with the HyPer3 experiments, which were also pointing to a more potent antioxidant system in G12V cells leading to a higher tolerance towards enhanced H_2O_2 concentrations (Figure 4.4, Figure 4.5). A direct comparison of both cell types

revealed that oxidation of SHP2 is higher in G12V cells at basal state and when treated with 0.5 and 2.5 mM H_2O_2 (Figure 4.29 C).

To investigate the proposed coupling between RTK activation and PTP inhibition, we stimulated both cell lines with EGF and detected SHP2 oxidation. Indeed, EGF stimulation led to the oxidation of SHP2 in both cell types, confirming the recursive interaction between EGFR activation and PTP inhibition. Again, the variation in SHP2 oxidation was far lower in wt cells when compared to G12V cells, possibly caused by a wider range of endogenous H_2O_2 concentrations generated by constitutively active HRas (Figure 4.29 B). However, the oxidation and thus inactivation of SHP2 was on average not higher in G12V transformed cells (Figure 4.29 C).

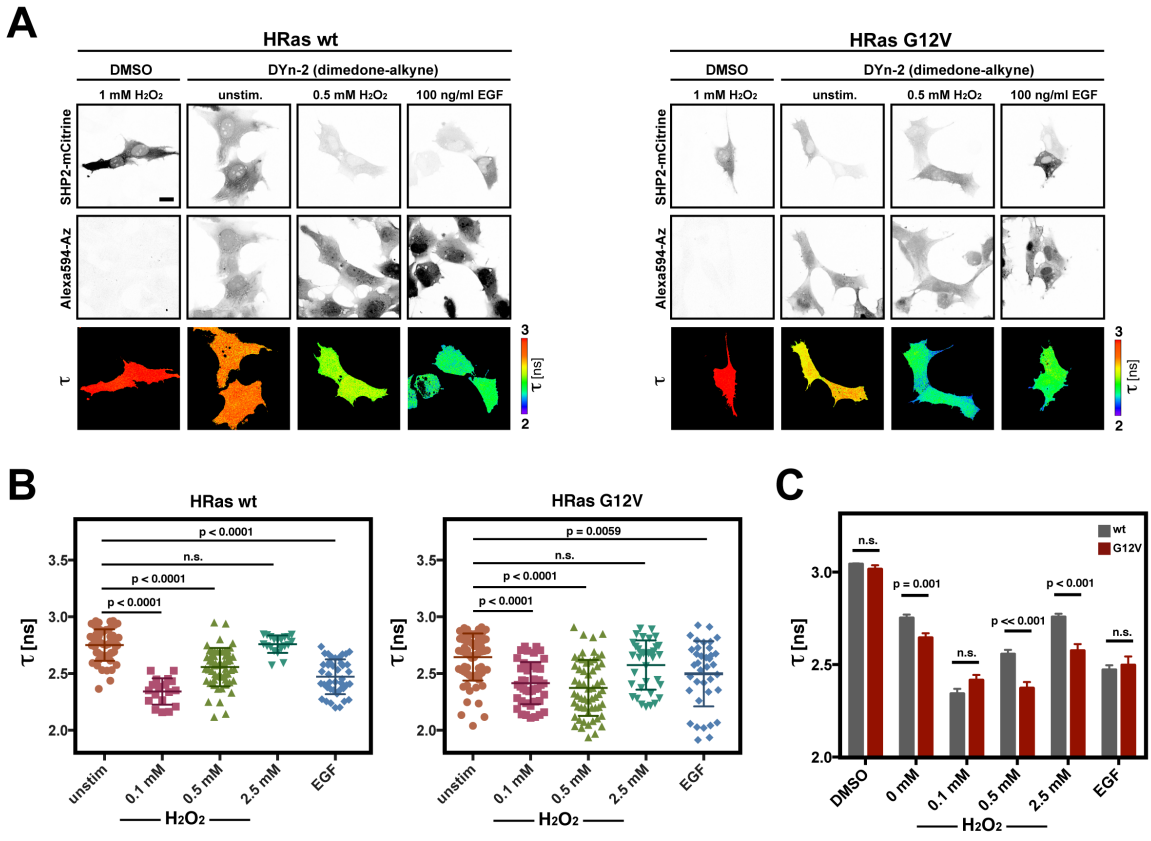

Figure 4.29: SHP2 oxidation in BJ cells upon H_2O_2 and EGF treatment
(A) Representative fluorescence images of SHP2-mCitrine (first row), Alexa594Az (second row), and fluorescence lifetime (τ) of SHP2-mCitrine (third row) showing SHP2-mCitrine oxidation in wt (left panel) and G12V cells (right panel) treated as indicated. Scale bar: 20 µm **(B)** Quantification of τ in single cells upon addition of different concentrations of H_2O_2 or 100 ng/ml EGF for 10 min. Horizontal line shows mean ± SD; two-way ANOVA was used for statistical tests. **(C)** Bar diagram showing mean ± SEM of τ from single cells plotted in (B) for direct comparison of oxidized SHP2-mCitrine between wt and G12V cells; p values were calculated by Student's t test.

To check if the here measured oxidation of SHP2 reflects indeed oxidation of the catalytic cysteine and thus leads to the inhibition of this PTP, we performed the same experiment with the catalytically inactive mutant (C/S)[137]. The staining intensity of DYn-2 – Alexa594Az was comparable to the SHP2-wt experiments showing once more that the pool of oxidized proteins in the cell is quite high and oxidation of specific proteins are hard to detect (Figure 4.29 A, Figure 4.30 A). However, in contrast to SHP2-wt, treatment with different H_2O_2 concentrations did not change τ of SHP2-C/S-mCitrine, indicating that we detected indeed oxidation of the catalytic cysteine in SHP2 (Figure 4.30).

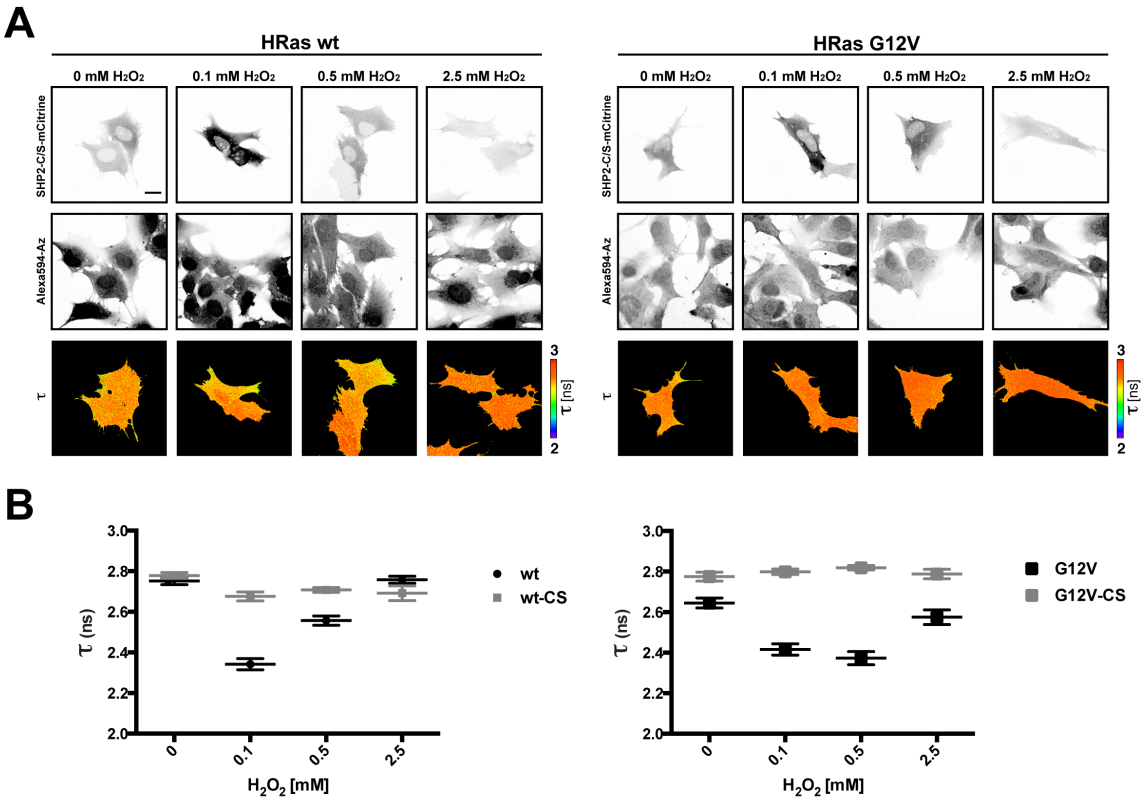

Figure 4.30: No oxidation detectable for SHP2-C/S mutant
(A) Representative fluorescence images of SHP2-C/S-mCitrine (first row), Alexa594Az (second row), and fluorescence lifetime (τ) of SHP2-C/S-mCitrine (third row) in wt (left panel) and G12V cells (right panel) treated as indicated. (B) Plot shows mean ± SEM for wt SHP2 (black, data from **Figure 4.29**) and C/S mutant (grey) for BJ wt cells on the left and G12V cells on the right for different H_2O_2 concentrations (n = min. 6 cells per condition).

In summary, we could show that the above-described approach is suitable for the detection of SHP2 oxidation and the resulting catalytic inactivation. Moreover, the data indicate that extracellular H_2O_2 and EGF-provoked H_2O_2 production inactivate SHP2 in both cell types, whereas G12V cells exhibit a higher cell-to-cell variability.

5 DISCUSSION

Cellular transformation by gain of function mutations of oncogenes is one of the major causes of cancer development and progression. The three Ras genes, comprising *KRAS*, *NRAS* and *HRAS*, were the first oncogenes being described and making up the most frequently mutated gene family in human cancer[138,139]. However, despite the extensive research that is focused on inhibiting Ras or its downstream effectors, clinical trials often resulted in unpredictable drawbacks showing that conventional therapy approaches are often too simplistic for treating a complex dynamic disease such as cancer. In the last years, systemic approaches gained more and more attention in the development of anti-cancer treatments. For example, identification of unknown feedback loops, which connect signaling nodes on all possible levels shifted the focus from the mutated gene itself to its effects on the dynamics of the signaling network, thus opening the door for more successful anti-cancer strategies, such as combinational therapy[140] and targeting of non-oncogene co-dependencies[109].

Here, we investigated how oncogenic HRas increases cellular H_2O_2 levels as a consequence of enhanced NOX activity. We showed that HRas G12V transformed cells are dependent on higher ROS levels and that increased production of H_2O_2 is affecting the RTK-PTP reaction network making these cells more susceptible for autonomous EGFR activation. To identify how the EGFR-PTP network dynamics determine the EGFR phosphorylation response, we developed a strategy to image protein oxidation revealing SHP2 oxidation in a spatial-temporal manner. Increased H_2O_2 levels in HRas G12V transformed cells are causing a higher basal oxidation of SHP2, which correlates with the increased autonomous EGFR activation in those cells. The further investigation of PTP oxidation could give new insights into how the EGFR-PTP network is affected by H_2O_2 in general and how high levels of H_2O_2, as common in cancer cells, could modulate it. We propose to study in the future the changes on the network level caused by oncogenic HRas to develop new strategies for the pharmacological treatment of Ras-driven cancer cells.

5.1 The spatial-temporal regulation of H_2O_2 production

Several studies have shown that elevated ROS levels are frequently linked to malignant transformation of cells making it a common phenomenon in human cancer[97,141]. Initially disregarded as irrelevant side product of a higher cellular metabolism, the role of ROS gained more and more interest in the scientific field revealing that it induces signaling cascades that mediate the oncogenic phenotype[142]. It was shown that oxidation of distinct signaling proteins

can increase tumor angiogenesis, drives the onset of inflammation and promotes the conversion of fibroblasts into myofibroblasts[142]. Those processes ultimately lead to tumor growth and metastatic dissemination indicating that a further investigation of ROS signaling in cancer cells can be beneficial for the development of new therapeutic approaches[143].

To date, literature about the diverse roles of ROS and their function in normal and cancer signaling is complex and in part conflicting[1,144]. In this work we used isogenic cell lines to specifically detect the changes in ROS signaling by introducing cellular transformation via HRas G12V[114]. We showed that intracellular H_2O_2 levels are increased in G12V cells and that the production depends on functional Ras signaling that mediates the activation of NOX proteins (Figure 4.1). Interestingly, abrogation of Ras signaling by PalmB and NOX inhibition by DPI also led to a significant decrease of H_2O_2 levels in unstimulated wt cells, showing that even untransformed cells produce H_2O_2 via Ras-NOX signaling at basal level. These results support the idea of H_2O_2 being a crucial signaling molecule not only in malignant cells, but also in untransformed cells. However, effects on cellular growth after inhibiting H_2O_2 production were only observed for HRas G12V transformed cells (Figure 4.2). High concentrations of DPI were necessary to inhibit cell growth in non-transformed cells, supporting the idea that ROS homeostasis is precisely balanced in transformed cells, whereas untransformed cells have a higher capacity for dealing with changing ROS level[143,145].

In order to fully understand the role of ROS and in particular H_2O_2 in normal and malignant cell signaling, it is necessary to consider the molecular mechanisms of oxidant actions. It has always been challenging to understand how target selectivity and spatial accumulation of H_2O_2 are achieved in a mainly reducing environment such as the cellular cytosol. With the discovery of NAPDH oxidases (NOXs) in leukocytes and later in various cell types, it was obvious that reactive oxidants are produced in regulated physiological processes[146].

In this study, we focused on the investigation of H_2O_2 production and its impact on EGFR signaling. Previous work showed that EGF stimulation leads to accumulation of H_2O_2, whereas treatment with exogenous H_2O_2 leads to ligand-independent EGFR activation[26,86]. Therefore, we investigated H_2O_2 production in dependence of the EGFR expression level showing that not only EGF stimulation and thus EGFR dimers, but also autonomously activated EGFR monomers can trigger the accumulation of H_2O_2 (Figure 4.3). In addition, the extent of H_2O_2 production in diverse cellular locations upon EGF stimulation was determined by using the genetically encoded sensor HyPer3[125] that was expressed in the cytosol or tagged

to the PM or ER. Spatial confinement of second messenger molecules like H_2O_2 is one key aspect of defining target specificity of ROS signaling[147]. Interestingly, our data indicates that the main increase of EGF induced H_2O_2 occurs in the cytosol (Figure 4.6, Figure 4.7, Figure 4.8). H_2O_2 produced by PM-associated NOX proteins first accumulates in the extracellular space and needs to diffuse back into the cell through the PM to reach intracellular target molecules. The H_2O_2 levels close to the PM possibly can not be detected with the here used HyPer3-TK version because it gets too fast diluted to provoke a significant change in the HyPer3-TK ratio. However, a better fold change upon EGF stimulation was achieved with the HyPer3/mCherry system, which was not tested for HyPer3-TK and HyPer3-ER. Further experiments with these combinations are needed to correctly compare H_2O_2 production in all three compartments. In summary, we could show though that EGF triggered a significant and fast increase of H_2O_2 in BJ cells and in MCF7 cells overexpressing EGFR. Upon EGF stimulation, EGFR gets internalized via packing into small endosomes, which could also serve as source of EGF-evoked H_2O_2. It was described before that activated NOX proteins could be also located on endosomes[148], which would rather lead to a cytosolic H_2O_2 accumulation, as detected with cHyPer3. A further investigation of the H_2O_2 dynamics upon EGF stimulation with HyPer tagged to endosomes could resolve its spatial accumulation more precisely.

However, a clear accumulation of NOX complexes was detectable at the PM in G12V cells indicating this compartment as main location for the increased H_2O_2 levels in G12V cells at basal level and upon EGF stimulation (Figure 4.9 C). In contrast to NOX2, the ER-anchored NOX4 complex is constitutively active and didn't show an elevated expression in HRas G12V transformed cells (Figure 4.9 B), therefore making it an unlikely source for stimulus-dependent H_2O_2 production[149]. The main problem in imaging H_2O_2 is its short-lived nature making a precise localization challenging even with advanced sensors like the here-used HyPer system. A combination with new imaging approaches such as on-stage cryo-arrest could provide new possibilities in uncovering ROS landscapes in normal and malignant cells and upon stimulation[150]. The detection of the distinct H_2O_2 sources in resting cells and upon GF stimulation would be a major step towards understanding the spatial and temporal regulation of ROS signaling. Since compartmentalization is also one of the main determinants of signal specificity of ROS, clear source localization would narrow down possible target proteins.

5.2 The effect of oncogene-induced H_2O_2 on EGFR activation

As described before, we showed that cellular transformation by HRas G12V increases cellular H_2O_2 levels both, at basal level and upon EGF stimulation. Additionally, EGFR itself leads to an accumulation of H_2O_2 when the receptor is highly overexpressed. In both cases, production of H_2O_2 seems to depend on stimulus-dependent NOX activation as shown by DPI treatment. Several reports document that GF evoked H_2O_2 production is necessary for inhibition of counteracting PTPs, one of the most famous target groups of ROS[86,151]. Elevated H_2O_2 levels should therefore increase tyrosine phosphorylation and thus receptor signaling activity. In case of HRas G12V transformed cells, we expected that the Ras induced H_2O_2 production can affect upstream RTKs like EGFR by inhibiting PTPs.

Therefore, we moved on to investigate EGFR activation in wt and G12V cells. Surprisingly, we could not detect any major differences in the EGFR phosphorylation profile between wt and HRas G12V transformed cells (Figure 4.10, Figure 4.11, Figure 4.13). However, basal EGFR phosphorylation in G12V cells was elevated, representing a higher activation of monomeric EGFR (Figure 4.11, Figure 4.13), which was lost upon DPI treatment (Figure 4.12). A higher EGFR phosphorylation in G12V cells was also observed upon treatment with exogenous H_2O_2 leading to solely autonomous receptor activation, which is characterized by phosphorylation of EGFR monomers (Figure 4.14)[80]. Various studies suggest different mechanisms that can lead to ligand-independent EGFR activation. Interestingly, two of them, namely phosphorylation of EGFR by Src and inhibition of PTPs, are thought to be regulated by ROS[79,86]. Therefore, it is interesting that higher H_2O_2 level as for instance caused by HRas G12V transformation enhance phosphorylation of monomeric EGFR, whereas phosphorylation levels of ligand-stimulated EGFR are comparable in both cells types. In summary, the here presented results show that inhibition of PTPs, as induced here by HRas G12V induced H_2O_2 production, does not mediate EGFR dimerization but facilitates a higher phosphorylation of the monomer. This points to different mechanisms for ligand-dependent vs. independent EGFR activation in BJ cells.

Ligand-independent EGFR activation has been already described before[80], but in how far signaling from the phosphorylated monomer differs to the one of phosphorylated dimers is still vaguely investigated. For a deeper understanding of the phosphorylation dynamics of EGFR, we performed single cell analysis of unstimulated and EGF stimulated BJ cells expressing EGFR-mCitrine and checked for phosphorylation of different tyrosine residues, each representing a distinct cellular function (Figure 4.16, Figure 4.17, Figure 4.18). For the

autocatalytic site Y845 a clear correlation between expression level and phosphorylation was detected in both cell types, indicating spontaneous phosphorylation of this site in the EGFR monomer. Interestingly, relative phosphorylation was higher in HRas G12V transformed cells when compared to similar EGFR expression levels in wt cells. This indicates that the threshold for spontaneous EGFR activation in G12V cells is lower than in wt cells, which might be caused by a lower PTP net activity in those cells. If this effect is purely determined by H_2O_2 remains to be further investigated by specific inhibitor experiments. In addition, it is also possible that HRas itself affects other network motifs that increase Y845 phosphorylation like increased Src activation, which in turn would activate EGFR.

When stimulated with EGF, the difference in Y845 phosphorylation between HRas G12V cells and wt cells is even more pronounced, with a higher phosphorylation in G12V cells (Figure 4.16). This is contradictory to the previous results, where no difference in EGFR phosphorylation between wt and G12V cells was detectable when stimulated with saturating EGF concentrations. One reason for that might be that detecting EGFR activation via PY72, PTB translocation or PhosTag, as used before, are not able to detect Y845 phosphorylation. This could indicate that both autonomous and EGF-induced autocatalytic EGF activation are indeed higher in G12V transformed cells but just specific phospho-sites are hyper-phosphorylated. The site-selective hyperphosphorylation caused by increased H_2O_2 levels was already shown for PDGFR, proposing a similar mechanism for EGFR[152]. Regulatory mechanisms that are unaffected by Ras signaling itself or H_2O_2 could keep relative phosphorylation of other tyrosines residues in check. For instance, PTPs that are not inhibited by H_2O_2 keep dephosphorylating distinct tyrosine of EGFR.

However, phosphorylation of Y845 is a prerequisite for EGFRs kinase activity and higher levels in pY845 should also be represented by other autophosphorylation sites[142]. Therefore, we checked for Y1068 phosphorylation, a signaling tyrosine that serves as docking site for Grb2. Interestingly, unstimulated G12V cells showed also a correlation between increasing Y1068 phosphorylation and higher receptor density (Figure 4.18). This effect was less pronounced in wt cells, although data are noisy and quantification of more cells is needed to draw a clear conclusion. Upon EGF stimulation, in particular G12V cells showed a fraction of cells with low EGFR expression level but high phospho-to-total ratio. This effect is probably caused by antibody binding to endogenous phosphorylated receptor creating artifacts in the here presented data. Therefore, this experiment should be repeated with a different antibody or in cells that express low levels of endogenous EGFR.

Another phosphorylation site that was investigated here is Y1045, a docking site for Cbl and therefore important for EGFR ubiquitination and degradation[153,154]. Interestingly, this site is not affected by oxidative stress[155] and just effectively phosphorylated in the dimer[80], which can be confirmed since no autonomous phosphorylation of this site was detected for both cell types (Figure 4.17). When stimulated with EGF, both cell types showed a clear increase in phosphorylation when compared to unstimulated cells. As for the other tyrosine residues, Y1045 phosphorylation was already saturated at low EGFR concentrations and no correlation between receptor expression and pY1045 was detectable. In accordance to Y845 phosphorylation, EGF-induced Y1045 phosphorylation was higher in G12V cells. However, as explained before, pY1045 leads to EGFR internalization and subsequent degradation. Thus, higher phosphorylation of this site in G12V cells could indicate an enhanced degradation rate, which could counteract the increased phosphorylation of Y845 leading to similar phosphorylation levels of other tyrosine residues that were investigated before (Figure 4.10, Figure 4.11, Figure 4.13). This hypothesis needs to be verified by further experiments, which should be emphasized on receptor ubiquitination and internalization rates.

By overexpressing EGFR, we provoked spontaneous phosphorylation due to high receptor density at the PM facilitating tyrosine phosphorylation by increasing the chance of random collisions. Under endogenous EGFR expression levels, the autocatalysis in the EGFR system can be detected by an EGF dose response, when a linear increase in ligand leads to a non-linear rather sigmoidal increase in receptor phosphorylation. This is accomplished by ligand-activated dimers that propagate the signal to non-ligand bound monomers and a simultaneous inhibition of PTPs by H_2O_2[86,94]. Under saturating ligand concentrations all receptors are fully active and in a dimeric state making higher H_2O_2 level in G12V cells probably redundant when it comes to EGFR phosphorylation. This is in line with the previously discussed experiments where no clear difference in EGFR phosphorylation between wt and G12V cells was detected. Therefore, we performed an EGF dose response experiment to identify the threshold at which EGFR gets activated in wt and G12V cells. However, no significant difference in tyrosine phosphorylation between both cell types was detected (Figure 4.15). Phosphorylation of Y845 was not detected here although this site showed clearly a higher phosphorylation when EGFR-mCitrine was overexpressed in G12V cells as compared to wt cells. This raises the question of how EGFR activation is defined. Simple antibody-stainings against one phospho-tyrosine do not adequately represent the complexity of EGFR activation and trafficking dynamics. Both of these processes combined

determine the EGFR activation status and should be therefore considered together. The combination of imaging experiments to map EGFR activation in a spatial context and biochemical experiments for the detection of the phosphorylation of distinct tyrosine could give a more detailed insight into the discrepancies in EGFR activation between wt and G12V cells caused by higher H_2O_2 levels.

Another way to investigate EGFR signaling activity is the analysis of downstream molecules, which get phosphorylated in response to EGF stimulation. Here, we focused on the two most prominent signaling cascades, the Ras/MAPK and PI3K/AKT pathway. Phosphorylation of ERK, representing activation of the MAPK pathway, was higher in unstimulated G12V cells as in wt cells, most likely caused directly by the constitutively active form of HRas. Upon EGF stimulation, phosphorylation levels between both cell types were comparable, in consistence with the similar pY1068 levels of EGFR obtained before (Figure 4.10). Interestingly, in unstimulated cells AKT activation, which is spatially restricted to the PM, was the same between both cell types but upon EGF stimulation G12V cells showed higher phospho-AKT level (Figure 4.19). This effect might be evoked either by HRas G12V itself or by the increased H_2O_2 levels, which have been shown to inhibit PTEN and thereby increase AKT activation[54,55].

Since the PI3K activity is also necessary for the formation of NOX complexes and H_2O_2 production[3,156], activation of its effector AKT is of main interest for this study. Therefore, we performed an EGF dose response experiment, detecting AKT phosphorylation as readout. The AKT phosphorylation profile differed significantly from the EGFR phosphorylation profile (Figure 4.15, Figure 4.20). In wt cells AKT phosphorylation saturated at a comparably low EGF concentration and even decreased with higher EGF concentrations. This phosphorylation profile indicates negative regulation of AKT signaling at high EGF concentrations[157]. It was shown before that EGF concentrations above 20 ng/ml induce the internalization via clathrin-independent pathways leading to EGFR degradation instead of recycling[118]. However, full AKT activation requires clathrin scaffolds suggesting that upon stimulation with high EGF concentrations, only a fraction of active EGFR leads to AKT phosphorylation[158]. Interestingly, AKT activation in G12V cells represents more a sigmoidal activation curve similar to the EGFR activation profile. Further experiments would be important to elucidate the mechanism behind these cell type specific variations. However, one can speculate that the more switch-like response of AKT phosphorylation in G12V cells could be generated for instance by a double-negative feedback as shown for EGFR[86,159]. The higher

production of H_2O_2 upon EGF stimulation in G12V cells would lead to an enhanced inhibition of PTEN in comparison to wt cells. Thus, PIP3 accumulates at the PM and NOX can be more efficiently activated leading to even higher levels of H_2O_2 resembling positive autoregulation[160]. Additionally, former results represented here show that G12V cells have a tendency to activate EGFR monomers, which have been shown to activate AKT but not ERK[80]. This would imply that in untransformed cells a switch from AKT to ERK activation occurs with increasing EGF concentrations caused by a change in the EGFR internalization mechanism (Figure 4.20). Consistent with this hypothesis, phosphorylation of AKT decreases at the same EGF concentration at which Y1045 phosphorylation of EGFR is highest indicating receptor ubiquitination (Figure 4.15 B, Figure 4.20). Although the relative pY1045 phosphorylation profile of G12V cells was similar to that observed in wt cells, the western blot analysis does not reveal how much EGFR is in a dimeric vs. monomeric state. A fraction of H_2O_2-activated monomers, negative for pY1045, in G12V cells would be able to activate AKT. In addition, this population of EGFR might be also promoting the here presented higher H_2O_2 production upon EGF stimulation (Figure 4.8). To proof this theory it would be important to investigate EGFR activity with regard to the receptors dimerization state and untangle signaling from EGFR monomers from that of EGFR dimers.

In summary, the simple explanation that an oncogene-induced raise in H_2O_2 decreases the net PTP activity resulting in a more trigger-friendly EGFR system was not fully confirmed by this study. These experiments illustrate that a simple detection of EGFR phosphorylation is not sufficient to map the distinct signaling modes of EGFR in relation to the spatial organization of the receptor and how these can be affected by HRas G12V dependent H_2O_2 production. However, the increased phosphorylation of the autocatalytic site Y845 in G12V cells indicates an increased autocatalytic activity of EGFR. Further investigations with regard to specific tyrosine residues are needed to reveal if the overall catalytic activity of EGFR is enhanced in G12V cells or if homeostatic mechanisms reduce an increased EGFR signal activity.

5.3 Homeostasis in HRas transformed cells

Malignant transformation of cells by the constitutive activation of an oncogene, as studied here, are frequently used model systems to investigate cancer signaling networks in cells. By introducing one oncogene, several networks motifs are getting perturbed and need to be integrated to ensure the survival of cancer cells[161]. This can lead to tumor specific drug

resistance, which could be prevented by understanding the effects on the signaling network level evoked by the oncogenic lesion[119,140].

Here, we found several indications that adaptive mechanisms in G12V cells are established to counteract the higher endogenous H_2O_2 level, thereby ensuring survival and proliferation rather than sensecence[109,162]. When the Hyper3 constructs were tested in BJ cells for their oxidation and reduction potential, G12V transformed cells showed a lower fold increase in the HyPer3 ratio than wt cells when treated with exogenous H_2O_2 (Figure 4.4, Figure 4.5). In line with that, all constructs showed a faster reduction in G12V cells when treated with DTT in particular the cytoplasmic construct cHyPer3 (Figure 4.4, Figure 4.5). This is counterintuitive to the higher basal H_2O_2 levels and the higher fold increase of H_2O_2 upon EGF stimulation in G12V cells (Figure 4.1, Figure 4.8). One explanation for this could be that the higher basal H_2O_2 levels in G12V cells already partially oxidize HyPer3 and treatment with exogenous H_2O_2 does not lead to the same fold increase as compared to wt cells due to sensor saturation. The fast reduction could be provoked by a more potent antioxidant system in BJ G12V cells that is necessary to cope with higher endogenous H_2O_2 concentrations. In line with this, it has been shown by other studies that adaption to high ROS levels is common in cancer cells[163,164].

We could also show that inhibition of NOX proteins via DPI leads to a significant decrease in cellular survival/proliferation in G12V cells, whereas a reduced growth rate in wt cells was only detected for high DPI concentrations (Figure 4.2). In addition to that, EGFR phosphorylation upon EGF stimulation was strongly reduced in G12V cells when treated with DPI, whereas no effect was detected for wt cells (Figure 4.12). In the opposite case, increasing ROS levels by treatment with exogenous H_2O_2, led to a striking autonomous activation of EGFR in G12V cells. In contrast, ligand-independent EGFR activation in wt cells could be only detected upon treatment with high H_2O_2 concentrations (Figure 4.14). This shows that G12V cells not only have to adapt to higher H_2O_2 levels to ensure survival but also are dependent on it for proper EGFR signaling and cellular growth.

In summary this points to the fact that, although not directly elevating EGFR phosphorylation, H_2O_2 production is necessary for full receptor activation upon EGF stimulation in G12V, where only a slight elevation of the intracellular H_2O_2 concentration led to autonomous receptor activation. This indicates that adaptive mechanisms keep EGFR phosphorylation under growth factor stimulation in check, whereas small perturbations such as higher ROS levels can lead to abnormal EGFR signaling. Several feedback loops might

downregulate EGFR phosphorylation in a more oxidative environment preventing hyperphosphorylation in G12V cells. For instance, it was shown that activation of ERK leads to the phosphorylation of Thr669 in EGFR correlating with decreased tyrosine phosphorylation and thus EGFR activation[165]. Constitutive activation of HRas enhanced ERK activation upon ligand stimulation resulting in Thr669 phosphorylation in G12V cells lowering EGFR tyrosine phosphorylation. Another negative feedback mechanism, which is regulated via the Ras/MAPK pathway, is the activation of the dual-specificity phosphatase CDC25c. EGFR dephosphorylation is correlated with CDC25c activation, a feedback loop causing drug resistance of colon cancer patients treated with a BRAF inhibitor[140]. Although there are also reports of H_2O_2 induced inhibition of CDC25c[166], its cytoplasmic localization could lead to a rapid exchange between inactivated and activated molecules still mediating EGFR dephosphorylation. Therefore, PTP localization could be a determinant for its oxidation susceptibility favoring PTP oxidation of spatially restricted PTPs like RPTPs or ER-anchored PTPs like PTP1B and TCPTP over cytoplasmic PTPs like CDC25c.

In general, we assume that PTPs catalyze dephosphorylation of their target proteins and thus mediate downregulation of RTK signaling. However, there are also oncogenic PTPs known that for example enhance EGFR activity like PTPD1[167] or mediate EGFR signaling and tumor growth as shown for SHP2[168-171]. Oxidation and inactivation of those PTPs would lead to decreased EGFR activity resulting in a negative feedback and not a double-negative feedback loop. Hence, a detailed investigation of the existing EGFR-PTP network topology in resting and EGF stimulated cells is necessary to elucidate how EGFR response properties are shaped by recursive interactions with PTPs and how those can be affected by H_2O_2.

5.4 PTP activity determining RTK phosphorylation dynamics

As stated out before, PTP oxidation and its effect on RTK activity is, despite great progress that was made over the last years, still one of the enigmas of RTK signaling. RTK phosphorylation dynamics are thought to be dictated by the receptors autocatalytic activity and its recursive interaction with PTPs[172]. Coupling between RTK activation and PTP inhibition is mediated by H_2O_2 and oxidation-mediated inactivation has been confirmed for several PTPs so far[42,57]. However, systematic approaches detecting the spatial-temporal dynamics of PTP oxidation upon GF stimulation and with respect to RTK activation are still missing.

5.4.1 HRas-induced H_2O_2 increases basal PTP oxidation

The challenge in studying ROS signaling is on the one hand the precise detection of ROS itself and on the other hand mapping the oxidation of target proteins correctly. Protein oxidation belongs like protein phosphorylation to the group of posttranslational modifications regulating protein activity, protein-protein interactions and protein stability. However, redox modifications such as the here-investigated S-sulfenylation (-SOH) are highly labile and dynamic making them hard to detect[173]. In this study, we used labeling of sulfenic acid with either native dimedone[20] or DYn-2, a cell-permeable alkyne-functionalized dimedone analogue[40]. Dimedone-derivatization of oxidized proteins in live cells, as used here, has the advantage of maintaining the native cellular redox environment whilst enabling the labeling of fixed cells for further analysis.

For the detection of dimedone-derivatized proteins an antibody was used that recognizes this epitope specifically[62]. We could show that the catalytic domain of PTP1B gets oxidized upon treatment with H_2O_2 *in vitro* (Figure 4.21). Further analysis of endogenous PTP1B in cells showed susceptibility of this PTP towards H_2O_2-mediated oxidation. However, the signal-to-noise ratio was quite low although exogenous treatment with H_2O_2 should exceed H_2O_2 levels that are produced upon GF stimulation leading to the full oxidation of PTP1B (Figure 4.22). Thus, we used ectopic expression of PTP1B-mCitrine and SHP2-mCitrine to provide a greater pool of available substrate for oxidation. In contrast to wt cells, HRas G12V transformed cells showed a significant increase in oxidation for both PTPs upon treatment with H_2O_2 (Figure 4.23). This indicates that higher endogenous H_2O_2 level caused by constitutively active HRas add up with exogenous H_2O_2, oxidizing and inhibiting PTPs more efficiently. This is in line with the higher ligand-independent activation of EGFR in G12V cells provoked by treatment with exogenous H_2O_2 (Figure 4.14). Basal oxidation of PTP1B-mCitrine and SHP2-mCitrine were also slightly increased in G12V cells when compared to wt cells, possibly causing the detected elevated EGFR phosphorylation in unstimulated G12V cells (Figure 4.11, Figure 4.13).

Without ligand stimulation, the ER-anchored PTP1B is important to suppress spontaneous RTK phosphorylation through the vesicular recycling of activated monomers from the PM to the perinuclear area, which is characterized by high PTP1B activity[80,81,90]. A higher basal oxidation of PTP1B might explain therefore the higher basal phosphorylation of EGFR in G12V transformed cells. However, it is still unclear why a higher inhibition of PTPs by HRas G12V-mediated H_2O_2 does not affect EGF-mediated receptor phosphorylation. For

further elucidating this discrepancy, we established an imaging approach for the spatial-temporal detection of protein oxidation by using the probe DYn-2 (Figure 4.27, Figure 4.28).

5.4.2 RTK activity patterns linked to PTP oxidation

By monitoring the spatially distinct phosphorylation pattern of EGFR upon EGF stimulation it is striking that upon ligand stimulation receptor activation is highest at the PM and declines upon internalization (Figure 4.11). Interestingly, when cells were treated with H_2O_2 to evoke ligand-independent EGFR activation, phosphorylation extended even to receptors on endomembranes since H_2O_2 levels and thus PTP inhibition are not spatially confined[86]. In contrast, EGF stimulation creates two opposite gradients; high H_2O_2 levels at the PM decreasing towards the cell interior[2] and high PTP activity in the perinuclear area declining towards the cell periphery[90]. This difference in spatial confinement of PTP inhibition could explain the discrepancy in EGFR phosphorylation between wt and G12V cells when treated with EGF vs. H_2O_2 (Figure 4.10, Figure 4.14, Figure 4.15). For instance, recycling/internalization in G12V cells could be faster upon EGF stimulation resulting in a more efficient dephosphorylation of receptors by ER-anchored PTPs, which are mostly unaffected by H_2O_2 accumulated at the PM. Although not detected at endogenous EGFR level, we could show a higher phosphorylation of Y1045 upon EGF stimulation in G12V cells when the receptor was overexpressed supporting this hypothesis (Figure 4.17). Another explanation could be a pool of PTPs that are freely diffusible and therefore less affected by spatially confined H_2O_2 production as stated before for CDC25c. A negative feedback created when those PTPs are either activated by EGFR, Ras or their downstream effectors could counteract an increased H_2O_2-mediated inhibition of other EGFR regulating PTPs.

To further investigate spatially distinct PTP inhibition, we developed an approach to monitor protein oxidation in cells. We focused on SHP2, a phosphatase that has been shown to be both a negative and a positive regulator of EGFR signaling. Once activated, SHP2 binds via its SH2 domain to phosphorylated EGFR directly or via tyrosine-phosphorylated adapter proteins stimulating the activity of Ras/ERK/MAPK signaling, marking SHP2 as a 'proto-oncogene'[174,175]. In addition, SHP2 also dephosphorylates the autophosphorylation site Y992 of EGFR, which acts as a binding site for RasGAP, a GTPase-activating protein catalyzing Ras inactivation[137]. On the other hand, phosphorylation of Y992 has been shown to mediate PLCγ1 activation resulting in Rac1 activation, important for membrane ruffling and H_2O_2 production[92,100,176].

ROS-dependent inhibition of SHP2 has been shown before for PDGF stimulation[45], EGF stimulation[40] and in this study upon treatment with H_2O_2 (Figure 4.23, Figure 4.28). Imaging SHP2 oxidation with the here established FRET-FLIM approach shows that it is higher in unstimulated G12V cells correlating with higher basal H_2O_2 level and autonomous EGFR activation (Figure 4.29). Upon treatment with H_2O_2 both cell types showed the formation of SHP2-SOH, whereas higher H_2O_2 concentrations led to the formation of irreversible oxoforms like sulfinic ($-SO_2H$) or sulfonic acid ($-SO_3H$) indicated by a decreased binding affinity of DYn-2 (Figure 4.29). EGF stimulation led to a significant oxidation of SHP2 in both cell types reflecting inhibition of the phosphatase since the catalytic deficient mutant (C/S substitution) was neither affected by H_2O_2 treatment nor by EGF stimulation (Figure 4.30). The unresponsiveness of the C/S mutant also proves that just the catalytic cysteine gets oxidized due to its low pKa value and that oxidation of PTPs thus inhibits their catalytic activity. In general, it is remarkable that G12V cells show a much higher variability than wt cells both upon H_2O_2 treatment and EGF stimulation. In general, it is beneficial for a cell population to maintain heterogeneity in a fluctuating, unpredictable environment, as it is the case for cancer. Cellular variation is thereby ensuring robustness and is in the case of cancer associated with resistance to anticancer therapies[83,177]. An enhanced variation is normally a characteristic of positive regulation and with regard to the RTK-PTP network an indication for the H_2O_2 mediated double negative feedback[160].

The here presented technique provides a first step towards the spatial-temporal monitoring of protein oxidation in single cells. This approach can be combined with immunostainings to map for instance EGFR phosphorylation simultaneously and can be extended to any protein of interest. With regard to our question it would be important to investigate oxidation of other PTPs important for generating the here observed EGFR phosphorylation profile in wt and G12V cells.

In summary, this and other studies suggest to divide PTPs in three different classes with regard to EGFR regulation:

- ER-anchored PTPs like PTP1B and TCPTP with high catalytic activity, dephosphorylating recycling EGFR molecules and terminating EGFR activity upon EGF stimulation

- Cytosolic, recruitable PTPs including SHP1 and SHP2 more important to activate/deactivate downstream effector proteins upon EGF stimulation
- Receptor PTPs, which are more likely to inhibit spontaneous EGFR activation at the PM and determining EGFRs responsiveness to EGF

Depending on the PTPs susceptibility to oxidation and its dephosphorylation target, distinct RTK-PTP network topologies can be distinguished creating different RTK activity patterns (Figure 5.1)[94,96]. It is important to separate, which PTPs are more important signal duration upon EGF stimulation and which regulate spontaneous activation and responsiveness. By untangling this, it would be possible to explain why autonomous activation is elevated in HRas G12V transformed cells whereas EGF induced phosphorylation is similar between both cell types.

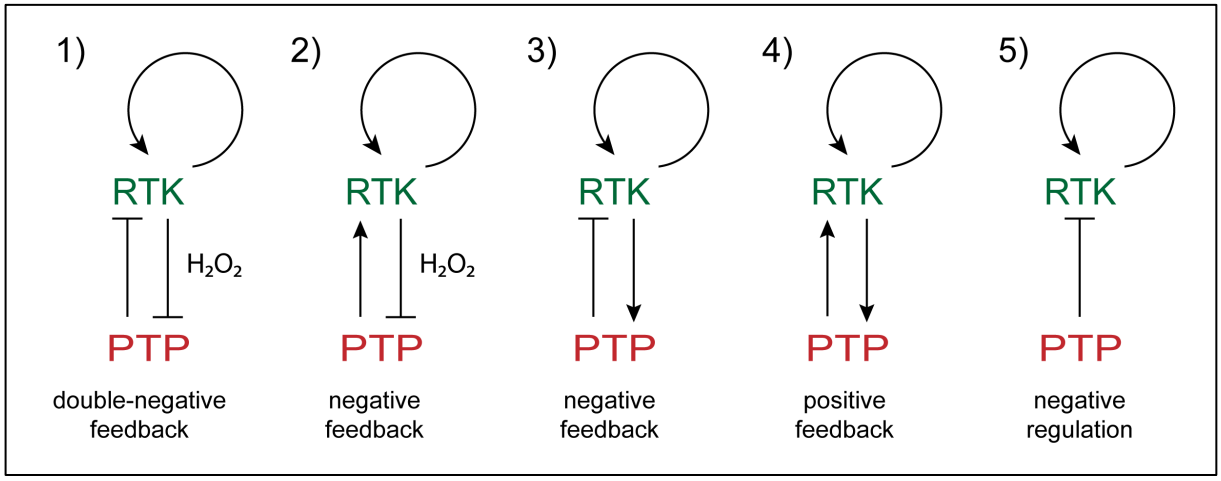

Figure 5.1: Examples of possible RTK-PTP network motifs
This scheme represents different possibilities for the interaction of PTPs with RTKs. When the PTP is inhibited upon RTK-induced H_2O_2 production either a double-negative feedback (1) or a negative feedback (2) can be generated. A negative feedback is created when the RTK activates its own inhibitor as for instance known for SHP1/SHP2 (3). When the PTP amplifies RTK activation e.g. by Src activation or by dephosphorylating tyrosine residues that negatively regulate RTK activation, a positive feedback is established (4). When the PTP just dephosphorylates the receptor the interaction is stated as simple negative regulation (5).

6 Outlook

With this work, we created the first step towards a more detailed understanding of the biology of ROS signaling. By generating an approach to detect protein oxidation in space and time it is possible to uncover several enigmas of ROS biology such as target selectivity or compartmentalization.

We focused our work on the RTK-PTP network and how this could be affected by the pathological rise of H_2O_2 caused by constitutively active HRas. In sum, we observed that EGF provoked EGFR phosphorylation is nearly unaffected in HRas G12V transformed cells whereas basal receptor activation is elevated. For a deeper understanding of the mechanism behind this finding, a detailed analysis of PTP oxidation is needed. By extending the here presented approach for imaging protein oxidation to other PTPs, different network motifs shaping the here detected EGFR phosphorylation profile could be identified. Interesting candidates are members of the RPTP family since their shared localization with EGFR might indicate that they are responsible for regulating autonomous receptor activation and ligand responsiveness. Structurally they also share the catalytic cysteine with a low pKa and oxidation and subsequent dimerization upon H_2O_2 treatment has been already shown for PTPRA[178]. This would create a double-negative feedback between EGFR activation and PTP oxidation at the PM, important for robust, threshold-controlled receptor activation. If this network topology exists under physiological H_2O_2 concentrations, as generated upon EGF stimulation, and which RPTPs regulate EGFR activation needs to be further verified.

It would be also important to identify PTPs that are not affected by EGF-induced H_2O_2 or even more active upon EGFR activation due to a positive feedback. This group of PTPs could sustain homeostasis of EGFR signaling keeping ligand-provoked receptor phosphorylation similar between wt and G12V cells. One possible candidate also belongs to the receptor-type PTPs. Former studies have shown that PTPRE dephosphorylates and thus actives Src[179,180]. Src activation is necessary for full EGFR activation and a PTP that activates Src would positively regulate EGFR activation. Interestingly, PTPRE is structurally related to PTPRA, which has been shown to be susceptible to oxidation-induced inhibition[178]. Therefore, inhibition of PTPRE through H_2O_2 would impair full EGFR activation in a negative feedback. In general, it would be necessary to globally identify, which PTPs are interacting with EGFR, the existing network topology and if this interaction is coupled by H_2O_2. This

would extend the knowledge of EGFR signaling to a new level by connecting protein phosphorylation with protein oxidation.

Another interesting aspect that was not investigated here is the direct oxidation of EGFR, which has been shown to increase its kinase activity[40]. So far it was just shown for A431 cells, a cell type with an extremely high expression rate of EGFR[181]. If EGFR oxidation is indeed important for physiological cell signaling needs to be verified in other cellular models. However, oxidation of EGFR and thereby increasing its own catalytic activity by triggering the production of H_2O_2 would be a new mechanism proving EGFR autocatalysis.

7 REFERENCES

1 D'Autreaux, B. & Toledano, M. B. ROS as signalling molecules: mechanisms that generate specificity in ROS homeostasis. *Nat Rev Mol Cell Biol* **8**, 813-824, doi:10.1038/nrm2256 (2007).

2 Dickinson, B. C. & Chang, C. J. Chemistry and biology of reactive oxygen species in signaling or stress responses. *Nat Chem Biol* **7**, 504-511 (2011).

3 Lambeth, J. D. NOX enzymes and the biology of reactive oxygen. *Nature reviews. Immunology* **4**, 181-189, doi:10.1038/nri1312 (2004).

4 Ray, P. D., Huang, B.-W. & Tsuji, Y. Reactive oxygen species (ROS) homeostasis and redox regulation in cellular signaling. *Cell Signal* **24**, 981-990, doi:doi:10.1016/j.cellsig.2012.01.008 (2012).

5 Aslund, F., Zheng, M., Beckwith, J. & Storz, G. Regulation of the OxyR transcription factor by hydrogen peroxide and the cellular thiol-disulfide status. *Proc Natl Acad Sci U S A* **96**, 6161-6165 (1999).

6 Dahlgren, C. & Karlsson, A. Respiratory burst in human neutrophils. *J Immunol Methods* **232**, 3-14 (1999).

7 Gough, D. R. & Cotter, T. G. Hydrogen peroxide: a Jekyll and Hyde signalling molecule. *Cell death & disease* **2**, e213, doi:10.1038/cddis.2011.96 (2011).

8 Burdon, R. H. & Rice-Evans, C. Free radicals and the regulation of mammalian cell proliferation. *Free Radic Res Commun* **6**, 345-358 (1989).

9 Suh, Y. A. *et al.* Cell transformation by the superoxide-generating oxidase Mox1. *Nature* **401**, 79-82, doi:10.1038/43459 (1999).

10 Bootman, M. D. & Berridge, M. J. The elemental principles of calcium signaling. *Cell* **83**, 675-678, doi:doi:10.1016/0092-8674(95)90179-5 (1995).

11 Stamler, J. S. Redox signaling: Nitrosylation and related target interactions of nitric oxide. *Cell* **78**, 931-936, doi:doi:10.1016/0092-8674(94)90269-0 (1994).

12 Bedard, K. & Krause, K.-H. The NOX Family of ROS-Generating NADPH Oxidases: Physiology and Pathophysiology. *Physiological Reviews* **87**, 245-313, doi:10.1152/physrev.00044.2005 (2007).

13 Lambeth, J. D., Cheng, G., Arnold, R. S. & Edens, W. A. Novel homologs of gp91phox. *Trends Biochem Sci* **25**, 459-461, doi:10.1016/S0968-0004(00)01658-3.

14 Giorgio, M., Trinei, M., Migliaccio, E. & Pelicci, P. G. Hydrogen peroxide: a metabolic by-product or a common mediator of ageing signals? *Nat Rev Mol Cell Biol* **8**, 722-728, doi:10.1038/nrm2240 (2007).

15 Zelko, I. N., Mariani, T. J. & Folz, R. J. Superoxide dismutase multigene family: a comparison of the CuZn-SOD (SOD1), Mn-SOD (SOD2), and EC-SOD (SOD3) gene structures, evolution, and expression. *Free Radical Biology and Medicine* **33**, 337-349, doi:doi:10.1016/S0891-5849(02)00905-X (2002).

16 Ago, T. *et al.* Phosphorylation of p47phox directs phox homology domain from SH3 domain toward phosphoinositides, leading to phagocyte NADPH oxidase activation. *Proc Natl Acad Sci U S A* **100**, 4474-4479, doi:10.1073/pnas.0735712100 (2003).

17 Groemping, Y., Lapouge, K., Smerdon, S. J. & Rittinger, K. Molecular basis of phosphorylation-induced activation of the NADPH oxidase. *Cell* **113**, 343-355 (2003).

18 Chamulitrat, W. *et al.* Association of gp91phox homolog Nox1 with anchorage-independent growth and MAP kinase-activation of transformed human keratinocytes. *Oncogene* **22**, 6045-6053, doi:10.1038/sj.onc.1206654 (2003).

19 Hilenski, L. L., Clempus, R. E., Quinn, M. T., Lambeth, J. D. & Griendling, K. K. Distinct subcellular localizations of Nox1 and Nox4 in vascular smooth muscle cells. *Arterioscler Thromb Vasc Biol* **24**, 677-683, doi:10.1161/01.ATV.0000112024.13727.2c (2004).

20 Miller, F. J., Jr. *et al.* Cytokine activation of nuclear factor kappa B in vascular smooth muscle cells requires signaling endosomes containing Nox1 and ClC-3. *Circ Res* **101**, 663-671, doi:10.1161/CIRCRESAHA.107.151076 (2007).

21 Brown, D. I. & Griendling, K. K. Nox proteins in signal transduction. *Free Radic Biol Med* **47**, 1239-1253, doi:10.1016/j.freeradbiomed.2009.07.023 (2009).

22 Van Buul, J. D., Fernandez-Borja, M., Anthony, E. C. & Hordijk, P. L. Expression and localization of NOX2 and NOX4 in primary human endothelial cells. *Antioxidants & redox signaling* **7**, 308-317, doi:10.1089/ars.2005.7.308 (2005).

23 von Lohneysen, K., Noack, D., Jesaitis, A. J., Dinauer, M. C. & Knaus, U. G. Mutational analysis reveals distinct features of the Nox4-p22 phox complex. *J Biol Chem* **283**, 35273-35282, doi:10.1074/jbc.M804200200 (2008).
24 von Lohneysen, K., Noack, D., Wood, M. R., Friedman, J. S. & Knaus, U. G. Structural insights into Nox4 and Nox2: motifs involved in function and cellular localization. *Molecular and cellular biology* **30**, 961-975, doi:10.1128/MCB.01393-09 (2010).
25 Sundaresan, M., Yu, Z.-X., Ferrans, V. J., Irani, K. & Finkel, T. Requirement for Generation of H2O2 for Platelet-Derived Growth Factor Signal Transduction. *Science* **270**, 296-299, doi:10.1126/science.270.5234.296 (1995).
26 Bae, Y. S. *et al.* Epidermal growth factor (EGF)-induced generation of hydrogen peroxide. Role in EGF receptor-mediated tyrosine phosphorylation. *J Biol Chem* **272**, 217-221 (1997).
27 Winterbourn, C. C. Reconciling the chemistry and biology of reactive oxygen species. *Nat Chem Biol* **4**, 278-286, doi:10.1038/nchembio.85 (2008).
28 Peskin, A. V. *et al.* The High Reactivity of Peroxiredoxin 2 with H2O2 Is Not Reflected in Its Reaction with Other Oxidants and Thiol Reagents. *Journal of Biological Chemistry* **282**, 11885-11892, doi:10.1074/jbc.M700339200 (2007).
29 Winterbourn, C. C. & Metodiewa, D. Reactivity of biologically important thiol compounds with superoxide and hydrogen peroxide. *Free Radic Biol Med* **27**, 322-328 (1999).
30 Woo, H. A. *et al.* Inactivation of peroxiredoxin I by phosphorylation allows localized H2O2 accumulation for cell signaling. *Cell* **140**, 517-528, doi:10.1016/j.cell.2010.01.009 (2010).
31 Wood, Z. A., Poole, L. B. & Karplus, P. A. Peroxiredoxin evolution and the regulation of hydrogen peroxide signaling. *Science* **300**, 650-653, doi:10.1126/science.1080405 (2003).
32 Bienert, G. P. *et al.* Specific Aquaporins Facilitate the Diffusion of Hydrogen Peroxide across Membranes. *Journal of Biological Chemistry* **282**, 1183-1192, doi:10.1074/jbc.M603761200 (2007).
33 Miller, E. W., Dickinson, B. C. & Chang, C. J. Aquaporin-3 mediates hydrogen peroxide uptake to regulate downstream intracellular signaling. *Proceedings of the National Academy of Sciences*, doi:10.1073/pnas.1005776107 (2010).
34 Spencer, N. Y. & Engelhardt, J. F. The basic biology of redoxosomes in cytokine-mediated signal transduction and implications for disease-specific therapies. *Biochemistry* **53**, 1551-1564, doi:10.1021/bi401719r (2014).
35 Sorkin, A. & von Zastrow, M. Endocytosis and signalling: intertwining molecular networks. *Nat Rev Mol Cell Biol* **10**, 609-622, doi:10.1038/nrm2748 (2009).
36 Schmick, M. & Bastiaens, P. I. The Interdependence of Membrane Shape and Cellular Signal Processing. *Cell* **156**, 1132-1138, doi:10.1016/j.cell.2014.02.007 (2014).
37 Cai, Z. & Yan, L.-J. Protein Oxidative Modifications: Beneficial Roles in Disease and Health. *Journal of biochemical and pharmacological research* **1**, 15-26 (2013).
38 Janssen-Heininger, Y. M. *et al.* Redox-based regulation of signal transduction: principles, pitfalls, and promises. *Free Radic Biol Med* **45**, 1-17, doi:10.1016/j.freeradbiomed.2008.03.011 (2008).
39 Zmijewski, J. W. *et al.* Exposure to hydrogen peroxide induces oxidation and activation of AMP-activated protein kinase. *J Biol Chem* **285**, 33154-33164, doi:10.1074/jbc.M110.143685 (2010).
40 Paulsen, C. E. *et al.* Peroxide-dependent sulfenylation of the EGFR catalytic site enhances kinase activity. *Nat Chem Biol* **8**, 57-64 (2012).
41 Tonks, N. K. Protein tyrosine phosphatases: from genes, to function, to disease. *Nat Rev Mol Cell Biol* **7**, 833-846, doi:10.1038/nrm2039 (2006).
42 Ostman, A., Frijhoff, J., Sandin, A. & Bohmer, F. D. Regulation of protein tyrosine phosphatases by reversible oxidation. *Journal of biochemistry* **150**, 345-356, doi:10.1093/jb/mvr104 (2011).
43 Salmeen, A. & Barford, D. Functions and Mechanisms of Redox Regulation of Cysteine-Based Phosphatases. *Antioxidants & Redox Signaling* **7**, 560-577, doi:10.1089/ars.2005.7.560 (2005).
44 Denu, J. M. & Dixon, J. E. Protein tyrosine phosphatases: mechanisms of catalysis and regulation. *Curr Opin Chem Biol* **2**, 633-641 (1998).
45 Meng, T.-C., Fukada, T. & Tonks, N. K. Reversible Oxidation and Inactivation of Protein Tyrosine Phosphatases In Vivo. *Molecular cell* **9**, 387-399, doi:10.1016/s1097-2765(02)00445-8 (2002).
46 Denu, J. M. & Tanner, K. G. Specific and reversible inactivation of protein tyrosine phosphatases by hydrogen peroxide: evidence for a sulfenic acid intermediate and implications for redox regulation. *Biochemistry* **37**, 5633-5642, doi:10.1021/bi973035t (1998).
47 Finkel, T. Oxidant signals and oxidative stress. *Current Opinion in Cell Biology* **15**, 247-254, doi:10.1016/s0955-0674(03)00002-4 (2003).

48 Mahadev, K., Zilbering, A., Zhu, L. & Goldstein, B. J. Insulin-stimulated hydrogen peroxide reversibly inhibits protein-tyrosine phosphatase 1b in vivo and enhances the early insulin action cascade. *J Biol Chem* **276**, 21938-21942, doi:10.1074/jbc.C100109200 (2001).
49 Lee, S. R., Kwon, K. S., Kim, S. R. & Rhee, S. G. Reversible inactivation of protein-tyrosine phosphatase 1B in A431 cells stimulated with epidermal growth factor. *J Biol Chem* **273**, 15366-15372 (1998).
50 Romsicki, Y., Kennedy, B. P. & Asante-Appiah, E. Purification and characterization of T cell protein tyrosine phosphatase reveals significant functional homology to protein tyrosine phosphatase-1B. *Archives of biochemistry and biophysics* **414**, 40-50 (2003).
51 Meng, T. C., Buckley, D. A., Galic, S., Tiganis, T. & Tonks, N. K. Regulation of insulin signaling through reversible oxidation of the protein-tyrosine phosphatases TC45 and PTP1B. *J Biol Chem* **279**, 37716-37725, doi:10.1074/jbc.M404606200 (2004).
52 Salmeen, A. *et al.* Redox regulation of protein tyrosine phosphatase 1B involves a sulphenyl-amide intermediate. *Nature* **423**, 769-773, doi:10.1038/nature01680 (2003).
53 Dagnell, M. *et al.* Selective activation of oxidized PTP1B by the thioredoxin system modulates PDGF-beta receptor tyrosine kinase signaling. *Proc Natl Acad Sci U S A* **110**, 13398-13403, doi:10.1073/pnas.1302891110 (2013).
54 Lee, S. R. *et al.* Reversible inactivation of the tumor suppressor PTEN by H2O2. *J Biol Chem* **277**, 20336-20342, doi:10.1074/jbc.M111899200 (2002).
55 Kwon, J. *et al.* Reversible oxidation and inactivation of the tumor suppressor PTEN in cells stimulated with peptide growth factors. *Proc Natl Acad Sci U S A* **101**, 16419-16424, doi:10.1073/pnas.0407396101 (2004).
56 Blanchetot, C., Tertoolen, L. G. & den Hertog, J. Regulation of receptor protein-tyrosine phosphatase alpha by oxidative stress. *Embo J* **21**, 493-503 (2002).
57 Karisch, R. *et al.* Global proteomic assessment of the classical protein-tyrosine phosphatome and "Redoxome". *Cell* **146**, 826-840, doi:10.1016/j.cell.2011.07.020 (2011).
58 Gupta, V. & Carroll, K. S. Sulfenic acid chemistry, detection and cellular lifetime. *Biochim Biophys Acta* **1840**, 847-875, doi:10.1016/j.bbagen.2013.05.040 (2014).
59 Allison, W. S. Formation and reactions of sulfenic acids in proteins. *Accounts of Chemical Research* **9**, 293-299, doi:10.1021/ar50104a003 (1976).
60 Poole, L. B. *et al.* Fluorescent and affinity-based tools to detect cysteine sulfenic acid formation in proteins. *Bioconjugate chemistry* **18**, 2004-2017, doi:10.1021/bc700257a (2007).
61 Reddie, K. G., Seo, Y. H., Muse Iii, W. B., Leonard, S. E. & Carroll, K. S. A chemical approach for detecting sulfenic acid-modified proteins in living cells. *Molecular bioSystems* **4**, 521-531, doi:10.1039/b719986d (2008).
62 Seo, Y. H. & Carroll, K. S. Profiling protein thiol oxidation in tumor cells using sulfenic acid-specific antibodies. *Proc Natl Acad Sci U S A* **106**, 16163-16168, doi:10.1073/pnas.0903015106 (2009).
63 Hunter, T. Tyrosine phosphorylation: thirty years and counting. *Current opinion in cell biology* **21**, 140-146, doi:10.1016/j.ceb.2009.01.028 (2009).
64 Lemmon, M. A. & Schlessinger, J. Cell signaling by receptor tyrosine kinases. *Cell* **141**, 1117-1134, doi:10.1016/j.cell.2010.06.011 (2010).
65 Schlessinger, J. & Lemmon, M. A. SH2 and PTB domains in tyrosine kinase signaling. *Sci STKE* **2003**, RE12, doi:10.1126/stke.2003.191.re12 (2003).
66 Cohen, S., Carpenter, G. & King, L., Jr. Epidermal growth factor-receptor-protein kinase interactions. Co-purification of receptor and epidermal growth factor-enhanced phosphorylation activity. *J Biol Chem* **255**, 4834-4842 (1980).
67 Ullrich, A. *et al.* Human epidermal growth factor receptor cDNA sequence and aberrant expression of the amplified gene in A431 epidermoid carcinoma cells. *Nature* **309**, 418-425 (1984).
68 Downward, J. *et al.* Close similarity of epidermal growth factor receptor and v-erb-B oncogene protein sequences. *Nature* **307**, 521-527 (1984).
69 Kovacs, E., Zorn, J. A., Huang, Y., Barros, T. & Kuriyan, J. A structural perspective on the regulation of the epidermal growth factor receptor. *Annu Rev Biochem* **84**, 739-764, doi:10.1146/annurev-biochem-060614-034402 (2015).
70 Arkhipov, A. *et al.* Architecture and membrane interactions of the EGF receptor. *Cell* **152**, 557-569, doi:10.1016/j.cell.2012.12.030 (2013).
71 Ferguson, K. M. *et al.* EGF activates its receptor by removing interactions that autoinhibit ectodomain dimerization. *Molecular cell* **11**, 507-517 (2003).

72 Zhang, X., Gureasko, J., Shen, K., Cole, P. A. & Kuriyan, J. An allosteric mechanism for activation of the kinase domain of epidermal growth factor receptor. *Cell* **125**, 1137-1149, doi:10.1016/j.cell.2006.05.013 (2006).
73 Endres, N. F. *et al.* Conformational coupling across the plasma membrane in activation of the EGF receptor. *Cell* **152**, 543-556, doi:10.1016/j.cell.2012.12.032 (2013).
74 Gotoh, N., Tojo, A., Hino, M., Yazaki, Y. & Shibuya, M. A highly conserved tyrosine residue at codon 845 within the kinase domain is not required for the transforming activity of human epidermal growth factor receptor. *Biochem Biophys Res Commun* **186**, 768-774 (1992).
75 Shan, Y. *et al.* Oncogenic mutations counteract intrinsic disorder in the EGFR kinase and promote receptor dimerization. *Cell* **149**, 860-870, doi:10.1016/j.cell.2012.02.063 (2012).
76 Huang, Y. *et al.* Molecular basis for multimerization in the activation of the epidermal growth factor receptor. *eLife* **5**, doi:10.7554/eLife.14107 (2016).
77 Clayton, A. H., Orchard, S. G., Nice, E. C., Posner, R. G. & Burgess, A. W. Predominance of activated EGFR higher-order oligomers on the cell surface. *Growth Factors* **26**, 316-324, doi:10.1080/08977190802442187 (2008).
78 Song, H. *et al.* Transphosphorylation of EGFR at Y845 plays an important role in its autophosphorylation and kinase activity. *Oncol Rep* **31**, 2393-2398, doi:10.3892/or.2014.3102 (2014).
79 Sato, K., Nagao, T., Iwasaki, T., Nishihira, Y. & Fukami, Y. Src-dependent phosphorylation of the EGF receptor Tyr-845 mediates Stat-p21waf1 pathway in A431 cells. *Genes Cells* **8**, 995-1003 (2003).
80 Baumdick, M. *et al.* EGF-dependent re-routing of vesicular recycling switches spontaneous phosphorylation suppression to EGFR signaling. *eLife* **4**, doi:10.7554/eLife.12223 (2015).
81 Sabet, O. *et al.* Ubiquitination switches EphA2 vesicular traffic from a continuous safeguard to a finite signalling mode. *Nature communications* **6**, 8047, doi:10.1038/ncomms9047 (2015).
82 Citri, A. & Yarden, Y. EGF-ERBB signalling: towards the systems level. *Nat Rev Mol Cell Biol* **7**, 505-516, doi:10.1038/nrm1962 (2006).
83 Kitano, H. Biological robustness. *Nat Rev Genet* **5**, 826-837, doi:10.1038/nrg1471 (2004).
84 Volinsky, N. & Kholodenko, B. N. Complexity of receptor tyrosine kinase signal processing. *Cold Spring Harbor perspectives in biology* **5**, a009043, doi:10.1101/cshperspect.a009043 (2013).
85 Kholodenko, B. N. Cell-signalling dynamics in time and space. *Nat Rev Mol Cell Biol* **7**, 165-176, doi:10.1038/nrm1838 (2006).
86 Reynolds, A. R., Tischer, C., Verveer, P. J., Rocks, O. & Bastiaens, P. I. EGFR activation coupled to inhibition of tyrosine phosphatases causes lateral signal propagation. *Nature cell biology* **5**, 447-453, doi:10.1038/ncb981 (2003).
87 Tischer, C. & Bastiaens, P. I. Lateral phosphorylation propagation: an aspect of feedback signalling? *Nat Rev Mol Cell Biol* **4**, 971-974, doi:10.1038/nrm1258 (2003).
88 Jallal, B., Schlessinger, J. & Ullrich, A. Tyrosine phosphatase inhibition permits analysis of signal transduction complexes in p185HER2/neu-overexpressing human tumor cells. *J Biol Chem* **267**, 4357-4363 (1992).
89 Ferrell, J. E., Jr. Building a cellular switch: more lessons from a good egg. *BioEssays : news and reviews in molecular, cellular and developmental biology* **21**, 866-870, doi:10.1002/(SICI)1521-1878(199910)21:10<866::AID-BIES9>3.0.CO;2-1 (1999).
90 Yudushkin, I. A. *et al.* Live-cell imaging of enzyme-substrate interaction reveals spatial regulation of PTP1B. *Science* **315**, 115-119, doi:10.1126/science.1134966 (2007).
91 Okutani, T. *et al.* Grb2/Ash binds directly to tyrosines 1068 and 1086 and indirectly to tyrosine 1148 of activated human epidermal growth factor receptors in intact cells. *J Biol Chem* **269**, 31310-31314 (1994).
92 Lambert, J. M. *et al.* Tiam1 mediates Ras activation of Rac by a PI(3)K-independent mechanism. *Nature cell biology* **4**, 621-625, doi:10.1038/ncb833 (2002).
93 Park, H. S. *et al.* Sequential Activation of Phosphatidylinositol 3-Kinase, Pix, Rac1, and Nox1 in Growth Factor-Induced Production of H2O2. *Molecular and Cellular Biology* **24**, 4384-4394, doi:10.1128/mcb.24.10.4384-4394.2004 (2004).
94 Grecco, H. E., Schmick, M. & Bastiaens, P. I. Signaling from the living plasma membrane. *Cell* **144**, 897-909, doi:10.1016/j.cell.2011.01.029 (2011).
95 Turing, A. M. The Chemical Basis of Morphogenesis. *Philosophical Transactions of the Royal Society of London. Series B, Biological Sciences* **237**, 37-72, doi:10.1098/rstb.1952.0012 (1952).
96 Villasenor, R., Nonaka, H., Del Conte-Zerial, P., Kalaidzidis, Y. & Zerial, M. Regulation of EGFR signal transduction by analogue-to-digital conversion in endosomes. *eLife* **4**, doi:10.7554/eLife.06156 (2015).

97 Szatrowski, T. P. & Nathan, C. F. Production of large amounts of hydrogen peroxide by human tumor cells. *Cancer Res* **51**, 794-798 (1991).
98 Weinberg, F. *et al.* Mitochondrial metabolism and ROS generation are essential for Kras-mediated tumorigenicity. *Proc Natl Acad Sci U S A* **107**, 8788-8793, doi:10.1073/pnas.1003428107 (2010).
99 Arnold, R. S. *et al.* Hydrogen peroxide mediates the cell growth and transformation caused by the mitogenic oxidase Nox1. *Proc Natl Acad Sci U S A* **98**, 5550-5555, doi:10.1073/pnas.101505898 (2001).
100 Sundaresan, M. *et al.* Regulation of reactive-oxygen-species generation in fibroblasts by Rac1. *Biochem J* **318 (Pt 2)**, 379-382 (1996).
101 Gorrini, C., Harris, I. S. & Mak, T. W. Modulation of oxidative stress as an anticancer strategy. *Nature reviews. Drug discovery* **12**, 931-947, doi:10.1038/nrd4002 (2013).
102 Schieber, M. & Chandel, N. S. ROS function in redox signaling and oxidative stress. *Current biology : CB* **24**, R453-462, doi:10.1016/j.cub.2014.03.034 (2014).
103 Cao, J. *et al.* Prdx1 inhibits tumorigenesis via regulating PTEN/AKT activity. *Embo J* **28**, 1505-1517, doi:10.1038/emboj.2009.101 (2009).
104 Ostman, A., Hellberg, C. & Bohmer, F. D. Protein-tyrosine phosphatases and cancer. *Nat Rev Cancer* **6**, 307-320, doi:10.1038/nrc1837 (2006).
105 Gao, P. *et al.* HIF-dependent antitumorigenic effect of antioxidants in vivo. *Cancer Cell* **12**, 230-238, doi:10.1016/j.ccr.2007.08.004 (2007).
106 Klein, E. A. *et al.* Vitamin E and the risk of prostate cancer: the Selenium and Vitamin E Cancer Prevention Trial (SELECT). *JAMA* **306**, 1549-1556, doi:10.1001/jama.2011.1437 (2011).
107 Omenn, G. S. *et al.* Effects of a combination of beta carotene and vitamin A on lung cancer and cardiovascular disease. *N Engl J Med* **334**, 1150-1155, doi:10.1056/NEJM199605023341802 (1996).
108 Yun, J. *et al.* Vitamin C selectively kills KRAS and BRAF mutant colorectal cancer cells by targeting GAPDH. *Science* **350**, 1391-1396, doi:10.1126/science.aaa5004 (2015).
109 Raj, L. *et al.* Selective killing of cancer cells by a small molecule targeting the stress response to ROS. *Nature* **475**, 231-234, doi:10.1038/nature10167 (2011).
110 Weinberg, S. E. & Chandel, N. S. Targeting mitochondria metabolism for cancer therapy. *Nat Chem Biol* **11**, 9-15, doi:10.1038/nchembio.1712 (2015).
111 Cairns, R. A., Harris, I. S. & Mak, T. W. Regulation of cancer cell metabolism. *Nat Rev Cancer* **11**, 85-95, doi:10.1038/nrc2981 (2011).
112 Koseska, A. & Bastiaens, P. I. Cell signaling as a cognitive process. *Embo J* **36**, 568-582, doi:10.15252/embj.201695383 (2017).
113 Sanger, F., Nicklen, S. & Coulsen, A. R. DNA sequencing with chain-terminating inhibitors. *Proceedings of the National Academy of Sciences* **74**, 5463-5467 (1977).
114 Hahn, W. C. *et al.* Creation of human tumour cells with defined genetic elements. *Nature* **400**, 464-468, doi:10.1038/22780 (1999).
115 Dickinson, B. C., Peltier, J., Stone, D., Schaffer, D. V. & Chang, C. J. Nox2 redox signaling maintains essential cell populations in the brain. *Nat Chem Biol* **7**, 106-112, doi:10.1038/nchembio.497 (2011).
116 Bastiaens, P. I. & Squire, A. Fluorescence lifetime imaging microscopy: spatial resolution of biochemical processes in the cell. *Trends Cell Biol* **9**, 48-52 (1999).
117 Clegg, R. M. Fluorescence resonance energy transfer. *Curr Opin Biotechnol* **6**, 103-110 (1995).
118 Verveer, P. J., Squire, A. & Bastiaens, P. I. Global analysis of fluorescence lifetime imaging microscopy data. *Biophysical journal* **78**, 2127-2137, doi:10.1016/S0006-3495(00)76759-2 (2000).
119 Grecco, H. E., Roda-Navarro, P. & Verveer, P. J. Global analysis of time correlated single photon counting FRET-FLIM data. *Opt Express* **17**, 6493-6508 (2009).
120 Kamentsky, L. *et al.* Improved structure, function and compatibility for CellProfiler: modular high-throughput image analysis software. *Bioinformatics* **27**, 1179-1180, doi:10.1093/bioinformatics/btr095 (2011).
121 O'Donnell, B. V., Tew, D. G., Jones, O. T. & England, P. J. Studies on the inhibitory mechanism of iodonium compounds with special reference to neutrophil NADPH oxidase. *Biochem J* **290 (Pt 1)**, 41-49 (1993).
122 Dekker, F. J. *et al.* Small-molecule inhibition of APT1 affects Ras localization and signaling. *Nat Chem Biol* **6**, 449-456, doi:10.1038/nchembio.362 (2010).
123 Avraham, R. & Yarden, Y. Feedback regulation of EGFR signalling: decision making by early and delayed loops. *Nat Rev Mol Cell Biol* **12**, 104-117, doi:10.1038/nrm3048 (2011).

124 Davidson, N. E., Gelmann, E. P., Lippman, M. E. & Dickson, R. B. Epidermal growth factor receptor gene expression in estrogen receptor-positive and negative human breast cancer cell lines. *Mol Endocrinol* **1**, 216-223, doi:10.1210/mend-1-3-216 (1987).
125 Bilan, D. S. *et al.* HyPer-3: A Genetically Encoded H2O2 Probe with Improved Performance for Ratiometric and Fluorescence Lifetime Imaging. *ACS Chemical Biology* **8**, 535-542, doi:10.1021/cb300625g (2012).
126 Belousov, V. V. *et al.* Genetically encoded fluorescent indicator for intracellular hydrogen peroxide. *Nat Methods* **3**, 281-286, doi:10.1038/nmeth866 (2006).
127 Kinoshita, E., Kinoshita-Kikuta, E., Takiyama, K. & Koike, T. Phosphate-binding tag, a new tool to visualize phosphorylated proteins. *Molecular & cellular proteomics : MCP* **5**, 749-757, doi:10.1074/mcp.T500024-MCP200 (2006).
128 Rowinsky, E. K. The erbB family: targets for therapeutic development against cancer and therapeutic strategies using monoclonal antibodies and tyrosine kinase inhibitors. *Annu Rev Med* **55**, 433-457, doi:10.1146/annurev.med.55.091902.104433 (2004).
129 Levkowitz, G. *et al.* c-Cbl/Sli-1 regulates endocytic sorting and ubiquitination of the epidermal growth factor receptor. *Genes Dev* **12**, 3663-3674 (1998).
130 Roberts, P. J. & Der, C. J. Targeting the Raf-MEK-ERK mitogen-activated protein kinase cascade for the treatment of cancer. *Oncogene* **26**, 3291-3310, doi:10.1038/sj.onc.1210422 (2007).
131 Bae, Y. S. *et al.* Platelet-derived growth factor-induced H(2)O(2) production requires the activation of phosphatidylinositol 3-kinase. *J Biol Chem* **275**, 10527-10531 (2000).
132 Gao, X. & Zhang, J. Akt signaling dynamics in plasma membrane microdomains visualized by FRET-based reporters. *Communicative & Integrative Biology* **2**, 32-34 (2009).
133 Gao, X. *et al.* PI3K/Akt signaling requires spatial compartmentalization in plasma membrane microdomains. *Proc Natl Acad Sci U S A* **108**, 14509-14514, doi:10.1073/pnas.1019386108 (2011).
134 Woolley, J. F., Corcoran, A., Groeger, G., Landry, W. D. & Cotter, T. G. Redox-Regulated Growth Factor Survival Signaling. *Antioxid Redox Signal*, doi:10.1089/ars.2012.5028 (2013).
135 Peralta, D. *et al.* A proton relay enhances H2O2 sensitivity of GAPDH to facilitate metabolic adaptation. *Nat Chem Biol* **11**, 156-163, doi:10.1038/nchembio.1720 (2015).
136 Benitez, L. V. & Allison, W. S. The inactivation of the acyl phosphatase activity catalyzed by the sulfenic acid form of glyceraldehyde 3-phosphate dehydrogenase by dimedone and olefins. *J Biol Chem* **249**, 6234-6243 (1974).
137 Agazie, Y. M. & Hayman, M. J. Molecular mechanism for a role of SHP2 in epidermal growth factor receptor signaling. *Molecular and cellular biology* **23**, 7875-7886 (2003).
138 Bos, J. L. ras oncogenes in human cancer: a review. *Cancer research* **49**, 4682-4689 (1989).
139 Stephen, A. G., Esposito, D., Bagni, R. K. & McCormick, F. Dragging ras back in the ring. *Cancer Cell* **25**, 272-281, doi:10.1016/j.ccr.2014.02.017 (2014).
140 Prahallad, A. *et al.* Unresponsiveness of colon cancer to BRAF(V600E) inhibition through feedback activation of EGFR. *Nature* **483**, 100-103, doi:10.1038/nature10868 (2012).
141 Pelicano, H., Carney, D. & Huang, P. ROS stress in cancer cells and therapeutic implications. *Drug Resistance Updates* **7**, 97-110, doi:10.1016/j.drup.2004.01.004 (2004).
142 Costa, A., Scholer-Dahirel, A. & Mechta-Grigoriou, F. The role of reactive oxygen species and metabolism on cancer cells and their microenvironment. *Semin Cancer Biol* **25**, 23-32, doi:doi:10.1016/j.semcancer.2013.12.007 (2014).
143 Trachootham, D., Alexandre, J. & Huang, P. Targeting cancer cells by ROS-mediated mechanisms: a radical therapeutic approach? *Nature reviews. Drug discovery* **8**, 579-591, doi:10.1038/nrd2803 (2009).
144 Holmstrom, K. M. & Finkel, T. Cellular mechanisms and physiological consequences of redox-dependent signalling. *Nat Rev Mol Cell Biol* **15**, 411-421, doi:10.1038/nrm3801 (2014).
145 Parkinson, E. I. & Hergenrother, P. J. Runaway ROS as a selective anticancer strategy. *ChemMedChem* **6**, 1957-1959, doi:10.1002/cmdc.201100381 (2011).
146 Bokoch, G. M. & Knaus, U. G. NADPH oxidases: not just for leukocytes anymore! *Trends in biochemical sciences* **28**, 502-508, doi:10.1016/S0968-0004(03)00194-4 (2003).
147 Ushio-Fukai, M. Compartmentalization of redox signaling through NADPH oxidase-derived ROS. *Antioxid Redox Signal* **11**, 1289-1299, doi:10.1089/ars.2008.2333 (2009).
148 Oakley, F. D., Abbott, D., Li, Q. & Engelhardt, J. F. Signaling components of redox active endosomes the redoxosomes. *Antioxidants & Redox Signaling* **11**, 1313-1333, doi:10.1089/ars.2008.2363. (2009).

149 von Lohneysen, K., Noack, D., Hayes, P., Friedman, J. S. & Knaus, U. G. Constitutive NADPH oxidase 4 activity resides in the composition of the B-loop and the penultimate C terminus. *J Biol Chem* **287**, 8737-8745, doi:10.1074/jbc.M111.332494 (2012).
150 Masip, M. E. *et al.* Reversible cryo-arrest for imaging molecules in living cells at high spatial resolution. *Nat Methods* **13**, 665-672, doi:10.1038/nmeth.3921 (2016).
151 Tonks, N. K. Protein tyrosine phosphatases--from housekeeping enzymes to master regulators of signal transduction. *The FEBS journal* **280**, 346-378, doi:10.1111/febs.12077 (2013).
152 Choi, M. H. *et al.* Regulation of PDGF signalling and vascular remodelling by peroxiredoxin II. *Nature* **435**, 347-353, doi:10.1038/nature03587 (2005).
153 Levkowitz, G. *et al.* Ubiquitin ligase activity and tyrosine phosphorylation underlie suppression of growth factor signaling by c-Cbl/Sli-1. *Mol Cell* **4**, 1029-1040 (1999).
154 Grovdal, L. M., Stang, E., Sorkin, A. & Madshus, I. H. Direct interaction of Cbl with pTyr 1045 of the EGF receptor (EGFR) is required to sort the EGFR to lysosomes for degradation. *Experimental cell research* **300**, 388-395, doi:10.1016/j.yexcr.2004.07.003 (2004).
155 Ravid, T., Sweeney, C., Gee, P., Carraway, K. L., 3rd & Goldkorn, T. Epidermal growth factor receptor activation under oxidative stress fails to promote c-Cbl mediated down-regulation. *J Biol Chem* **277**, 31214-31219, doi:10.1074/jbc.M204677200 (2002).
156 Baumer, A. T. *et al.* Phosphatidylinositol 3-kinase-dependent membrane recruitment of Rac-1 and p47phox is critical for alpha-platelet-derived growth factor receptor-induced production of reactive oxygen species. *J Biol Chem* **283**, 7864-7876, doi:10.1074/jbc.M704997200 (2008).
157 Tyson, J. J., Chen, K. C. & Novak, B. Sniffers, buzzers, toggles and blinkers: dynamics of regulatory and signaling pathways in the cell. *Current opinion in cell biology* **15**, 221-231 (2003).
158 Garay, C. *et al.* Epidermal growth factor-stimulated Akt phosphorylation requires clathrin or ErbB2 but not receptor endocytosis. *Mol Biol Cell* **26**, 3504-3519, doi:10.1091/mbc.E14-09-1412 (2015).
159 Ferrell, J. E., Jr. Feedback regulation of opposing enzymes generates robust, all-or-none bistable responses. *Curr Biol* **18**, R244-245, doi:10.1016/j.cub.2008.02.035 (2008).
160 Alon, U. Network motifs: theory and experimental approaches. *Nat Rev Genet* **8**, 450-461 (2007).
161 Creixell, P., Schoof, E. M., Erler, J. T. & Linding, R. Navigating cancer network attractors for tumor-specific therapy. *Nature biotechnology* **30**, 842-848, doi:10.1038/nbt.2345 (2012).
162 Lee, A. C. *et al.* Ras Proteins Induce Senescence by Altering the Intracellular Levels of Reactive Oxygen Species. *Journal of Biological Chemistry* **274**, 7936-7940, doi:10.1074/jbc.274.12.7936 (1999).
163 Shi, X., Zhang, Y., Zheng, J. & Pan, J. Reactive oxygen species in cancer stem cells. *Antioxid Redox Signal* **16**, 1215-1228, doi:10.1089/ars.2012.4529 (2012).
164 Liou, G. Y. & Storz, P. Reactive oxygen species in cancer. *Free Radic Res* **44**, 479-496, doi:10.3109/10715761003667554 (2010).
165 Sato, K. *et al.* Inverse correlation between Thr-669 and constitutive tyrosine phosphorylation in the asymmetric epidermal growth factor receptor dimer conformation. *Cancer science* **104**, 1315-1322, doi:10.1111/cas.12225 (2013).
166 Savitsky, P. A. & Finkel, T. Redox regulation of Cdc25C. *J Biol Chem* **277**, 20535-20540, doi:10.1074/jbc.M201589200 (2002).
167 Roda-Navarro, P. & Bastiaens, P. I. Dynamic recruitment of protein tyrosine phosphatase PTPD1 to EGF stimulation sites potentiates EGFR activation. *PLoS ONE* **9**, e103203, doi:10.1371/journal.pone.0103203 (2014).
168 Cunnick, J. M., Dorsey, J. F., Munoz-Antonia, T., Mei, L. & Wu, J. Requirement of SHP2 binding to Grb2-associated binder-1 for mitogen-activated protein kinase activation in response to lysophosphatidic acid and epidermal growth factor. *J Biol Chem* **275**, 13842-13848 (2000).
169 Ren, Y. *et al.* Roles of Gab1 and SHP2 in paxillin tyrosine dephosphorylation and Src activation in response to epidermal growth factor. *J Biol Chem* **279**, 8497-8505, doi:10.1074/jbc.M312575200 (2004).
170 Ren, Y. *et al.* Critical role of Shp2 in tumor growth involving regulation of c-Myc. *Genes Cancer* **1**, 994-1007, doi:10.1177/1947601910395582 (2010).
171 Aceto, N. *et al.* Tyrosine phosphatase SHP2 promotes breast cancer progression and maintains tumor-initiating cells via activation of key transcription factors and a positive feedback signaling loop. *Nature medicine* **18**, 529-537, doi:10.1038/nm.2645 (2012).
172 Harris, I. S. *et al.* Glutathione and thioredoxin antioxidant pathways synergize to drive cancer initiation and progression. *Cancer Cell* **27**, 211-222, doi:10.1016/j.ccell.2014.11.019 (2015).
173 Yang, J., Carroll, K. S. & Liebler, D. C. The Expanding Landscape of the Thiol Redox Proteome. *Molecular & cellular proteomics : MCP* **15**, 1-11, doi:10.1074/mcp.O115.056051 (2016).

174 Gu, H. & Neel, B. G. The "Gab" in signal transduction. *Trends in cell biology* **13**, 122-130 (2003).
175 Bunda, S. *et al.* Inhibition of SHP2-mediated dephosphorylation of Ras suppresses oncogenesis. *Nature communications* **6**, 8859, doi:10.1038/ncomms9859 (2015).
176 Nogami, M. *et al.* Requirement of autophosphorylated tyrosine 992 of EGF receptor and its docking protein phospholipase C gamma 1 for membrane ruffle formation. *FEBS Lett* **536**, 71-76 (2003).
177 Kitano, H. Cancer as a robust system: implications for anticancer therapy. *Nat Rev Cancer* **4**, 227-235, doi:10.1038/nrc1300 (2004).
178 van der Wijk, T., Overvoorde, J. & den Hertog, J. H2O2-induced intermolecular disulfide bond formation between receptor protein-tyrosine phosphatases. *J Biol Chem* **279**, 44355-44361, doi:10.1074/jbc.M407483200 (2004).
179 Gil-Henn, H. & Elson, A. Tyrosine phosphatase-epsilon activates Src and supports the transformed phenotype of Neu-induced mammary tumor cells. *J Biol Chem* **278**, 15579-15586, doi:10.1074/jbc.M210273200 (2003).
180 Berman-Golan, D. & Elson, A. Neu-mediated phosphorylation of protein tyrosine phosphatase epsilon is critical for activation of Src in mammary tumor cells. *Oncogene* **26**, 7028-7037, doi:10.1038/sj.onc.1210505 (2007).
181 Zidovetzki, R., Yarden, Y., Schlessinger, J. & Jovin, T. M. Rotational diffusion of epidermal growth factor complexed to cell surface receptors reflects rapid microaggregation and endocytosis of occupied receptors. *Proc Natl Acad Sci U S A* **78**, 6981-6985 (1981).

8 ACKNOWLEDGEMENTS

Firstly, I would like to thank my advisor Prof. Dr. Philippe I. H. Bastiaens. I appreciate all his contributions of time, ideas and way of thinking, making my time as a PhD student one of the most exciting, challenging and rememberable phases of my life.

Besides my advisor, I would like to thank Prof. Dr. Roger S. Goody for taking over the second revision.

I would also like to thank Dr. Astrid Krämer and Tanja Forck for organizing the lab, helping with various issues and keeping the overview when it comes to proper timing.

Furthermore I would like to thank our technicians who have supported me all the way through my PhD with their careful organization of the labs, protocols, common stocks and a list of several other aspects that is too long to be given here. Thank you Hendrike, Kirsten, Michael, Jutta, Lisaweta, Petra, Manuela, Kirsten and Nimetka!

People of Dep. II; what would be my PhD time without you? Thanks for scientific discussions, embracing creative solutions, filling up free time with enjoyable moments and bringing me back to the ground when I was freaking out. You lightened up my PhD during and after work. Cheers, guys!

Special thanks to my amazing friends for being very kind when it seemed I forgot about them due to busy and stressful times but were always available when I needed distraction, someone to talk and a glass/bottle of wine. You helped me with not getting lost, getting intentionally lost and remembering me that many problems are not as huge as they seem in the first place. Hugs and kisses to you!

Mein besonderer Dank gilt meiner Familie! Mama, von dir habe ich wohl die Antriebskraft und den dicken Kopf, der nötig ist, um auch schwer erreichbare Ziele zu verfolgen und darin aufzugehen. Danke euch allen für das Vertrauen und die unendliche Unterstützung, vor allem in Phasen, in denen ich in verschiedenster Weise an meine Grenzen gestoßen bin! Ihr habt mich unter Druck gesetzt, wenn es nötig war und mich entlastet, wenn ich mir selbst im Weg stand. Danke!